System Integration and Optimization of Copper-Chlorine Thermochemical Cycle with Various Options for Hydrogen Production

By

SEYEDALI AGHAHOSSEINI

A Thesis Submitted in Partial Fulfillment
of the Requirements for the degree of Doctor of Philosophy
in
Mechanical Engineering

Faculty of Engineering and Applied Science
University of Ontario Institute of Technology

Oshawa, Ontario, Canada

Infinite Intelligence…

I ask not for more riches, but for more wisdom with which to make better use of blessing with which I was endow with birth through the privilege of embracing my own mind and directing it ends into my own choice.

Abstract

The Copper-Chlorine (Cu-Cl) thermochemical water splitting cycle is one of the most attractive alternative thermochemical cycles for clean hydrogen production due to its lower temperature requirement and better overall efficiency. CuCl electrolysis is considered a key process in the Cu-Cl cycle of hydrogen production where H_2 gas is produced by oxidation of CuCl particles dissolved in concentrated HCl solution. A lower electrochemical cell voltage than water electrolysis is a significant advantage of CuCl electrolysis and makes this process attractive for hydrogen production. Nevertheless, an integration of both hydrolysis and electrolysis processes is one of the most important engineering challenges associated with the Cu-Cl cycle of hydrogen production. The kinetics of the hydrolysis reaction indicates the reversibility of this process. This requires H_2O in excess of the stoichiometric quantity which significantly decreases the overall thermal efficiency of the Cu-Cl cycle. Moreover, the HCl concentration in the produced gas mixture of H_2O and HCl in the hydrolysis reaction is in much lower concentration of the electrolysis reaction requirement for an effective electrolytic cell performance.

In this PhD thesis, an integrated process model of the hydrolysis and electrolysis processes is simulated by introducing intermediate heat recovery steam generator (HRSG) and HCl-H_2O separation process consisting of rectification and absorption columns. In the separation processes, the influence of operating parameters including reflux ratio, mole fraction of HCl in the feed stream, solvent flow rate and temperature, and column configuration variables, such as the location of feed stage and number of stages on the heat duty requirements and the composition of products are investigated and analyzed. It is shown that the amount of steam generated in the HRSG unit satisfies the

extra steam requirement of the hydrolysis reaction up to 14 times more than its stoichiometric value and the separation process effectively provides HCl acid up to the concentration of 22 mol% for the electrolysis reaction.

In order to achieve an effective integration of the electrolysis process with hydrolysis and decomposition reactions of the Cu-Cl cycle, a lab-scale CuCl electrolysis unit is designed, fabricated and tested. The influences of operational factors on the cell performance are then investigated. In the experiments, the effects of operating parameters, including HCl and CuCl concentrations, applied current density, temperature and solution flow rate on the cell potential and hydrogen production rate are experimentally investigated and analyzed. A fractional factorial design is performed, based on design of experiment methods, to find a correlation between cell voltage and operation factors. The present model predicts the effects of various operating variables on the cell voltage to provide new insight into an integration of the electrolysis process. A close agreement of the measured and theoretical hydrogen production rate confirms the accuracy of measurements and reliability of the experimental studies.

An innovative integration of gasification process and Cu-Cl cycle, which can effectively contribute to hydrogen production with higher efficiency and lower environmental impact, is also studied and evaluated. In this study, the effects of using oxygen instead of air in the gasification process, where it is produced and supplied by the integrated Cu-Cl cycle is investigated. It is shown that using oxygen instead of air in the gasification process increases the gasification temperature and helps to eliminate NOx emissions. It is demonstrated that increasing the equivalence ratio (ER) from 0.1 to 0.4 improves the gasification exergy efficiency by about 10%. The influence of ER on the

syngas composition is also studied. The gasification products rely on specific syngas compositions and could potentially provide a precursor to the combined cycle for power generation in an Integrated Gasification Combined Cycle (IGCC) power plant. The process model of a gasification process is simulated based on the industrial Texaco IGCC plant in which the heat of syngas cooling process is utilized to supply extra steam requirement of the hydrolysis reaction in the Cu-Cl cycle. The effects of steam recovery in the hydrolysis reaction on energy and exergy efficiencies of the Cu-Cl cycle are analyzed and discussed.

Acknowledgements

I would like to thank my supervisor Dr. Ibrahim Dincer and my co supervisor Dr. Greg Naterer for their invaluable advice and contributions to this work. Their insights at high standards have definitely helped to shape this work. It is a pleasure to have supervisors being so supportive in the work and creative in the research.

I would like to thank all my committee members for their valuable time in reading and providing their comments to improve the content of my thesis.

I am in particular indebted to Dr. Forest Wang for his significant impact on the course of this work. His insight to the field of Chemical Engineering and to the Cu-Cl cycle operation has been most valuable. Our discussions have been most amusing and enlightening. My thanks go to Edward Secnik for great and inspiring years in Clean Energy Research Laboratory, supporting me to purchase equipment and setting up the experiment test bench.

Thanks to my colleagues at UOIT for making an enjoyable working environment, and to my friends Patrick Edge, Mehdi Hosseini, Pouria Ahmadi, and Behnaz Rezaie for being my confidant.

Finally, I want to express gratitude to my parents and sister for their unconditional support and encouragement. My warmest thanks go to my amazing wife Mona, without her love, support, and continued patience my contribution to this work wouldn't be possible.

The financial support provided by the Ontario Research Excellence Fund and Atomic Energy of Canada Limited is gratefully acknowledged.

Table of Contents

List of Tables

List of Figures

Nomenclature

A	heat transfer surface area, m^2
B_Y	bias error
a_i	activity of chemical species *i*
C_p	heat capacity, kJ K^{-1}
c_p	molar heat capacity at constant pressure, kJ $kmol^{-1}$ K^{-1}
$\dot{E}$	energy flow rate, kW
E^m	molar energy, kJ mol^{-1}
$\dot{E}x$	exergy flow rate, kW
Ex_{ch}^o	standard chemical exergy, kJ $kmol^{-1}$
F	feed stream flow rate, kmol h^{-1}
f	fugacity, kPa
H	enthalpy, kJ
HHV	higher heating value, kJ kg^{-1}
h	molar enthalpy, kJ $kmol^{-1}$
h^m	specific enthalpy, kJ kg^{-1}
I	current density, A
K	chemical equilibrium constant
L	liquid stream flow rate, kmol h^{-1}
LHV	lower heating value, kJ kg^{-1}
$\dot{m}$	mass flow rate, kg s^{-1}
MW	molecular weight, kg $kmol^{-1}$
$\dot{n}$	molar flow rate, kmol s^{-1}
n_i	number of moles of species *i*
P	pressure, kPa
P_Y	precision error
P_0	ambient pressure, kPa
$\dot{Q}$	heat flow rate, kW
Q_c	electric charge, C (coulomb)
R	universal gas constant, kJ $kmol^{-1}K^{-1}$
S	entropy, kJ K^{-1}
Sr	solvent flow rate, kmol h^{-1}
s	specific entropy, kJ kg^{-1} K^{-1}
s^o	standard molar entropy, kJ $kmol^{-1}$ K^{-1}
T	temperature, K
t	temperature, K
T_0	ambient temperature, K

t_s	time duration, s
U	liquid side stream flow rate, kmol h^{-1}
U_h	heat transfer coefficient, kW m^{-2} K^{-1}
U_Y	uncertainty
v_i	mole fraction of species *i*
V	vapor flow rate, kmol.h^{-1}
W	vapor side stream flow rate, kmol h^{-1}
$\dot{W}$	power, kW
x	liquid mole fraction
X	amount of reactant moles
$\overline{X}$	mean value
y	vapor mole fraction
z	feed stream mole fraction
$\Delta H°$	enthalpy of reaction, kJ
$\overline{\Delta h_f}$	standard enthalpy of formation, kJ $kmol^{-1}$
Δh^*_{Vap}	molar enthalpy of vaporization, kJ $kmol^{-1}$

Greek letters

α	relative volatility
β	temperature coefficient
γ	activity coefficient
θ	factorial coefficient
λ	chemical exergy coefficient
ζ	sensitivity coefficient
η	energy efficiency
φ	fugacity coefficient
ψ	exergy efficiency

Subscripts and Superscripts

aq	aqueous
C	condenser
ch	chemical
des	destruction
eq	equilibrium
Fe	feed stream

g	gas
i, j, k	component index
ig	ideal gas
in	inlet
Li	liquid phase property
M	number of outlet streams
N	number of inlet streams
out	outlet
ph	physical
pr	product stream
R	reboiler
ref	reference condition
s	solid
sat	saturation
Sl	solvent
tot	total
Vap	vapor phase property
k	inlet process stream
l	outlet process stream

Acronyms

AECL	Atomic Energy of Canada Limited
ANL	Argonne National Laboratory
ANOVA	Analysis of Variance
ASU	Air Separation Unit
CERL	Clean Energy Research Laboratory
CRL	Chalk River Laboratory
DAQ	Data Acquisition
DI	De-Ionized
DOE	Department of Energy
ED	Extractive Distillation
ER	Equivalence Ratio
FDS	Fraction of Design Space
GHG	Greenhouse Gas Emission
HENs	Heat Exchanger Networks

HRSG	Heat Recovery Steam Generator
ICE	Initial-Change-Equilibrium
IGCC	Integrated Gasification Combined Cycle
LLE	Liquid-Liquid Equilibrium
LMTD	Log Mean Temperature Difference
LSV	Linear Sweep Voltammetry
MEA	Membrane Electrode Assembly
Mt	Million tonnes
NRTL	Non-Random-Two-Liquid
ORC	Organic Rankine Cycle
PED	Process Flow Diagram
PEM	Proton Exchange Membrane
PI	Process Integration
PPE	Porous Poly Ethylene
PJ	Petajoule (10^{15} Joules)
PSD	Pressure-Swing Distillation
PSU	Pennsylvania State University
RSS	Root-Sum-Square
RESS	Residual Sum of Squares
SCWR	Super-Critical Water Reactor
SMR	Steam Methane Reforming
SS	Sum of Squares
UOIT	University of Ontario Institute of Technology
VLE	Vapor-Liquid Equilibrium

Chapter 1: Introduction

1.1 Energy and environment

The increase in the average temperatures over the globe since the mid-20th century is mainly related to the recorded increase in the greenhouse gas concentration. Carbon dioxide (CO_2), water vapor and methane known as greenhouse gases (GHGs) absorb solar radiation and create a natural greenhouse cover effect around the Earth. It is predicted that the earth average temperatures could be 30°C lower without this effect [1]. CO_2 can remain in the atmosphere for hundreds of years. Human activities have been the significant contributor to GHGs emission which has been significantly increased since pre-industrial times. As an example, carbon dioxide (CO) concentration has been increased by over one third from 280 parts per million (ppm) in 1750, to 379 ppm in 2005 [2]. It has been also estimated that CO_2 concentration level could reach 550 ppm by 2050, leading to warming of at least 2°C. Some effects of the global warming on earth are the rise of sea level, glacial decline, species extinction, and the increased possibility of extreme weather condition. For example, a temperature rise of just 2.7°C could lead to the melting of the Greenland ice cap [2]. Therefore, it is crucial to start taking actions to control global warming and its effects.

Energy is a driving force of industry and is a key in the development of the human society. It is considered as one of the important factors in sustainable development. Energy resources are necessary to fulfill human needs and enhance life quality which could harm the environment. United Nations obligated the energy sector to follow effective environmental protection strategies to increase efficiency. Transition to

alternative energy sources results in decrease in the use of fossil fuels in industry. This can significantly help to mitigate CO_2 emissions [3]. Fossil fuels are used commonly to generate heat and power which are enormously dangerous to environment and global sustainability [4].

1.2 Energy utilization and sectors in Canada

Canada is a country rich in a variety of energy resources. According to Statistics Canada, Canada is a big energy consumer, almost equal to the USA and number one in the G8 nations [4]. Long travel distance, cold winters, and the dependency of Canada's economy to the energy intensive industries such as mining, pulp and paper, refining and steel manufacturing, are the main reasons that Canada is on the list of big energy consumer countries. Three main resources of energy in Canada are electricity, natural gas, and motor gasoline which all are main sources of producing GHG emissions. In other words, Canada contributes largely to GHG emissions. According to the Kyoto Protocol, Canada should reduce fossil-fuel based energy consumption in order to mitigate related environmental damages [4].

The industrial sector accounts for the largest share of energy use in Canada and is second in terms of GHG emissions [5]. Energy is used in five sectors of residential, commercial, industrial, transportation, and agriculture for a total of 8,541.6 petajoule of energy [1]. One petajoule (PJ), or 10^{15} Joules, is equivalent to the energy required by more than 9,000 households (excluding transportation requirements) over one year. The industrial sector has the largest share of energy, followed by transportation, residential, commercial/institutional, and agriculture. The total GHG emissions associated with the

energy use of the mentioned five sectors was approximately 463.9 million tonnes (Mt) in 2009 [5]. Figure 1.1 depicts Canada energy use by the sectors in 2009.

The GHG emissions related to the electricity generation systems are sometimes referred to as indirect emissions. Therefore, it is a common practice in analysis to allocate GHG emissions associated with electricity production to the sector that uses that electricity. This calculation is carried out by multiplying the amount of electricity used by a national average to the emission factor which indicates the average mix of fuels used to generate electricity in Canada [5]. Figure 1.2 shows the amount of GHG emissions by energy consuming sectors. As it is illustrated, energy consumed by the transportation sector is considerably more GHG-intensive than the other sectors.

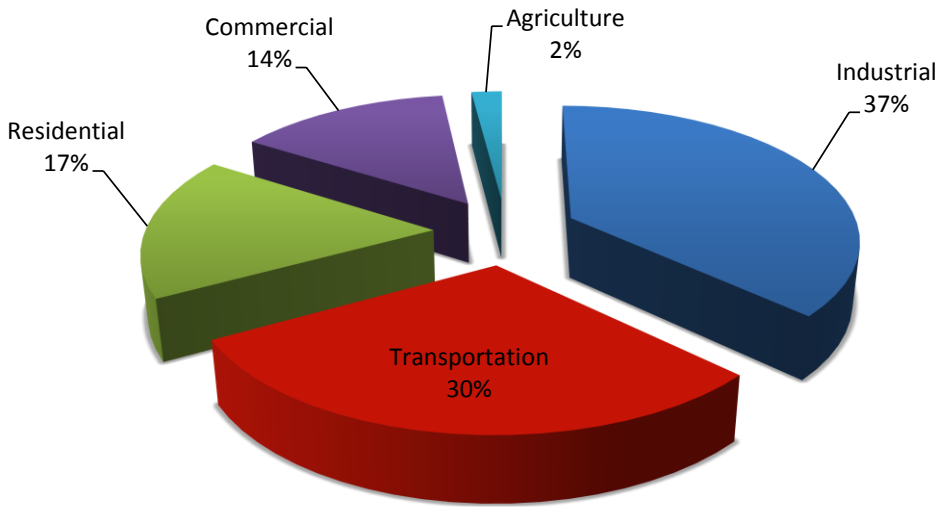

Figure 1.1 Canada energy use by the sectors.

It is rational to consider that a growth in energy use corresponds to the growth of GHG emissions. In 2009, Canada's GHG emissions excluding related emissions to electricity generation declined 1% compared to 2008, while emissions including those from electricity generation decreased 4% [5]. Decrease in the generated electricity from

coal contributes to 52% of the total reduction in electricity generated between 2008 and 2009 [5]. The CO_2 emissions mitigated from the reduction of coal-based electricity contributed 83.6% of the total CO_2 decrease. The total CO_2 emissions from different energy consuming sectors in Canada are depicted and compared in Figure 1.3 for 1990 and 2009 [5].

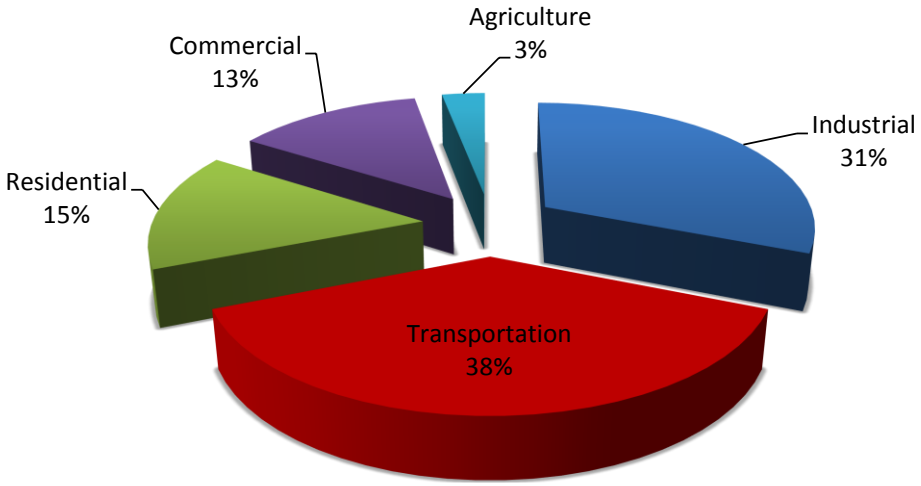

Figure 1.1 GHG emissions in Canada by energy consuming sectors.

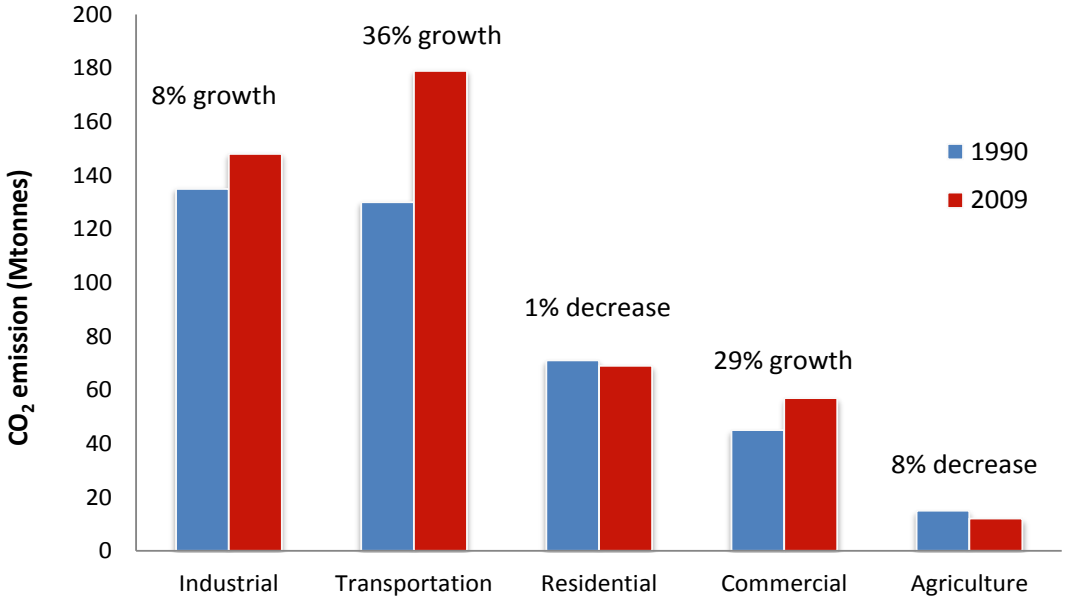

Figure 1.2 CO_2 emission growth in Canada by energy consuming sectors.

1.3 Hydrogen and energy industry

A growing shortage of conventional energy sources for heat, power, and fuels is driving the exploration and development of alternative fuels [1]. The concentration of conventional fossil fuel resources in specific regions of the world represents a threat to the reliability and security of global energy supply [2]. Furthermore, there is a need to decarbonize global energy systems to mitigate the risks associated with climate change and greenhouse gas emissions [4]. Comparing the growth rate of oil consumption and the rate of discovered oil reserves around the world predicts the end of oil supply tentatively about 2050 [3]. The same scenario for natural gas as an alternative suggests its complete consumption in 70 to 100 years.

Various alternative energy options such as solar, wind, hydropower, geothermal, and nuclear energy have been introduced to provide large and stable energy supply and to mitigate climate change by controlling the GHG emissions [6]. Nuclear energy has the potential to provide considerable share of world energy supply where utilization of the natural sources of energy are limited due to their quantity and stability. Since utilization of the nuclear energy is almost focused on direct power generation, there is a good opportunity to use nuclear thermal energy and waste heat from nuclear power plants for energy savings. Hydrogen production is one of the most attractive technologies can benefit from direct use of nuclear thermal energy.

Hydrogen is a promising clean energy carrier of the future, and a potentially best solution to climate change. It is widely used in numerous industry applications. Steam-methane reforming (SMR), gasification, and electrolysis are the most common existing technologies for hydrogen production [7]. Global demand for hydrogen production has a

value of $300 billion/year and is still increasing in a very rapid rate [8]. Hydrogen can be used as a fuel for power generation, as a transportation fuel, as an energy carrier, or for the production of other chemicals such as ammonia for fertilizers [9]. Hydrogen can also be used in refineries in various processes such as hydrocracking, desulfurization and upgrading of heavy oils such as bitumen in Alberta's oil sands. Methanol, alcohols, acetic acid, and Fischere-Tropsch liquids can be produced from synthesis gas as well. Hydrogen as a fuel has the advantage of zero CO_2 emission with a lower heating value (LHV) of about 120 MJ/kg [10]. This is very important for the transportation sector which contributes about 18% of world energy consumption [1].

Unfortunately, 98% of annual hydrogen production in the globe is coming from the reforming of fossil fuels which contributes to GHG emission [11]. The main technical and environmental challenges of current hydrogen production technologies have been investigated and analyzed [10]. Clean hydrogen production is a key challenge for energy industries and has been the point of interest for many researchers [12-15]. Hydrogen as a carrier of energy is expected to facilitate the integration of some renewable energy sources to the current energy systems. Canada, the US, Japan, and Germany are the leading countries increasing their investment to implement clean hydrogen production in their energy systems, targeting markets for power plants, cars, buses, ships, rockets and etc. [11].

In order to produce hydrogen, the hydrogen bonds in water or any kind of hydrocarbon must be broken which requires considerable amount of energy in the form of electricity and heat. Then, the produced hydrogen should be separated from the reactant. Hydrogen production from water electrolysis is a relatively costly process which provides

an overall efficiency of 18% to 24% [16]. Numerous thermochemical cycles have been proposed as alternatives with higher efficiency and lower cost of production which work at elevated temperatures up to 2000˚C [16-19]. Thermochemical cycles with a moderate operating temperature in the range of 400˚C to 600˚C have been extensively studied. These cycles have the advantage of being integrated with low-grade heat sources such as solar concentrators or industrial waste heat to produce hydrogen more efficiently at lower costs [20]. The utilization of heat which is used directly from nuclear or solar energy sources make the thermochemical cycles more attractive. The estimated cost of hydrogen production using integrated nuclear and thermochemical systems could be as low as 60% of the H_2 production by water electrolysis coupled with nuclear energy sources [21].

Investigation on development of the thermochemical hydrogen production cycles has been conducted since the 1970s and potentials for integration with nuclear and solar energy systems have been comprehensively analyzed [16, 22-24]. In thermochemical hydrogen production cycles in which H_2 and O_2 are produced separately, operating temperature reduces below 1000˚C [25]. This makes the process more efficient and cost effective than direct thermal splitting of water in typical electrolysis process. The Copper-Chlorine (Cu-Cl) cycle is one of the most attractive alternative thermochemical cycles for clean hydrogen production due to its lower temperature requirement and better overall efficiency [26]. In comparison to the other thermochemical cycles, it has the advantage of lower operating temperatures of about 500˚C to 530˚C, lower requirements on materials of construction, and a relatively low electrochemical cell voltage [27]. The low operating temperature allows integration of this cycle with Generation IV Super-Critical Water Reactor (SCWR) or high temperature solar energy systems. The efficiency of the Cu-Cl

cycle is about 43% when coupled to a thermal power plant, which is a substantial margin of improvement over water electrolysis [28]. There are different variations of the Cu-Cl cycle consisting of 3 to 5 main reactions which net reaction decomposes water into hydrogen and oxygen [29]. The Cu-Cl cycle can be also coupled with process or waste heat sources like Integrated Gasification Combined Cycle (IGCC) power plants to be even more efficient and competitive [7].

1.4 Motivation and objectives

1.4.1 Motivation

The Cu-Cl cycle is one of the promising emerging technologies which thermochemically decomposes water into hydrogen and oxygen using low temperature waste heat. The Cu-Cl cycle is a closed loop of thermally driven chemical reactions which consists of four main steps of hydrolysis, electrolysis, decomposition, and drying. In this cycle water is decomposed into H_2 and O_2, and all other intermediate compounds are recycled with no emission to environment. It was mentioned earlier that in comparison to the other thermochemical cycles, this has the advantage of lower operating temperatures, lower requirements on materials of construction, and a relatively low electrochemical cell voltage. However, there are many engineering challenges for the Cu-Cl cycle to become industrially adopted and used for hydrogen production. This makes the aim of University of Ontario Institute of Technology (UOIT), Atomic Energy of Canada Limited (AECL), and other partner institutions to be the development of the cycle through integrated experimental work, advanced modeling and simulation, thermochemistry, corrosion

resistant materials, safety, reliability and linkage between nuclear and solar energy systems and hydrogen plants.

Despite reported theoretical investigation and experimental analysis which successfully demonstrates advanced development for most of the processes of the Cu-Cl cycle, process integration of reactions and analysis of the interaction between processes as a closed cycle are neglected [30, 31]. So, the main focus of this thesis is to address and investigate three major challenges for the Cu-Cl cycle to enable industrial application of this technology for green hydrogen production. The three main objectives of this research proposal are detailed below.

1.4.1.1 Process integration of hydrolysis and electrolysis processes in the Cu-Cl cycle

The hydrolysis process and its integration with the electrolysis reaction impose significant challenges to achieve high efficiency in the Cu-Cl cycle. In order to achieve >95% yield of Cu_2OCl_2 production in the hydrolysis reaction, the amount of steam should be supplied to the process is considerably higher than its stoichiometric requirement [30, 32]. Moreover, concentration of the produced Hydrochloric acid (HCl) in the hydrolysis reaction is not enough or even close to the minimum HCl concentration required in the electrolysis reaction. This difference increases by increasing the steam to $CuCl_2$ ratio. Furthermore, the difference exists between operating temperature of the hydrolysis and electrolysis processes requires considerable quantity of heat flow condenses the high temperature products which then must be reheated for succeeding processes [33].

In this thesis, an integrated process model of the hydrolysis and electrolysis processes is simulated by introducing intermediate heat recovery steam generator

(HRSG) and HCl-H_2O separation process consists of rectification and absorption columns. Simulation of the proposed system is conducted using Aspen HYSYS process modelling software. In the separation system, the influence of operation factors on the heat duty requirements and also the composition of products are investigated and analysed. Operation factors include reflux ratio, mole fraction of HCl in the feed stream, solvent flow rate and temperature, and column configuration variables such as the location of the feed stage and number of stages. Moreover, the influence of adding extractive agent $CaCl_2$ to the distillation process, when the concentration of produced HCl in the hydrolysis reaction is below the azeotropic point, is investigated. As well, the effects on HCl-H_2O phase equilibrium and heat duty requirements are analysed. It is shown that the amount of steam generated in the HRSG unit satisfies the extra steam requirement of the hydrolysis reaction and the separation process effectively provides HCl acid at the concentration required for the electrolysis reaction.

1.4.1.2 Experimental development of the electrolysis process in the Cu-Cl cycle

One of the other main challenges associated with the Cu-Cl cycle is system integration of its unit operations. Although performance of the individual steps has been successfully analyzed, and some small lab-scale experiments of individual reactions have been developed and studied, there is still a need to link all sub-steps of the cycle and build a pilot plant to facilitate analysis of the cycle overall performance and its eventual commercialization. Research at UOIT shows the importance of system integration of the experimental units including integration of the electrolysis and hydrolysis processes [30]. In the Cu-Cl cycle, a key step is H_2 gas production in the electrolysis process when

dissolved CuCl in concentrated HCl solution, which comes from hydrolysis reaction, is oxidized to $CuCl_2$. The steam quantity required by the hydrolysis reaction is a key parameter that influences the produced HCl concentration and subsequent integration of the electrolysis and hydrolysis processes. Moreover, the concentration of Cu(II) chloride exiting the electrolytic cell is another important factor in the integration of the electrolysis process. These facts necessitate making an accurate model of the electrolysis operation which can provide reliable prediction of the electrolytic cell performance. Effective integration of the electrolysis and hydrolysis processes has a major role towards industrial adaptation of the Cu-Cl cycle. Although, many published work studied different aspects of the electrolysis process individually, a holistic approach to investigate the effects of operation factors on the cell performance from the integration viewpoint, is neglected.

In this thesis, an experimental investigation and modeling of the electrolysis process is also conducted to find a correlation between the cell voltage and the hydrogen production rate with the operating parameters. A lab-scale CuCl electrolysis process is designed, fabricated, and tested. The influence of operation factors including HCl and CuCl concentrations, applied current density, temperature, and solution flow rate on the cell potential and hydrogen production rate are experimentally investigated. A fractional factorial design is performed to make a model predict the cell voltage for different operating conditions. Analysis of variance (ANOVA) confirms the accuracy of the proposed model. Calculations are based on design of experiment methods, using Design-Expert software to find a correlation. The model permits the prediction and comparison of all main effects and interaction effects on the cell voltage to provide valuable insight into integration of the electrolysis process.

1.4.1.3 System integration analysis of a gasification process and the Cu-Cl cycle

The world energy demand is increasing at a very rapid rate where there is a crucial need for a significant reduction of greenhouse gas emissions. A limited supply of fossil fuel reserves for heat and power makes development of alternative fuels necessary. Future of the global energy supply is relying on the energy supply security, sustainable development and environmental protection, and utilization of energy sources in more efficient and cost effective ways.

Gasification process has drawn widespread attention in recent years because it addresses each of the above concerns. Gasifiers operate at high temperatures (>700°C) and can accept a wide variety of low-value feedstocks such as heavy oil, refinery residues or refuse-derived fuels [34]. One of the most important gasification products with a wide range of applications is hydrogen. However, the concentration of H_2 in produced synthesis gas (syngas) is variable and strongly depends on the operating condition of a gasification process. Another important parameter is the lower heating value (LHV) of the syngas which is directly related to its composition.

In order to offset the disadvantages of gasification-based energy systems such as lower heating value of syngas, complexity of operation, and to increase its efficiency and reduce its environmental impacts, oxygen can be utilized instead of air to improve the combustion efficiency, increase the hydrogen content of produced syngas, and reduce the CO_2 and NOx emissions [35]. This can be achieved by process integration of the gasification process and the Cu-Cl cycle of hydrogen production. Oxygen as a by-product in the Cu-Cl cycle can be considered as a key for integration of this cycle to the well-established gasification systems which brings more attention, creates market, and makes

it more competitive. The other benefit of the suggested integration is that the excess steam requirement of the hydrolysis reaction in the Cu-Cl cycle is supplied from the syngas cooling unit of the integrated gasification and combined cycle (IGCC) power plant. This could significantly increase the energy efficiency of the Cu-Cl cycle.

1.4.2 Objectives

The objectives of the present thesis are subdivided into three major areas. In the process integration of the hydrolysis and electrolysis processes,

- One of the most important engineering challenges associated with the Cu-Cl cycle of hydrogen production is addressed. This thesis investigates process integration of the hydrolysis and electrolysis processes which has been neglected in previous research.
- Integrated process model of HRSG and HCl-H_2O separation process, which consists of rectification and absorption columns, is designed and simulated. The effects of operating parameters on the system performance are analysed and discussed.
- It is demonstrated that the steam generated in the HRSG unit satisfies the extra steam requirement of the hydrolysis reaction which significantly improves the Cu-Cl cycle efficiency. It is also shown that the separation process effectively produces HCl acid at the concentration required for the electrolysis reaction.

A summary of the present approach is written below:

- Problem synthesis and investigation through the most feasible separation configuration.
- Identification of binary parameters for HCl-water liquid phase activity coefficient model.

- Modelling and simulation of the coupled distillation and absorption processes.
  - Identification of design (fixed) and operating (variable) parameters.
  - Sensitivity analysis of the separation system considering main operation factors.
  - Configuration analysis of the simulated processes.
  - Calculation of the required input heat for the separation process.
  - Estimation of a heat recovery potential by HRSG for the hydrolysis reaction.
  - Validation of the simulation results and parametric studies.
  - Search for optimal process parameter values.
- Process integration analysis with the hydrolysis and electrolysis processes.
- Making recommendations to implement the proposed integrated process design.

A summary of approach in the experimental development of the CuCl electrolysis process and factorial modeling of its operation is listed below,

- Selection of appropriate instruments for sampling and experimental design.
- Selection of suitable measuring instruments and control for data collection.
- Fabrication of the electrochemical cell and selection of measurements taken.
- Statistical modeling and analysis of the process operation.
- Identification of the effects of operation condition on the cell performance.
- Analysis of the electrolysis operation from the system integration perspective.

In the system integration analysis of a gasification process and the Cu-Cl cycle, the effects of using oxygen instead of air on the gasification process are investigated where it is supplied by the Cu-Cl cycle of hydrogen production as the by-product. A parametric sensitivity analysis is conducted and the influence of equivalence ratio (ER) on the gasification temperature, exergy efficiency, and composition of the produced

syngas are analyzed and discussed. The effects of moisture content of feedstock and steam to carbon ratio on the gasification temperature and LHV of produced syngas are also studied. The conceptual model of a gasification process based on Texaco IGCC power plant is simulated using Aspen HYSYS. Moreover, the effect of steam recovery in the hydrolysis reaction on the Cu-Cl cycle energy efficiency is examined.

1.5 Thesis Outline

This thesis is organized in seven chapters as described below:

Chapter 1 provides introductory information about energy industry and outlines the motivation and objectives of the present thesis.

Chapter 2 presents background information about the Cu-Cl cycle of hydrogen production and process integration of the hydrolysis and electrolysis reactions. The process integration technology and its tie for further development and commercialization of the Cu-Cl cycle are introduced. The concept of HCl-H_2O separation process as an azeotropic mixture is explained. Gasification process in an IGCC power generation system is introduced and the opportunity of its integration with the Cu-Cl cycle is described.

Chapter 3 provides a literature review on the hydrolysis reaction of the Cu-Cl cycle and its integration with the electrolysis process. Alternative separation technologies for HCl and water mixture are reviewed and pros and cons of each are analyzed. Efforts on the experimental development of the electrolysis process are reviewed and described. As well, literature survey on the gasification process and its application is included.

Chapter 4 illustrates the fabricated experimental setup and test bench instrumentation of the electrolysis process of the Cu-Cl cycle including description of measurement devises and techniques.

Chapter 5 describes the methodology to model and simulate the HCl-H_2O separation process, to model the electrolysis process of the Cu-Cl cycle based on experimental results, and to conduct exergy analysis of the gasification process when integrated to the Cu-Cl cycle.

Chapter 6 presents the results and discussion about conceptual modeling and simulation of the HCl-H_2O separation process, experimental development and statistical modeling of the electrolysis process, and system integration of the gasification process in an IGCC power plant with the Cu-Cl cycle.

Chapter 7 summarizes the conclusions and provides recommendations for future research.

Chapter 2: Background

2.1 Thermochemical Cu-Cl cycle

The Copper-Chlorine cycle (Cu-Cl) cycle is a sequence of processes for hydrogen production by thermochemical water splitting. This cycle has been identified by Atomic Energy of Canada Limited (AECL) [36, 37] at its Chalk River Laboratories (CRL) as a highly promising cycle for thermochemical hydrogen production. The Cu-Cl cycle involves four main chemical reactions for water splitting, whose net reaction decomposes water into hydrogen and oxygen. All other chemicals are recycled. The Cu-Cl cycle can be linked with nuclear plants and/or other heat sources such as solar and industrial process/waste heat (i.e. incinerators, chemical plants or waste energy from furnaces) to potentially achieve higher efficiencies, lower environmental impact and lower costs of hydrogen production than other conventional technologies [38].

The Cu-Cl thermochemical cycle uses a series of reactions to achieve the overall splitting of water into hydrogen and oxygen. There are three variations of the Cu-Cl cycle: 5-step, 4-step, and 3-step cycles [36]. In the 5-step cycle, copper is first produced and then moved to an exothermic hydrogen reactor to react with HCl gas and produce hydrogen. The 4-step cycle combines the hydrogen and electrochemical reactions together to eliminate the intermediate production and handling of copper solids. AECL has successfully demonstrated this combined process through a CuCl-HCl electrolyser which produces hydrogen and aqueous $CuCl_2$ [31]. The 3-step cycle further combines the cycle steps by supplying aqueous $CuCl_2$ directly into the hydrolysis chamber. In this thesis, the main focus is the 4-step cycle since separation of hydrolysis and drying

processes provides the advantages of higher thermal efficiency and more viable practical adaptation. Table 2.1 shows the reactions involved in the 4-step Cu-Cl cycle.

Advantages of the Cu-Cl cycle over other thermochemical cycles include lower operating temperatures, ability to utilize low-grade waste heat to improve energy efficiency, and potentially lower cost materials of construction. In comparison to other thermochemical cycles, the Cu-Cl process requires lower maximum temperatures of about 500°C to 530°C [27]. Another significant merit of this cycle is a relatively lower electrochemical cell voltage in the electrolysis reaction comparing to typical water electrolysis [39]. The overall efficiency of the Cu-Cl cycle is estimated to be just over 43% [40], excluding the additional potential gains of utilizing waste heat in the cycle. Figure 2.1 presents a schematic diagram of the Cu-Cl cycle.

Table 2.1 Reactions in the 4-step Cu-Cl cycle.

Step, (Temp. range (°C))	Reaction	Feed - Output*
1- Electrolysis, (<80)	$2CuCl(aq) + 2HCl(aq) \rightarrow H_2(g) + 2CuCl_2(aq)$	Aqueous CuCl and HCl +V+Q
		H_2 +$CuCl_2$(aq)
2- Drying, (<70)	$CuCl_2(aq) \rightarrow CuCl_2(s)$	Slurry containing HCl and $CuCl_2$ +Q
		Granular $CuCl_2$ +H_2O/HCl vapours
3- Hydrolysis, (400)	$2CuCl_2(s) + H_2O(g) \rightarrow Cu_2OCl_2(s) + 2HCl(g)$	Powder/granular $CuCl_2$ + H_2O(g) +Q
		Powder/granular Cu_2OCl_2 + 2HCl(g)
4- Decomposition, (500)	$Cu_2OCl_2(s) \rightarrow 2CuCl(l) + 1/2O_2(g)$	Powder/granular Cu_2OCl_2(s) +Q
		Molten CuCl salt +Oxygen
*Q = Thermal energy, V = Electrical energy		

In the Cu-Cl cycle, a key step is H_2 gas production in the electrolysis process when dissolved CuCl in concentrated HCl solution is oxidized to $CuCl_2$. The CuCl-HCl electrolyser uses a proton-conducting membrane in which oxidation of CuCl occurs

during an electrochemical reaction in the presence of hydrochloric acid to generate hydrogen.

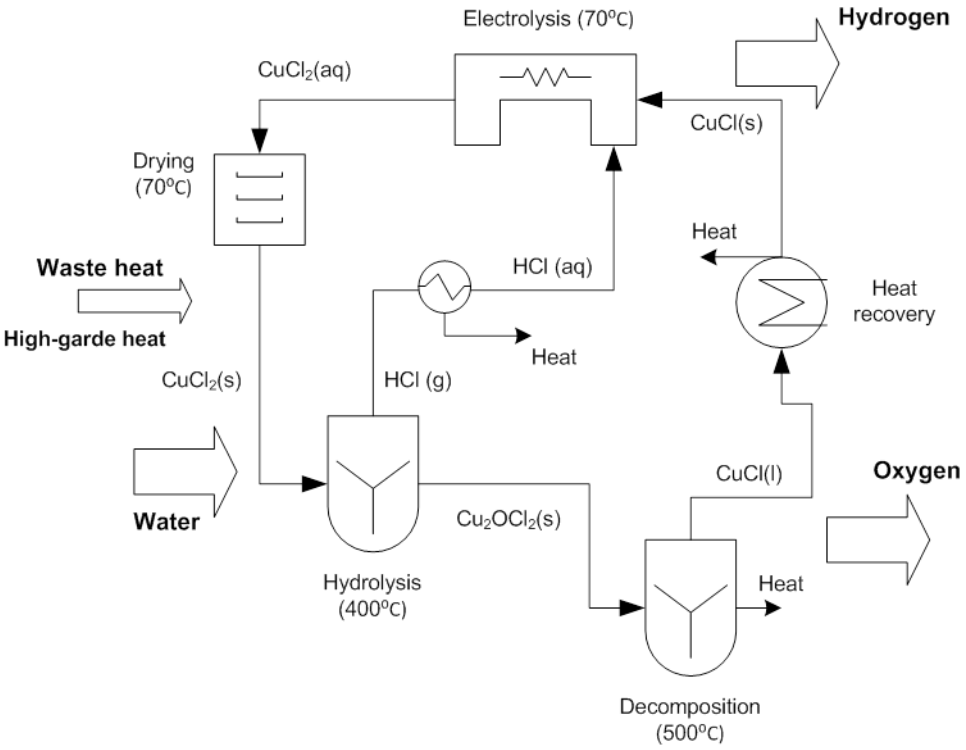

Figure 2.1 Schematic diagram of the Cu-Cl cycle.

In the electrolysis reaction, the Cu^{+} ions are oxidized to Cu^{++} in the anode side of an electrochemical cell, and the hydrogen ions are reduced in the cathode side. The overall reaction can be expressed as follows [41]:

$$2CuCl + 2HCl \rightarrow 2CuCl_2 + H_2 \tag{2.1}$$

In the anode side, several Cu^{+} and Cu^{++} chloride species can form with the following reactions, where relative ratios of each species are dependent on the concentration of chloride ions [42]:

$$Cu^{+}(aq) + nCl^{-} \leftrightarrow CuCl_n^{1-n} \tag{2.2}$$

$$Cu^{2+}(aq) + nCl^{-} \leftrightarrow CuCl_n^{2-n} \tag{2.3}$$

The net reactions in the anode and cathode side can be presented as follows. The anode reaction proceeds readily on graphite electrodes and doesn't require any metal catalyst. However, hydrogen production in the cathode reaction requires a catalyst which is a fuel cell graphite separator plate coated with a Pt electrocatalyst [27]:

$$CuCl(aq) + HCl \rightarrow CuCl_2(aq) + H^{+} + e^{-} \tag{2.4}$$

$$H^{+}(aq) + e^{-} \rightarrow \frac{1}{2} H_2(g) \tag{2.5}$$

A schematic of the electrolysis cell is depicted in Figure 2.2. The efficiency in the electrolysis process is defined as the multiplication of voltage efficiency and hydrogen production ratio, where the voltage efficiency is the decomposition potential divided by the applied potential. The H_2 production ratio is defined as the experimental H_2 production divided by the theoretical H_2 production. For the electrolysis reaction to proceed, energy must be added to the system.

The hydrolysis process and its integration with the electrolysis reaction impose significant challenges to achieve higher cycle efficiencies. These include firstly, the excess steam requirement of the hydrolysis reaction above the stoichiometric amount to obtain >95% yield of Cu_2OCl_2. Secondly, the concentration of the produced HCl in the hydrolysis reaction is not enough or even close to the minimum HCl concentration required in the electrolysis reaction and getting worse by increasing the steam to $CuCl_2$ ratio, and lastly the difference exists between operating temperature of the hydrolysis and

electrolysis processes which requires considerable quantity of heat flow condense the high temperature products which then must be reheated for succeeding processes [30, 32]. It means providing excess steam to the hydrolysis reaction requires an intermediate HCl separator for the integration to the electrolysis process [33] which could also provide HCl solution to the electrolysis process at the required concentration. In other word, the overall thermal efficiency of the Cu-Cl cycle is very sensitive to the percentage of heat recovered from the steam utilized in the hydrolysis reaction and hence is very sensitive to the separated percentage of excess steam from HCl. Therefore, in the Cu-Cl cycle, HCl must be separated from steam and recovered in appropriate concentration for the electrolysis reaction. At the same time the steam could be recovered for the hydrolysis reaction. So, effective process integration approach for the hydrolysis and electrolysis processes of the Cu-Cl cycle could significantly improve the cycle performance and efficiency.

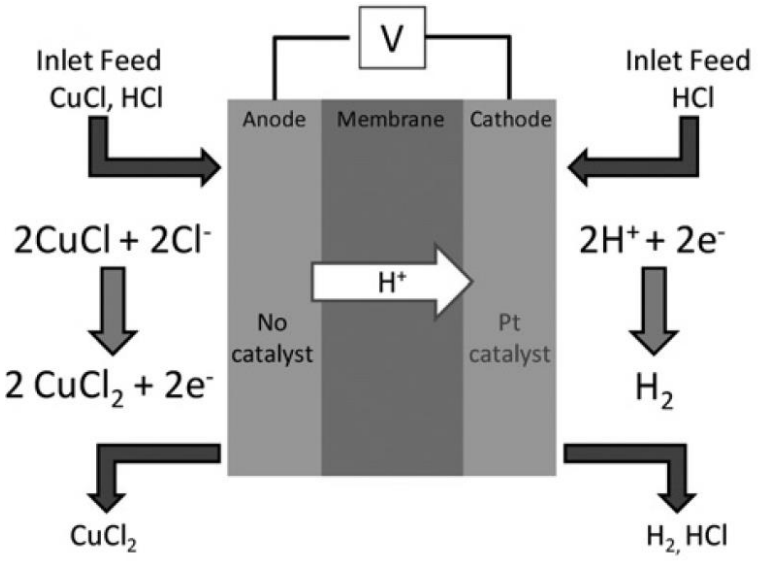

Figure 2.2 Schematic diagram of CuCl-HCl electrolyser [43].

2.2 Process integration technology

The past decade has seen significant industrial and academic efforts devoted to the development of process design methodologies. These efforts improve energy conservation and waste reduction for a large variety of chemical and energy industries such as refineries, power plants, pulp and paper, pharmaceutical, food products, and plastics producing industries. In response to the environmental and energy problems associated with industrial facilities, the process industry has recently dedicated more attention and resources to mitigating its detrimental impact on the environment, conserving resources, and reducing energy consumption. These efforts have gradually shifted from a unit-based approach to a systems-level paradigm. This means that the various process objectives, from technical and economic to environmental and safety, must be integrated and reconciled. These challenges call for the application of a systematic approach that targets the specific circumstances of the process and views the environmental, energy, and resource conservation problems from a holistic perspective.

Process Integration (PI) is an integrated methodology to design a series of consecutive systems which emphasizes the unity of the process [44]. Process integration design has been developed to achieve process improvement, productivity enhancement, conservation of mass and energy resources, and reductions in the operating costs of energy and process industries. Its primary applications are focused on resource conservation, pollution prevention and energy management. The initial efforts in the field of process integration were focused on the energy dimension of a chemical process. The primary efforts occurred during the late 1970s and 1980s and resulted in the development

of several novel design methodologies. These include pinch analysis and heat exchange networks (HENs) design which collectively involves heat integration analysis [45-48].

The field of process integration has been expanded to address the mass dimension of a chemical process. This has resulted in the development of new design methodology, which requires accurate process simulation to analyze the effects of operating variables on the integrated system performance. The combination of energy and mass analysis efforts are called mass integration methodology [49]. Mass integration is a systematic approach that requires process simulation to analyze the flow of mass and energy within and beyond each process and employs this understanding to identify optimum system performance [50].

Process integration analysis which is developed to simultaneously address both the mass and energy aspects of the process has been successfully applied in many industrial systems such as various separation processes [51-54]. The development of this integrated methodology has been advanced to address waste reduction complex by the announcement of more stringent environmental regulations coupled with the desire to improve industrial competitiveness. Process integration combined with process simulation, is a powerful approach that allows engineers to systematically analyze an industrial process and the interactions between its various parts. It may be applied to address the following industrial issues:

- Energy saving, and GHGs emission reduction
- Identification of the critical areas in a given process
- Optimization of separation processes and their sequence
- Optimization of hydrogen production network

- Minimization of water/steam usage and wastewater production
- Multi-generation system design and waste minimization

2.3 Azeotropic mixture separation

The system of HCl and water mixture displays a maximum azeotrope at a boiling temperature of 108.6°C, for a system pressure of 1 bar and HCl concentration of 20.2wt%**,** about 11.1mol% [48]. If the acid concentration is lower than the azeotrope mixture, the acid can be concentrated only up to the azeotropic point. Further concentration needs special and complex procedures. Separation of azeotropic mixtures is a topic of significant practical and industrial interest. Some mixtures have non-ideal behavior, so the separation will only be possible with significant complexity, which is not possible through regular distillation process.

Although many alternatives to distillation process have been developed such as membrane and adsorption processes, distillation is one of the main unit operations in thermal separation especially for the separation of non-ideal liquid mixtures [55]. In most cases, azeotropic mixtures require special methods to facilitate their separation. All liquid mixtures have forces of intermolecular attraction. The molecular interactions when two or more components are mixed may cause the mixture to form certain inseparable components where the vapor and liquid compositions at the equilibrium state are equal for a given pressure and temperature range. These specific mixture compositions are called azeotropes. Azeotropy significantly influences the vapor-liquid equilibrium in separation processes such as distillation. In order to develop separation methods for azeotropic mixtures, there is a need for better insight into the fundamental phenomena of

azeotropic phase equilibria, different azeotropic separation technologies and their energy consumption, and a search for a separating agent.

2.3.1 General background – distillation of azeotropic mixtures

Separation of homogeneous liquid mixtures requires addition of another phase within the system. The most common method is repeated vaporization and condensation with a distillation process where the vapor phase becomes gradually enriched in the more volatile component(s) compared to the liquid. Alternatives to distillation are adsorption, membrane separation, crystallization, liquid-liquid extraction, chromatography, and others [56]. Separation of a liquid mixture by distillation is dependent on the fact that when a liquid is partially vaporized, the vapor and liquid compositions are different. The vapor phase becomes enriched in the more volatile components and it is depleted in the less volatile ones with respect to its equilibrium liquid phase. By dissociation of the phases and repeating the partial vaporization, it is often possible to achieve the desired degree of separation.

An azeotrope cannot be separated by ordinary distillation since no enrichment of the vapor phase occurs at this point. Therefore, in most cases, azeotropic mixtures require special methods to facilitate their separation. Such methods utilize a mass separating agent to enhance mass transfer selectivity of the azeotrope-forming elements. This agent might be a membrane material for pervaporation or an entrainer for Extractive Distillation (ED). The Pressure-Swing Distillation (PSD) is an alternative process that uses the dependency of azeotropic composition on the system pressure [57].

The degree of enrichment, or the ease of separation, is measured with the relative volatility between a pair of components which changes with temperature, pressure and composition. The relative volatility for a two-component mixture is expressed as follows:

$$\alpha_{ij} = \frac{\frac{y_i}{x_i}}{\frac{y_j}{x_j}} = \frac{\gamma_i P_i^{sat}}{\gamma_j P_j^{sat}} \tag{2.6}$$

where α_{ij} is the relative volatility and *y* and *x* are the vapor and liquid compositions of component *i and j*, respectively. *P* and *T* are the system pressure and temperature, γ is the activity coefficient of component *i and j* in the liquid phase, and P^{sat} is the saturated vapor pressure [58]. The activity coefficient is a measure of the non-ideality of a mixture and changes both with temperature and composition. The vapor-liquid phase equilibrium for a two-component mixture is expressed as

$$y_i P = x_i \gamma_i(T, x) P_i^{sat}(T) \tag{2.7}$$

Here, the mixture with an activity coefficient of unity, which is called ideal mixture, follows Raoult's law: non-ideal mixtures exhibit positive (>1) or negative (<1) deviations from Raoult's law. If these deviations become so large that the vapor pressure exhibits a maximum or minimum point at constant temperature, or, equivalently, a maximum or minimum point in the boiling temperature at constant pressure, the mixture is azeotropic [58]. At azeotropic points, the liquid phase and its equilibrium vapor phase have the same composition (x = y) and the condensation and boiling temperature curves are tangential with zero slope. Figure 2.3 depicts deviations from Raoult's law for non-ideal mixtures

where the total vapor pressure of mixtures is a function of composition at a chosen constant temperature. If the positive deviations are sufficiently large typically more than 4, phase splitting occurs to form a heteroazeotrope where the vapor phase is in equilibrium with two liquid phases [59].

The relative volatility of most mixtures, as defined in equation (2.6), changes with temperature, pressure and composition. The more α_{ij} deviates from unity, the easier it is to separate component *i* from component *j*. At an azeotropic point, the relative volatility of the azeotrope-forming components equals one (α_{ij} = 1) and further enrichment of the vapor is impossible. In such a way, azeotropes cannot be separated into pure components by ordinary distillation. Similarly, any mixture where the relative volatilities are close to unity is difficult to separate by distillation since little enrichment occurs with each partial vaporization step. Typically, conventional distillation becomes uneconomical when 0.95< α_{ij} <1.05, but there are some exceptions, since a high reflux ratio and a large number of theoretical equilibrium stages are required [60]. Special methods to facilitate the separation of azeotropic mixtures may also be applied to close-boiling zeotropic mixtures.

2.3.2 Vapor-liquid phase equilibrium

For two particular volatile components at a certain pressure such as atmospheric pressure, a boiling point diagram shows what vapor compositions are in equilibrium with given liquid compositions depending on temperature. In a typical binary boiling point diagram, temperature is plotted on a vertical axis and mixture composition on a horizontal axis. For

azeotropic mixtures, the boiling point temperature of an azeotrope is either less than the boiling point temperatures of any of its constituents, which is called a positive azeotrope, or greater than the boiling point temperatures of any of its constituents which is called a negative azeotrope [59].

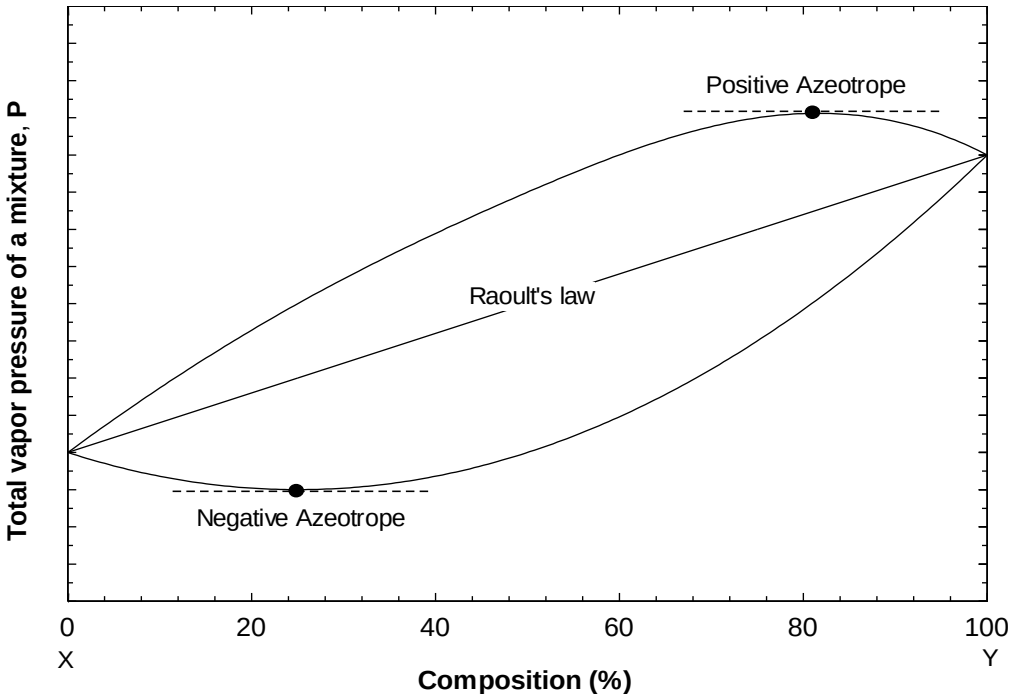

Figure 2.3 Positive and negative deviation from Raoult's law (modified from [61]).

In general, a positive azeotrope boils at a lower temperature than any other ratio of its constituents. Positive azeotropes are also called minimum boiling mixtures or pressure maximum azeotropes. A well-known example of a positive azeotrope is 95.63wt% ethanol and 4.37wt% water [58]. Ethanol boils at 78.4°C, water boils at 100°C, but the azeotrope boils at 78.2°C, which is lower than either of its constituents [58]. Indeed 78.2°C is the minimum temperature at which any ethanol/water solution can boil at atmospheric pressure. Figure 2.4 illustrates a positive azeotrope of hypothetical constituents, X and Y.

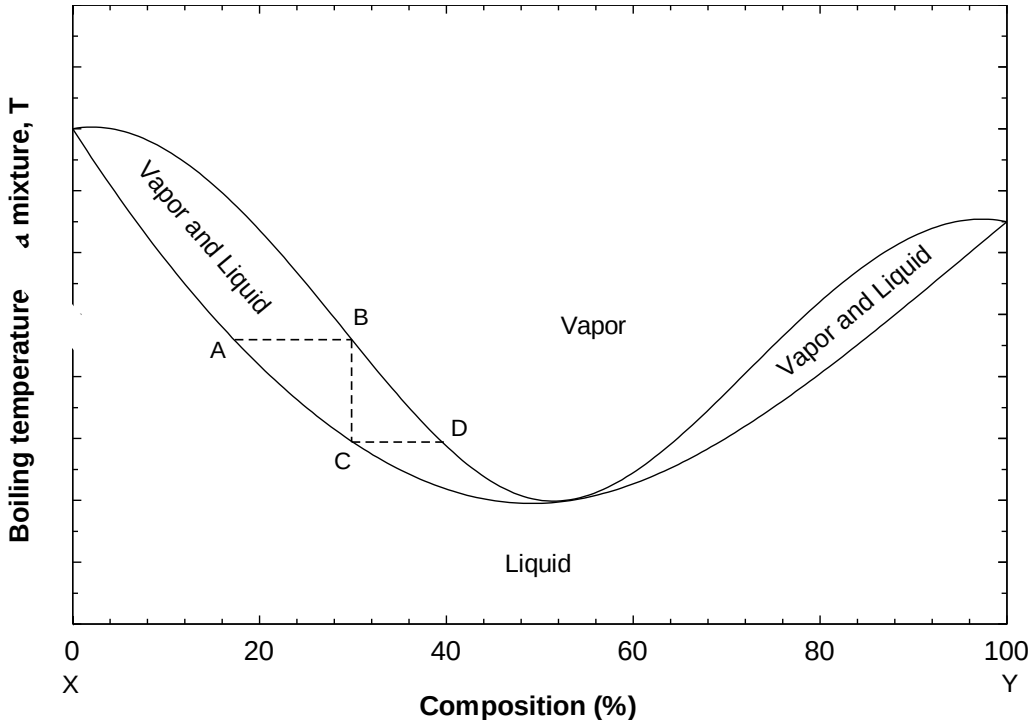

Figure 2.4 Phase diagram of a positive azeotrope (modified from [61]).

As depicted in the above diagram, the horizontal line illustrates the boiling temperature of various compositions. The vapor and liquid phase are in equilibrium between the upper and lower curves respectively which liquid and vapor phases exist simultaneously in equilibrium. For example, heating a 25wt% X – 75w% Y mixture to the temperature AB would generate vapor of composition B over liquid of composition A. The azeotrope is the point on the diagram where the two curves touch each other. The horizontal and vertical steps show the path of repeated distillations. Point A is the boiling point of a non-azeotropic mixture. The vapor which separates at that temperature has composition B. The shape of the curves requires that the vapor at point B is richer in constituent X than the liquid at point A [62]. The vapor is then physically separated on the vapor-liquid equilibrium (VLE) system and it is cooled to the point C, where it condenses. The resulting liquid is now richer in X than at point A. The step by step

progression shows how consecutive distillation can never produce a distillate that is more concentrated in component X than the azeotropic point.

A negative azeotrope boils at a higher temperature than any other ratio of its components. Negative azeotropes are also called maximum boiling mixtures or pressure minimum azeotropes. An example of a negative azeotrope is hydrochloric acid at a concentration of 20.2%wt and 79.8%wt water. HCl boils at −84°C and water at 100°C, but the azeotrope boils at 110°C, which is higher than either of its constituents. The maximum temperature at which any hydrochloric acid solution can boil is 110°C. Figure 2.5 depicts a negative azeotrope of hypothetical constituents, X and Y.

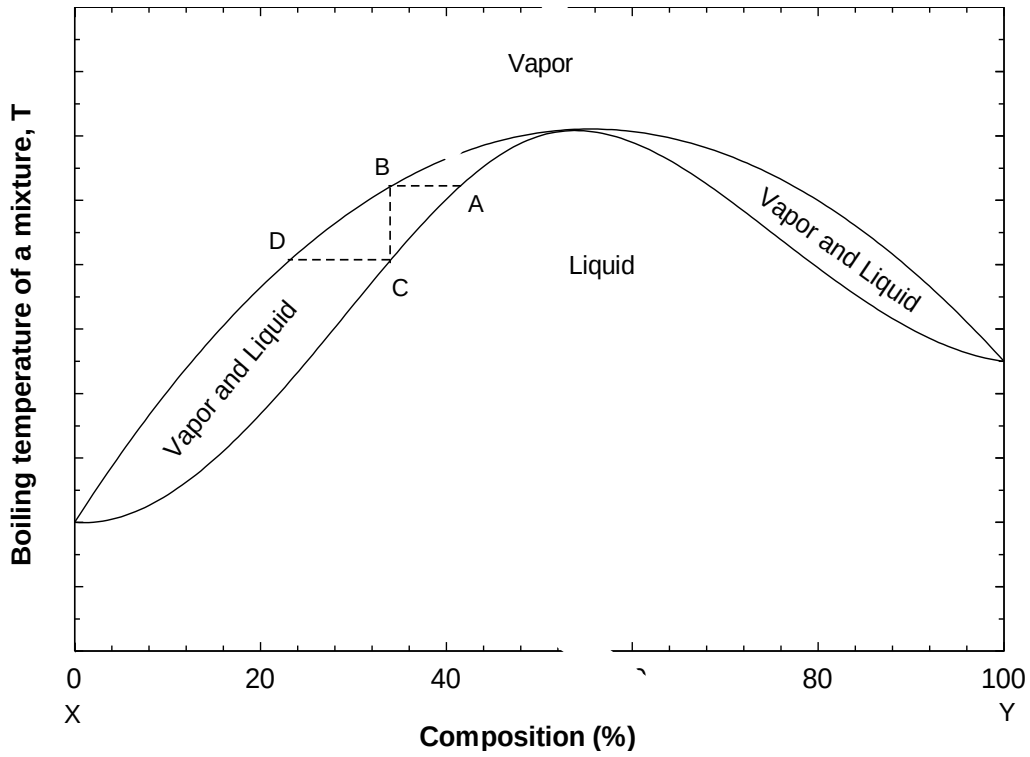

Figure 2.5 Phase diagram of a negative azeotrope (modified from [61]).

In the above diagram, point A has a boiling point with a composition chosen very near to the azeotrope. The vapor is in the same temperature at point B. That vapor is

cooled, condensed, and collected at point C. Because of negative azeotrope behavior, the distillate is in more distance from the azeotropic point than the original liquid mixture. Consequently, the distillate is less concentrated in component X and richer in component Y in comparison to the original mixture.

2.3.3 Azeotropic mixture separation processes

There are various methods for separating liquid mixtures that form one or more homoazeotropes. Distillation methods are the well-established and most performed systems in industry. Distillation process either by pressure variation or the addition of an agent, called an entrainer, alters the phase equilibria of a mixture and makes the separation possible. Other alternative separation techniques for azeotropic mixtures, such as membrane separation, are usually combined with distillation to be more efficient and cost effective [60]. Integration of a distillation process with complementary separation technologies are commonly called hybrid distillation systems. Enhanced distillation is another common term used for distillation systems that utilize mass separating agents, entrainer, other than energy. This term means the use of entrainers or other separating techniques to complement distillation. It does not necessarily involve azeotropes [63]. Study in this thesis is limited to the separation of homoazeotropic mixtures, like HCl and water and is focused on pressure-swing distillation and extractive rectification.

2.3.3.1 Pressure-swing distillation

Pressure changes can have a large effect on the vapor-liquid equilibrium compositions of azeotropic mixtures and provides opportunity to separate a mixture by ordinary

distillation. Increase or decrease in the operating pressure of an individual distillation column moves distillation boundaries of a mixture composition and could even make azeotropes appear or disappear [64]. For an azeotropic mixture, a simple alteration in pressure can result in a significant change in the azeotrope composition and enable a complete separation by pressure-swing distillation. Separation schematic of a maximum boiling point azeotropic mixture by pressure-swing distillation is illustrated in Figure 2.6. A binary homoazeotropic mixture is introduced as feed to the low-pressure column. The top product of the first column with the pressure of P_1 is relatively pure A, whereas the bottom product is still an azeotrope of A and B. This azeotrope is then fed to the high-pressure column, which produces relatively pure B in the top of the column. The final azeotropic mixture could be recycled back into the low-pressure column. For a small change in azeotropic composition with pressure, there is a large amount of azeotrope is recycled.

In principle, the pressure swing distillation can be operated in three different modes: of continuous, discontinuous, and semi-continuous process [65, 66]. In the continuous process, feed streams with different concentrations are put into the suitable column, depending on the concentration under or above the azeotropic point. For concentrations under the azeotropic point, the feed is put into the low pressure column. For concentrations above the azeotropic point, the feed is put into the high pressure column. In both columns pure product is withdrawn from the overhead process line. At the bottom of the columns there are azeotropic mixtures with concentrations depending on the pressure in the column. Each of them is recycled into the other column, so there is a mass integration between the columns. The pressure-swing distillation is a very energy

intensive process and has a high degree of complexity in operation [65]. However, Because of the pressure difference, both columns can be energetically coupled. The high pressure vapor stream at the top of the high pressure column is used to heat up the low pressure column at the bottom. It means that the pressure difference between two columns is high enough to have a significant temperature difference between the condenser of the high pressure column and the reboiler of the low pressure column. The main advantage of this integration is an energy savings of up to 40% [67]. The separation of ethanol and water in a thermally coupled column system is an example of such integration [68]. It can be concluded that the pressure-swing distillation is not an efficient and economically viable separation method without heat integration which itself brings more complexity to the system [69-71].

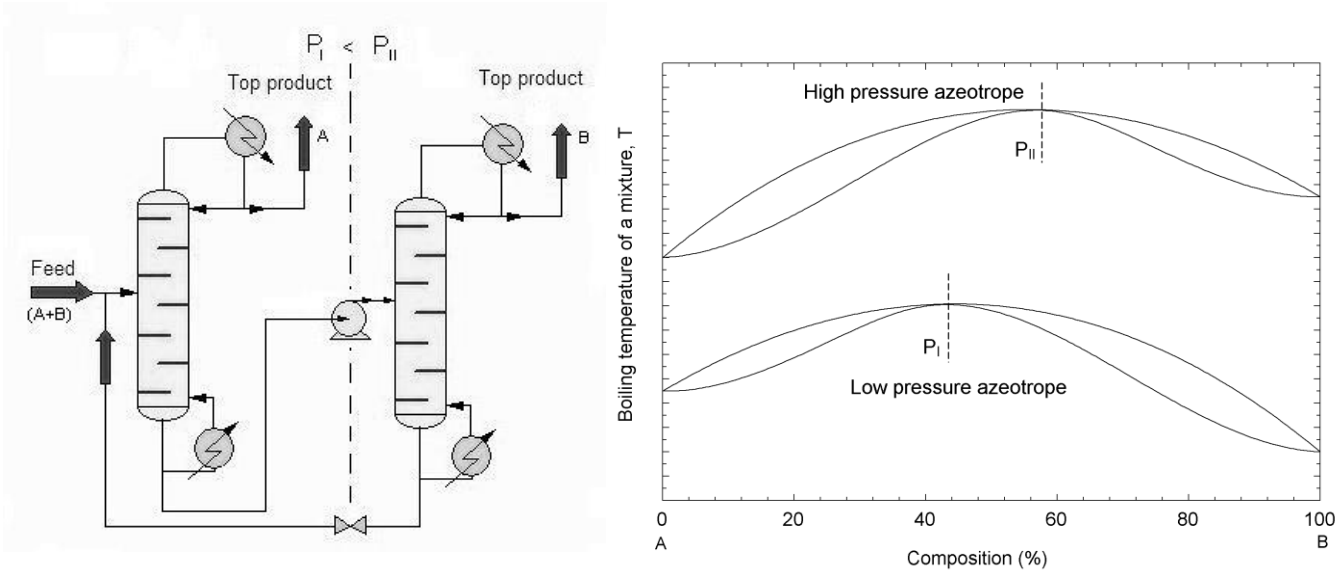

(a) (b)

Figure 2.6 (a) Schematic diagram and (b) phase equilibrium of a pressure-swing distillation system.

2.3.3.2 Extractive distillation

Change in the VLE behavior of an azeotropic mixture by addition of an external component to a distillation process offers effective separation results. The mixture to be separated is named as the original mixture and the added component that facilitates the separation is the entrainer. The basic principle is that the extractive entrainer interacts differently with the components of the original mixture and thereby alters their relative volatility. These interactions occur mainly in the liquid phase. An entrainer is basically introduced above the original mixture feed point in a distillation column to ensure that the entrainer remains at a sufficient concentration in the liquid phase in the column stage below [72]. A common restriction on extractive distillation is that the entrainer should not introduce new azeotropes in the system [73]. However, if he entrainer forms new azeotropes with one of the original mixture components, it should be selective to the other constituent. In that case, the separation process is named hetero-extractive distillation where the entrainer forms a heteroazeotrope in a distillation. The main disadvantage of the hetroazeotropic distillation against the extractive distillation is a higher energy demand of separation process since the entrainer is vaporized, and is not preferable [60].

For better explanation, the simplest example of extractive distillation occurs when the original mixture is a binary maximum-boiling homoazeotrope, like HCl and water mixture, and the entrainer is miscible and zeotropic. The main conditions that a candidate extractive entrainer, or solvent, must satisfy in order to make the separation feasible are given below:

- The entrainer has a boiling-point that is substantially higher than the original mixture components and it is selective to one of the components. It means the entrainer must cause a substantial change in the relative volatility of the azeotrope forming components.
- The main part of entrainer is removed as a bottom product of the distillation process.
- Entrainer is fully recovered in the solvent recovery column and recycled back to the extractive distillation process.

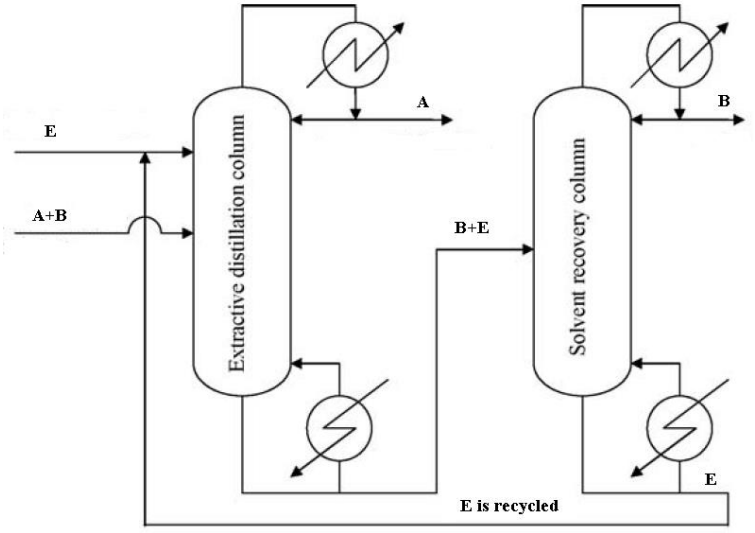

Figure 2.7 Schematic diagram of an extractive distillation process.

An illustration of extractive distillation is shown above in Figure 2.7. As it was mentioned earlier, the entrainer must have a higher boiling-point than the original mixture components. The relative volatility between the entrainer (E), or solvent, and the component that is recovered as a distillate (A) in the first column should preferably be large. The higher the boiling-point difference between the entrainer and the distillate component, the less reflux flow and fewer stages are required in the distillation column.

Moreover, the greater entrainer flow rate generally yields better separation, but increases the energy demand in both columns and also increases the reboiler temperature in the extractive column [74]. High reflux flow is harmful in extractive distillation because it weakens the effects of extractive agent since it decreases the entrainer concentration on the top of the distillation column.

2.4 Gasification and IGCC power plant

One of the most important advantages of the Cu-Cl cycle over other thermochemical water splitting systems is a lower operating temperature and ability to utilize low-grade heat to improve energy efficiency. Moreover, oxygen as a by-product in the Cu-Cl cycle could be used in other chemical processes and is an opportunity for process integration purposes. Oxygen could be used instead of air in a gasification process to improve its combustion efficiency and increase the hydrogen content of produced synthesis gas. Also, the external heat required in the Cu-Cl cycle could be supplied by a gasification process. This would significantly increase the energy efficiency of the Cu-Cl cycle. So, it is a point of interest to analyze process integration of the Cu-Cl cycle with a gasification process. Gasification is the thermochemical conversion of either a solid (coal, coke, biomass, solid waste) or liquid (oil, tar, pitch) fuel into a synthesis gas (or syngas) composed primarily of H_2 and carbon monoxide (CO) [75]. Unlike combustion processes that only produce carbon dioxide (CO_2) and water, gasification is a partial oxidation process that occurs in an oxygen-limited environment. The resulting syngas is more useful than combustion flue gas and it has the potential to generate electricity more efficiently. During the last century, gasification has been used to convert coal into fuel

gas for domestic heating and lighting. More recently, gasification has been used in the petrochemical industry for the production of chemical products [76].

The chemistry of gasification is complex since there are several processes occurring simultaneously. The initial stages of gasification are partial oxidation and pyrolysis, which occurs in the absence of oxygen. Partial oxidation occurs when a carbonaceous fuel reacts with less than the stoichiometric amount of oxygen. Once all of the oxygen is consumed, the high operating temperature of the gasifier devolatilizes the volatile components of the feedstock. These processes result in a two-phase system consisting of a gas phase and a carbon-based solid phase known as char. The main components of syngas, CO and H_2, are then produced by steam reforming of the carbon-based char. If the temperature of the gasifier is high enough, all the char can be converted to CO and H_2 and the 'water-gas' reaction goes to completion. The most desired product of a gasification process is usually hydrogen. In the final stage of gasification, steam reforming of CO produces H_2 according to the 'water-gas shift' reaction. Unlike partial oxidation and steam reforming, the water-gas shift does not convert all reactants into products. The extent of reaction is determined by its equilibrium point, which is a function of temperature and steam concentration. The partial oxidation, water-gas, and water-gas shift reactions are shown in the following equations respectively:

$$C + O_2 \rightarrow CO_2 \tag{2.8}$$

$$C + H_2O \rightarrow CO + H_2 \tag{2.9}$$

$$CO + H_2O \longleftrightarrow CO_2 + H_2 \tag{2.10}$$

$$C + 2H_2 \longleftrightarrow CH_4 \tag{2.11}$$

The one-sided arrows in equations (2.8) and (2.9) indicate that the reactions are irreversible in the forward direction. The double-sided arrow for equation (2.10) indicates that the reaction can proceed in either the forward or reverse direction. Equilibrium is reached when the rate of change of the forward and reverse reactions are equivalent.

Modern gasification technologies can be integrated with power generation cycles, acting as a link between coal or heavy fuel oils and gas turbines and its subsequent steam cycle. Schematic diagram of an Integrated Gasification Combined Cycle (IGCC) power plant is illustrated in Figure 2.8. Syngas from gasification can be cleaned to very low levels of contaminants, such as sulfur compounds and particulates [77]. After cleaning, syngas can be utilized in gas-steam turbine combined cycle power plants to generate electricity more efficiently than traditional combustion-based systems [78]. The resulting process configuration of IGCC is the only for power generation purposes, including burning coal or high sulfur residues, that can approach the technical and environmental performance of natural gas-fired systems.

The environmental impact of IGCC systems can be minimized even further when coupled with carbon capture and storage techniques. Oxygen-fired gasification systems can be designed to produce a material stream composed almost entirely of CO_2, which can be captured and sequestered [79]. Inputs to a typical gasification reactor include feedstock, steam, and air. The resulting syngas is cooled and cleaned of impurities before combustion in a gas turbine. The resulting hot exhaust gases from gas turbine are then used in a heat recovery steam generator (HRSG) to boil high-pressure steam for expansion in a steam turbine. The low-pressure exhaust from the steam turbine is then recycled back into the HRSG and reused.

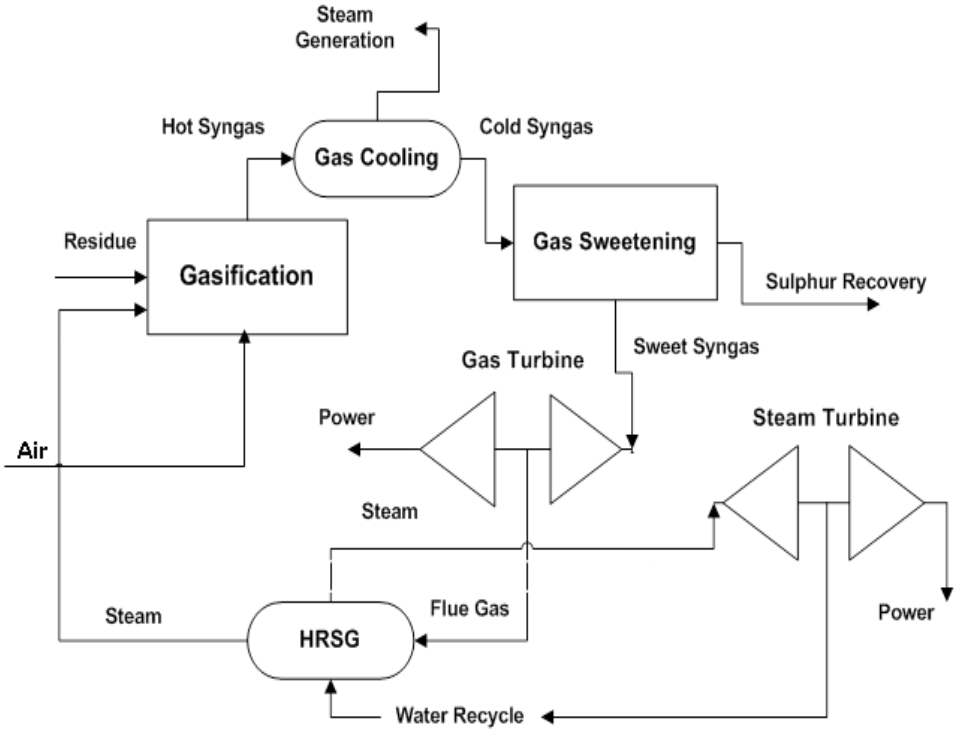

Figure 2.8 Schematic diagram of an IGCC power plant.

IGCC is one of the most promising technologies for the production of electricity, steam and hydrogen. Gasifiers operate at high temperatures of >700°C and can accept a wide variety of low-grade feedstocks, such as heavy oil refinery residues or refuse-derived fuels [34]. Gasification of heavy oil residues has been shown to be a cleaner alternative to conventional processing methods of fossil fuels. The gasifier can be used to process refinery waste, avoiding waste disposal costs and improving the yields from crude oil distillation process [80, 81]. The co-generation part of the system can produce electricity and steam needed by a refinery.

Commercial IGCC power plants have proven capable of exceeding the most tight emissions regulations currently applicable to comparable combustion-based power plants. They have achieved the lower levels of NOx, SOx and CO pollutant air emissions

comparing to any coal-fuelled power plants in the world [35]. Another significant environmental benefit is a reduction of CO_2 emissions, by at least 10% for an equivalent net production of electricity, due to higher operating efficiency comparing to existing coal-fuelled combustion-based power generation technology [35]. If more significant CO_2 reduction is required in the process, gasification technology has substantial operating advantages that can be achieved to capture CO_2 more efficiently than currently possible with combustion technology [80].

In order to increase the efficiency and reduce economic and environmental costs of gasification processes, oxygen can be used instead of input air to improve the combustion efficiency, increase the hydrogen content of produced syngas, and reduce the NOx emissions [7]. This can be achieved by linkage of the gasification and Cu-Cl processes. This innovative approach is to use oxygen instead of air in the gasification process, where it is supplied from the Cu-Cl cycle and utilizes heat provided by the syngas cooling section of an IGCC plant, previously used for low-pressure steam generation, as the major input of external heat required for the hydrolysis reaction of the Cu-Cl cycle. Figure 2.9 shows a schematic diagram of this integrated system.

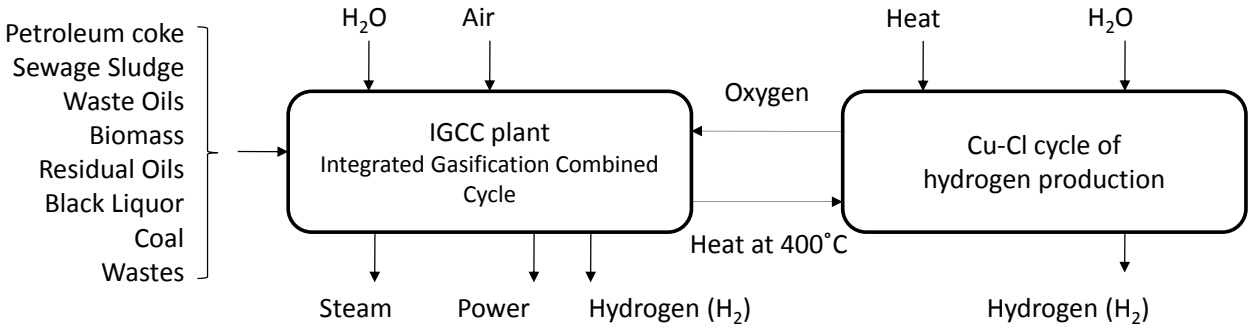

Figure 2.9 Schematic diagram of an integrated IGCC and Cu-Cl cycle.

To summarize this chapter, it is emphasized that in spite of reported theoretical investigation and experimental analysis which successfully demonstrate advanced development for most of the processes of the Cu-Cl cycle individually, process integration of reactions and analysis of the interaction between processes as a closed cycle are neglected. So, the main focus of this thesis is to address and investigate three major challenges for the Cu-Cl cycle which are process integration of the hydrolysis and electrolysis processes, experimental analysis of the electrolysis process and statistical modelling of its operation from integration standpoint, and process integration of a gasification process with the Cu-Cl cycle. This research enables commercialization and industrial adaptation of the Cu-Cl cycle for more efficient and cost effective hydrogen production.

Chapter 3: Literature Review

3.1 Hydrolysis and electrolysis processes in the Cu-Cl cycle

It is mentioned earlier that despite reported theoretical investigation and experimental analysis which successfully demonstrates advanced development for most of the processes of the Cu-Cl cycle, process integration analysis of the reactions in the cycle hasn't been a point of close attention. The hydrolysis process and its integration with the electrolysis impose significant challenges to achieve higher cycle efficiencies. These include the excess steam requirement of the hydrolysis reaction above the stoichiometric amount to obtain >95% yield of Cu_2OCl_2, and secondly, the concentration of the produced HCl in the hydrolysis reaction is not enough or even close to the minimum HCl concentration required in the electrolysis reaction and even getting worse by increasing the steam to $CuCl_2$ ratio. The last challenging point is the difference exists between operating temperature of the hydrolysis and electrolysis processes which requires considerable quantity of heat flow condense the high temperature products which then must be reheated for succeeding processes [30, 31, 33].

The hydrolysis reaction operates between 350˚C and 400˚C [41]. It is endothermic and doesn't require catalyst. The higher temperature of the reaction increases the formation chance of side products and also opposes the aim of using low-grade heat in the Cu-Cl cycle [82]. In this reaction, the solid $CuCl_2$ particles react with the superheated steam to produce Cu_2OCl_2 and HCl. The kinetics of the hydrolysis reaction indicates the reversibility of this reaction. It means that the quantity of H_2O must be in excess of the stoichiometric quantity to reach the stoichiometric yield of Cu_2OCl_2. The effects of

excess steam on the desirable yield of Cu_2OCl_2 in the hydrolysis reaction have been experimentally investigated. In order to reach the Cu_2OCl_2 yield higher than 70%, the molar ratio of H_2O to $CuCl_2$ must be higher than 5:1 [83], and to reach a yield higher than 95%, this ratio is around or higher than 17:1 [32]. Increasing the ratio beyond this point which corresponds to the excessive amount of steam is not recommended. It also directly reduces the concentration of the produced HCl which is not beneficial for the successor electrolysis reaction. Moreover, it is demonstrated that the higher HCl concentration in the gas mixture of H_2O and HCl in the hydrolysis reaction decreases the conversion rate of $CuCl_2$ to Cu_2OCl_2 which potentially increases the demand of excess steam for the complete conversion. [33].

Experimental study on the hydrolysis reaction is successfully demonstrated with a 100% rate of $CuCl_2$ conversion in a spray reactor using an ultrasonic atomizer [84]. The operating temperature of a hydrolysis reactor has substantial effect on the conversion extent of $CuCl_2$ [85]. The higher operating temperature, results in higher rate of conversion. Undesired production of Cl_2 is experimentally identified when the operating temperature increases beyond 400°C [84]. Therefore, decreasing the operating pressure in the hydrolysis could potentially increase product yields while limiting the CuCl production. The ideal working temperature of the hydrolysis reaction is then proposed to be below 375°C since the amount of CuCl in the reaction is estimated to increase beyond this temperature [86]. The accurate calculation of equilibrium conversion in the hydrolysis reaction has recommended temperature of 400°C for the complete conversion of $CuCl_2$ [85].

The results of thermodynamic calculation by [84] show that changing the hydrolysis reaction pressure from 1bar to 0.5 bar, could decrease the steam to Cu molar ratio from17 to 13 for 100% conversion. Although benefits from decreasing the energy required for water vaporization is significant, conducting the hydrolysis reaction at pressures less than atmospheric pressure is more complicated. Experiment at the University of Ontario Institute of Technology (UOIT) suggest that the amount of required excess steam for the hydrolysis reaction could be reduced when the inlet steam mixed with an inert gas like nitrogen to decreases the steam partial pressure. The results indicate the steam to Cu molar ratio of 3 is feasible by the packed bed reactor to generate HCl and Cu_2OCl_2 which is significantly lower than previously reported results [87]. The outcome is not confirmed for complete conversion of $CuCl_2$ and the produced HCl is not concentrated enough to be used in the electrolysis process. Also, it is suggested that gaseous stream should flow through a separation process before entering the electrolyser.

The experiments confirm that the required HCl concentration for effective operation of the electrolysis process is 6M to 11M [30, 41, 88]. The higher HCl concentration corresponds to the lower flux of copper species through the membrane from the anolyte to the catholyte which results in lower electrolytic cell voltage. The copper species crossing over the membrane would deposit on the membrane catalyst layer and interrupt the hydrogen production reaction. The stable operation of the electrolysis reaction is experienced over 50 hours with 11M HCl concentration [30]. However, the maximum value of 7.4M for the HCl concentration is estimated for the hydrolysis reaction from the minimum steam to $CuCl_2$ ratio of 7 which has been approached in the experiments [83].

It is concluded that providing excess steam to the hydrolysis reaction requires an intermediate HCl separator for the integration to the electrolysis process [33] which could also provide HCl solution at the required concentration. It means that the overall thermal efficiency of the Cu-Cl cycle is very sensitive to the percentage of heat recovered from the steam utilized in the hydrolysis reaction and hence is very sensitive to the separated percentage of excess steam from HCl. For a Cu-Cl cycle in which the excess steam is 100% separated from HCl and the heat is 100% recovered, the cycle thermal efficiency is around 88.6% [89]. If the steam cannot be separated efficiently, the thermal efficiency could be as low as 23.1%, even lower than water electrolysis which is currently used in industry [89]. This makes the Cu-Cl cycle less competitive than water electrolysis. Therefore, in the Cu-Cl cycle, HCl must be separated from steam and recovered in appropriate concentration for the electrolysis reaction. At the same time the steam could be recovered for the hydrolysis reaction. This would significantly increase the cycle thermal efficiency.

In the Cu-Cl cycle, H_2 gas production in the electrolysis reaction is the most important process in the Cu-Cl cycle where dissolved CuCl in concentrated HCl solution is oxidized to $CuCl_2$. Experiments of the CuCl electrolysis process were successfully demonstrated by Atomic Energy of Canada Limited (AECL) [90, 91]. It was shown that the anode reaction is mass transfer limited, in which stirring and the operation at higher temperature could increase current density for a given cell voltage [91]. Successful performance of the electrochemical cell was also shown by AECL for 2-3 days of continuous operation with the voltage of 0.7V at room temperature. Although the reported current density is lower than the Department of Energy (DOE) target value of

0.5A/cm^2, the operation at higher temperature could improve the cell current density [92]. Experiments on the electrolyser as conducted by Pennsylvania State University (PSU) demonstrate the possibility of copper crossing over the membrane from the anode to the cathode. This phenomenon results in a large increase in cell voltage and considered a main challenge to reach the DOE target values [91]. The concentration of copper ions in the anode solution is identified to be dependent on pH and oxidation-reduction potential (Eh) of the solution [93]. Recent development of the CuCl electrolysis process at PSU, which is based on a 5cm^2 proton exchange membrane (PEM) fuel cell using a Nafion-based membrane and pure water as catholyte, demonstrates promising performance at 0.5V and 0.1A.cm^{-2} with the H_2 production ratio of 98% [88]. Electrochemical impedance spectroscopy (EIS) is also used for measurement of the total ohmic and polarization resistance in the cell. Inconsistency between theoretical and experimental dependence of the current density to the anolyte flow rate suggests an improvement in the cell and membrane design to assist reagent transport to the electrode and improve the overall process kinetics.

In order to mitigate the adverse effect of copper crossover on the cell voltage, past research has focused on development of alternative membranes which are capable of stopping copper species crossover [94]. Moreover, material properties of the anode that influence the cell performance have been a main interest of some researchers [43, 95]. Experimental research at the Argonne National Laboratory (ANL) shows that Nafion-based and porous polyethylene (PPE) membranes can inhibit copper transport while using HCl as a catholyte [96]. It was demonstrated that the H_2 production ratio is more than 95% when the cell potential is stable at 0.7V with a current density of 0.5A.cm^{-2}, for a 36

hour test using a customized Nafion-based membrane. It was also estimated that the cost of a PPE membrane is about 55 times less than a tailor-made Nafion-based membrane. The cost of coating for PPE membranes was not included [96]. In the experiments, the HCl concentration of anolyte and catholyte was 6 to 7 M, for safer and more reliable operation, and the CuCl concentration was set to be 2M. The hydrogen production rate was measured by weighting the water displaced by the outlet gas after drying and HCl removal [94]. AECL demonstrated successful operation of the CuCl/HCl electrolysis process for a period of 341 hours with a cell potential of about 0.7V and a current density of about $0.2A.cm^{-2}$ [94]. The membrane was a customized Nafion-based material. It was shown that the cell resistance and voltage decrease with an increment of operating temperature at constant current density. It was also found that the cell voltage escalates with an increase in HCl concentration [94]. The change in temperature causes thermodynamic irreversibilities which decrease the open circuit potential and concentration gradients that lead to irreversibility within the cell. The activation losses are relatively small which indicates a weak reliance on temperature.

3.2 Separation techniques for azeotropic mixtures

Separating azeotropic mixtures into pure components is a challenge commonly encountered in commodity and fine chemical processes. There are many techniques for separation of azeotropic mixtures, such as pressure-swing distillation, extractive and azeotropic distillation, liquid-liquid extraction, adsorption, prevaporation using a membrane, and crystallization [59-61]. There are some new coupling separation techniques that using integration of the mentioned processes. Designing an appropriate

separation process and optimize the operating condition are complicated among the various techniques available for breaking azeotropes. Distillation is the separation method most frequently applied in the chemical industry, which is based on the difference of volatility of the components of a liquid mixture [60]. For the separation of two components (A and B) forming an azeotrope, a special distillation method must be applied.

The term azeotrope denotes a mixture of two or more components where the equilibrium vapor and liquid compositions are equal at a given pressure and temperature. More specifically, the vapor has the same composition as the liquid and the mixture boils at a temperature different from the boiling points of its pure components. Azeotropes have sometimes been mistaken for single components because they boil at a constant temperature. The term azeotropy was introduced by Wade and Merriman in 1911 to designate mixtures characterized by a minimum or a maximum in the vapor pressure under isothermal conditions or in the boiling temperature at constant pressure [97]. The term has been used for liquid systems forming one or several azeotropes. The mixture whose composition corresponds to the maximum point is called an azeotrope. If at the equilibrium temperature the liquid mixture is homogeneous, the azeotrope is a homoazeotrope. If the vapor phase coexists with two liquid phases, it is a heteroazeotrope. Systems which do not form azeotropes are called zeotropic [62].

Many mixtures form an azeotrope are pressure sensitive in which the azeotropic point can be shifted or even disappear by changing the system pressure. This effect can be applied to separate azeotropic mixtures without using a separating agent and is called pressure-swing distillation and has been suggested as an effective way to separate many

azeotropic mixtures [64-66]. In literature, details of PSD process have been extensively studied and pros and cons of this process have been investigated [64, 98]. Although, PSD is a very energy-consuming process comparing to the other separation techniques using an extractive agent, But with help of energy integration techniques, the pressure-swing distillation process can become an economically viable solution [67-70]. In this case the heat of the condenser of the high pressure column (HP) is used for heating up the low pressure column (LP). Phimister and Seider [66] studied the separation of a minimum azeotrope of Tetrahydrofuran (THF)-water mixture by semi-continuous PSD and reverse-batch operation. In the semi-continuous column, better performance was achieved than in a batch stripper. In their research, the control and other practical aspects of suggested configurations are analyzed and compared. Wasylkiewicz et al. [99] developed an algorithm which allows tracking of composition variations with operating pressure in which new azeotropes appears.

Examples of application of PSD process for various binary azeotropic mixtures are given in Table 3.1. As an example, the THF-water azeotrope could be separated by two columns operated at P_1 = 1atm and P_2 = 8atm [100]. The example of the ethanol-water azeotrope is not considered to be sufficiently pressure sensitive for the pressure-swing distillation process to be competitive. However, a hybrid system of pressure-swing adsorption and distillation is reported to be an effective alternative to the conventional methods [101]. The reason behind the fact that designers do not consider PSD process as an attractive separation technique is that azeotropic data frequently is not available at non-atmospheric pressures and the collection of such data is expensive [102]. In that case, an algorithm is developed that applies specific mathematical theory and a rigorous

stability analysis to find all homogeneous and heterogeneous azeotropes at a specified pressure [103]. Since the property data of azeotrpic mixtures is a key to analyze their behavior, some thermodynamic property databases for pure components and mixtures has been developed [104-106].

Table 3.1 Examples of binary azeotropes in PSD separation process.

Aazeotropic Mixtures in PSD
Carbon tetrachloride / Ethyl acetate
Propanol / Toluene
Methanol / Ethyl acetate
Acetone / Methanol
Ethanol / 1,4-dioxane
Benzene / Isopropanol
Acetonitrile / Water
Aniline / Octane
Phenol / Butyl acetate
Tetrahydofuran (THF) / water
Methanol / Methyl Ethyl Ketone (MEK)
Propanol / cyclohexane
Ethanol / Ethyl acetate
MEK / Benzene
Acetic acid / Toluene

Extractive distillation, as an effective alternative separation technique, is a partial vaporization process using a non-volatile and high boiling point separating mass agent that is called an entrainer, solvent, or separating agent. The entrainer is added to the azeotropic mixture to change the relative volatility of the key component without

additional formation of azeotrope [72, 107]. Extractive distillation is being used broadly in the energy industry as a batch and continuous operations but, no detail explanation of the process has been reported in literature [107]. De Dietrich Process Systems group and Aker Solutions are examples of companies working widely on different distillation technologies.

In the extractive distillation process, generally, a solvent is fed in the upper part of the column, above the feed stream and it remains in the liquid phase along the column. It is withdrawn as a bottom product with one of the components that are separated and then is sent to a second regeneration column to be recovered and recycled back to the distillation column. The most common solvents used in extractive distillation are glycols [108], glycerol [109], gasoline [110] and for the case of saline extractive distillation, acetate and inorganic salts such as $CaCl_2$, $AlCl_3$, KNO_3, and K_2CO_3 [111–113]. In the extractive distillation using salt as an entrainer, the activity coefficients of two volatile components are altered when the dissolved salt associates with one component and changes the solubility relationship of two components and composition of the equilibrium vapor phase [112]. It should be mentioned that no salt presents in vapor phase and would only appear in the liquid phase. Extractive distillation using salts and solvents together as separating agents is an alternative that can obtain high purity products. In this combined method, it is possible to solve several problems of dissolution and obstruction found when only salt is used as a separating agent [114].

Analysis of the ethanol-water separation system was conducted on experimental data of the mixture vapor-liquid equilibrium and the effects of using glycol-calcium chloride as a solvent on the separation process are examined [114]. It is observed that the

solvent effectively helps the separation process. The application of extractive distillation process is successfully conducted to separate close boiling points hydrocarbons such as C_4, C_5, C_6 mixtures [115]. Moreover, application of extractive distillation is examined for mixtures such as alcohol/water, acetic acid and water, acetone and methanol, methanol and methyl acetate, ethanol and ethyl acetate, acetone and ethyl ether [116-120]. Effective separation of HCl and water mixture with the extractive distillation is shown both in literature and industry [121-124]. $CaCl_2$, $MgCl_2$, and H_2SO_4 are suggested as the appropriate extractive agents. It is demonstrated that adding 25wt% $CaCl_2$ to the HCl and water mixture could eliminate the azetrope completely. The addition of $MgCl_2$ is experienced to have similar effects. It is also suggested to separate water from HCl partially upstream of the extractive distillation in order to reduce the amount of water that needs to be removed in the distillation column. The benefits of using $CaCl_2$ because of availability reasons and ease of operation make it the most attractive choice as a solvent for the separation of HCl and water.

The advantages of distillation process are the potential for high throughput, any feed concentration, and high purity [56]. Comparing to other thermal separation processes, distillation is used in 90% of cases for the separation of binary and multi-component liquid mixtures [125]. The distillation technique itself is a mature technology, in terms of design, operation and control, in contrast to other promising technologies such as using membranes. On the negative side, distillation tends to use large amounts of energy and the introduction of an additional liquid entrainer to the mixture system causes additional complexities. Distillation is particularly energy intensive when the heat of vaporization of the mixture to be separated is high, such as water and alcohols. For these

particular separation tasks, heat integration could significantly reduce the total energy consumption of the process [126]. Distillation, and in particular batch distillation, is based on robust and flexible equipment that can handle a wide range of feed compositions and often has considerable economic advantage at large throughputs.

Adsorption distillation as a newer separation method is proposed which can be compared with extractive distillation. There are two types of adsorption distillation. One has been proposed by Abu Al-Rub [127, 128] which involves replacement of the inert packing components in a packed-bed distillation column by active packing materials. The active packing materials used by Abu Al-Rub for separating ethanol and water are able to alter the VLE of ethanol and water considerably and make the separation possible. In the second type of adsorption distillation, which is presented by Cheng et al. [129, 130], small solid particles are used as an adsorption agent and blended with the liquid phase in the column. This process doesn't involve replacement of internals of distillation. The enhancement of gas-liquid mass transport by solid particles has been proven, and the mechanism model is proposed. However, adding solid particles to a liquid phase causes the packed column frequently plugged. So, the tray column is suggested to be more suitable for this kind of adsorption distillation.

3.3 Gasification process and IGCC power plant

Gasification is the thermochemical conversion of either a solid (coal, coke, biomass, solid waste) or liquid (oil, tar, pitch) fuel into a synthesis gas (or syngas) composed primarily of H_2 and CO [75]. Unlike combustion processes that only produce CO_2 and water, gasification is a partial oxidation process that occurs in an oxygen-limited environment.

The resulting syngas is more useful than combustion flue gas and it has the potential to generate electricity more efficiently. During the last century, gasification has been used to convert coal into fuel gas for domestic heating and lighting. More recently, gasification has been used in the petrochemical industry for the production of chemical products [76].

Research on the gasification process could be divided up into two major categories. The majority of efforts are focused on the methods to improve the heating value of produced syngas where the others are concentrated on techniques to increase the concentration of produced hydrogen. Many works investigate the overall conversion efficiency of the gasification process based on the first law of thermodynamics, where others analyze irreversibilites in the process and the quality of energy at various operating conditions based on the second law of thermodynamics and exergy analysis concept [131]. Two methods are suggested to model and simulate the gasification process. The first approach is based on the minimization of the Gibbs free energy that requires advanced mathematical calculation. The second approach of equilibrium models are based on equilibrium constant which is on the basis of the same concept but is preferred to predict the composition of the produced syngas [132-134]. Calculation of exergy efficiency is vital to estimate the amount of useful energy is utilized in the process. The exergy analysis of the biomass gasification process is conducted by Abuadala et al. and the effects of temperature and the amount of steam injection on the hydrogen yield and energy and exergy efficiencies are investigated [135]. Energy and exergy efficiencies of steam gasification of biomass are analyzed and compared for different type of raw materials [136]. It is shown that the exergy efficiency, which is a function of feedstock, gasification temperature, and steam to biomass ratio, varies from 65% to 80%. Results

from an investigation of the change in exergy content of syngas and the exegetic efficiency of the gasification process reveal that municipal solid wastes are a competitive fuel to biomass in this process [137]. Energy and exergy efficiencies of steam and air fed biomass gasification processes are analyzed and compared for different operation conditions [138]. It is shown that the adiabatic temperature of the gasifier substantially changes with the type of gasifying medium. It is found that the efficiency of air gasification is higher that steam gasification process since the gasifier operates at higher temperature. The effect of moisture content of input material on the heating value of the produced syngas and the process exergy efficiency is analyzed in the gasification of municipal solid waste [139]. The higher moisture content of feedstock results in the lower heating value of syngas and exergetic efficiency of the process.

The influence of operation factors like temperature and the equivalent ratio (ER) on the gasification performance process irreversibilities are assessed considering steam and steam-air mixture as gasifier mediums [140-142]. ER is defined as the ratio of used oxygen for gasification of any material divided by the required oxygen for its stoichiometric combustion. In the mentioned research, ER is considered as a key factor in the operation of gasification systems. Different options are then suggested to improve the exergy efficiency of the process. The effect of fuel composition on the thermodynamic efficiency of gasifiers and gasification systems is studied and it is found that highly oxygenated biofuels are not ideal fuels for gasifiers from an exergetic point of view [143]. It is also demonstrated that the higher gasification temperature minimizes kinetic restrictions of the process. The influence of ER on the efficiency of the biomass

gasification with air is conducted and results shows that increase in ER corresponds to the higher exergy and energy efficiencies [144].

An Integrated Gasification Combined Cycle (IGCC) is a successful integrated process concept that combines modern gasification technology with both gas and steam turbine power generation systems for tri-generation of electricity, steam and hydrogen [35]. IGCC features higher efficiency and lower emissions in comparison to a conventional pulverized coal combustion power generation system. It also provides the opportunity of using variety of low value fuels and producing multiple products [81]. An air separation unit (ASU) could be integrated to the gasification process to improve its efficiency by substituting air with oxygen which makes an oxygen-fired IGCC power plant more attractive [77]. Although using oxygen instead of air improves the gasification efficiency and reduces NOx emissions, but it will impose extra capital investment to an IGCC power plant. It is estimated that about 8% of the capital investment for a conventional IGCC power generation system is related to the ASU [77]. IGCC can be extended beyond the combined cycle power generation application and has a potential to be a foundation for modern energy systems. It could be used to produce high quality steam for heating application, or produce transportation fuels and variety of chemicals through catalytic conversion of the clean syngas. It could be also coupled with advanced fuel cell technology to generate clean electricity with high efficiency.

Chapter 4: Experimental Apparatus and Procedures for the CuCl Electrolysis Process

4.1 Experimental test bench and measurement devices

The experimental test bench of the CuCl electrolysis process is shown in Figure 4.1. A solution of CuCl, HCl, and deionized (DI) water is supplied from the anolyte container to the anode side of the electrolysis cell. CuCl and HCl concentrations are varied between 0.5M to 1M and 6M to 10M, respectively. The solution of HCl and DI water is supplied from the catholyte container to the cathode side of the cell simultaneously with the same flow rate and HCl concentration. Figure 4.2 illustrates a process flow diagram of the CuCl electrolysis experiment.

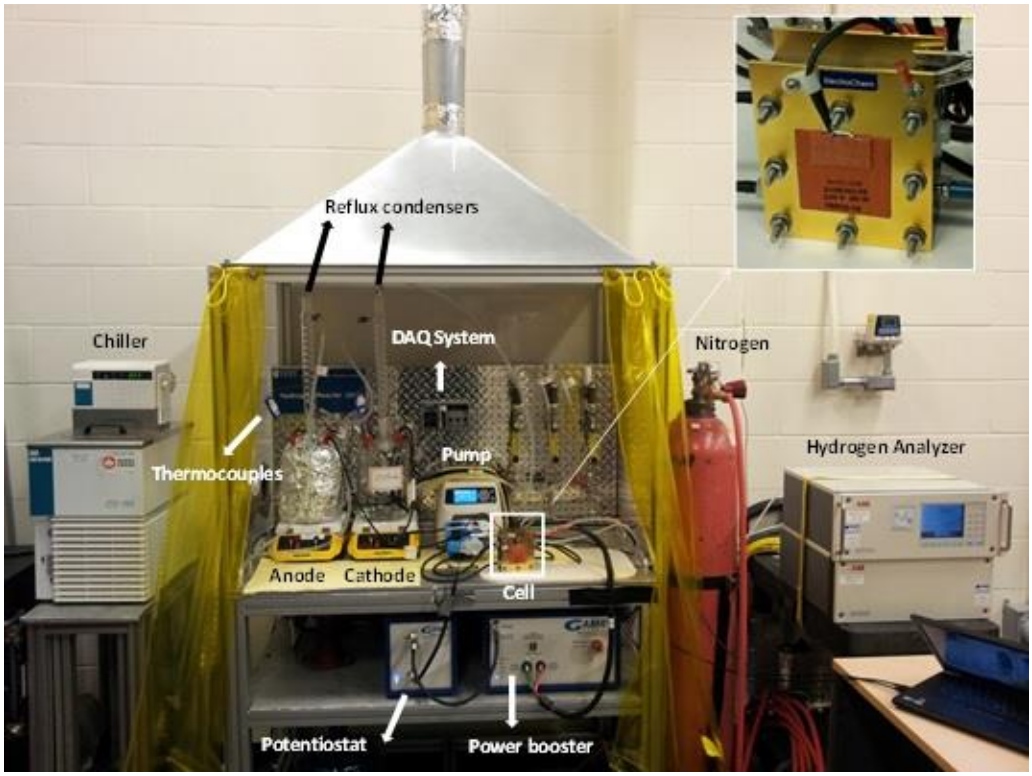

Figure 4.1 Experimental apparatus for the CuCl electrolysis process.

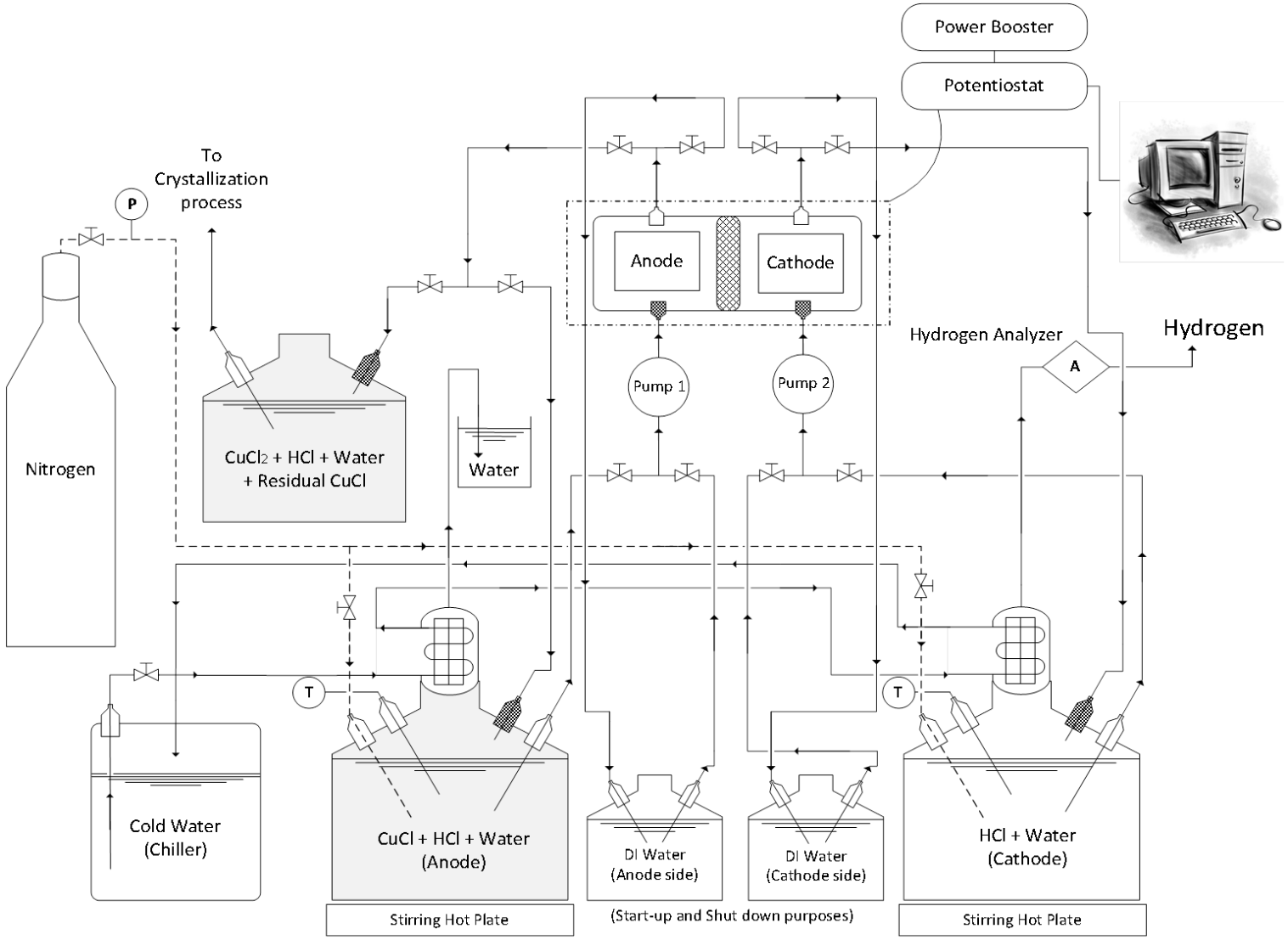

Figure 4.2 Process flow diagram of the CuCl electrolysis experiment.

Anolyte and catholyte containers are custom-made 4L flat bottom vessels made of Borosilicate glass with a 24/40 center neck and four #14 Chemglass screw-thread connectors. Since the CuCl solution is light sensitive, the anolyte container is covered with aluminum foil. The four connections of each container are dedicated to the solution inlet and outlet streams, thermocouple, and nitrogen supply. Black L/S® 16 Viton tubing by Coleparmer with a hose barb size of 1/8 inch is used for all main process lines because it is resistant to concentrated HCl solution at elevated temperatures up to 205°C and offers ultra-low gas permeability [145]. The tubing is manufactured to tight tolerances that match L/S® pump heads which ensures accurate flow rates and a long tubing life.

A Masterflex peristaltic pump, L/S® 600rpm Digital Drive, manufactured by Coleparmer with two pump heads of L/S Easy-Load® 3 SS, is used to avoid direct contact of the pump with the solution. The pump drive offers flow rate capacities from $0.001 mL.min^{-1}$ to $3400 mL.min^{-1}$ using different Masterflex pump heads and compatible tubing. The Masterflex digital pump provides a motor speed repeatability of 0.1 percent to maximize productivity in precision liquid dosing, batch dispensing and filling applications. A turndown ratio up to 6000 to 1, bidirectional flow and self-priming capabilities allow for smooth, seamless operation and an extremely broad flow range within selected tubing size [145].

This L/S® Easy-Load® 3 pump heads are selected to provide a simple, easy-to-use peristaltic pump system. The pump heads accepts several different tubing sizes for a wide range of flow rates. The unique lever actuator design and automatic tubing retention allow quick tubing changes. The heads have 3 rollers each with a maximum speed of

600rpm and rotor, bearing, and rollers are all made of stainless steel. The Masterflex pump with attached Easy-Load heads is depicted in Figure 4.3.

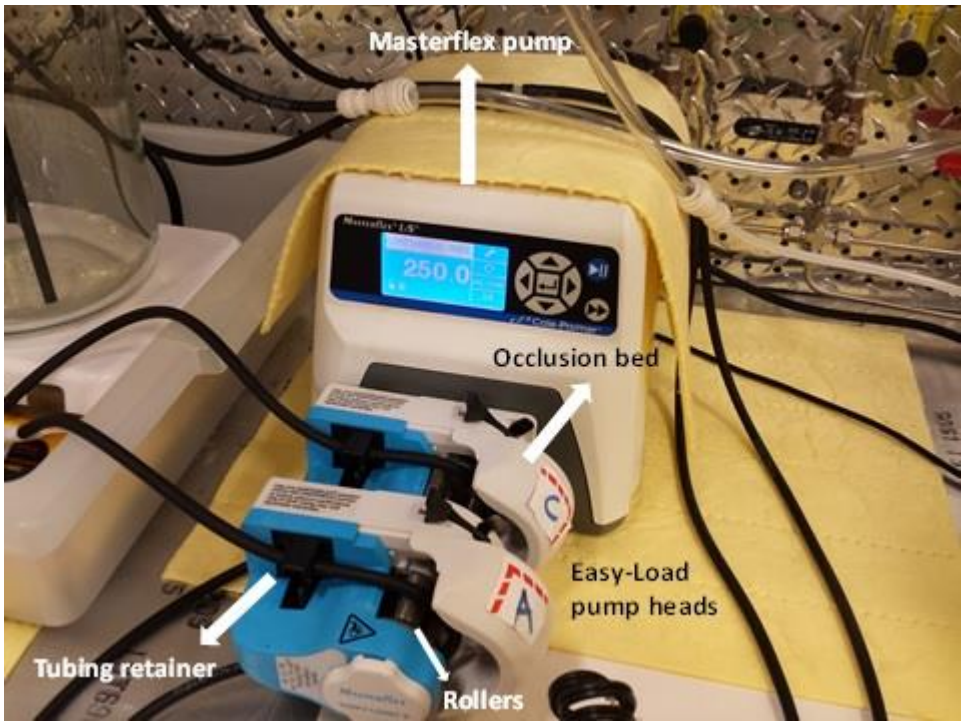

Figure 4.3 Pumping system in the CuCl electrolysis experiment.

The pure nitrogen gas is constantly purged into the anode solution to prevent oxidation of CuCl. Nitrogen is also purged at a flow rate of 0.5L.min^{-1} into the catholyte to carry produced H_2 gas to the hydrogen analyzer. A start-up process consists of preparation of solutions and calibration of measurement devices. For the preparation of the anode solution, nitrogen is first purged into DI water for 15 minutes and then HCl acid is added. Nitrogen is purged again into the solution for another 15 minutes and then CuCl powder is added inside a glove box filled completely with nitrogen to prevent pre-oxidation of CuCl in the anolyte solution.

In order to achieve complete dissolution of CuCl powder and control the solution temperature, the anolyte container is placed on the top of a stirring hot plate. The temperature of anode and cathode solutions is controlled with two stirring hot plates underneath the containers in a range of 25˚C to 60˚C. The temperature of both solutions is continually monitored by type T thermocouples and a National Instruments DAQ-9174 data acquisition system. The Data Acquisition (DAQ) system and a block diagram of the designed temperature measurement system are depicted in Figure 4.4.

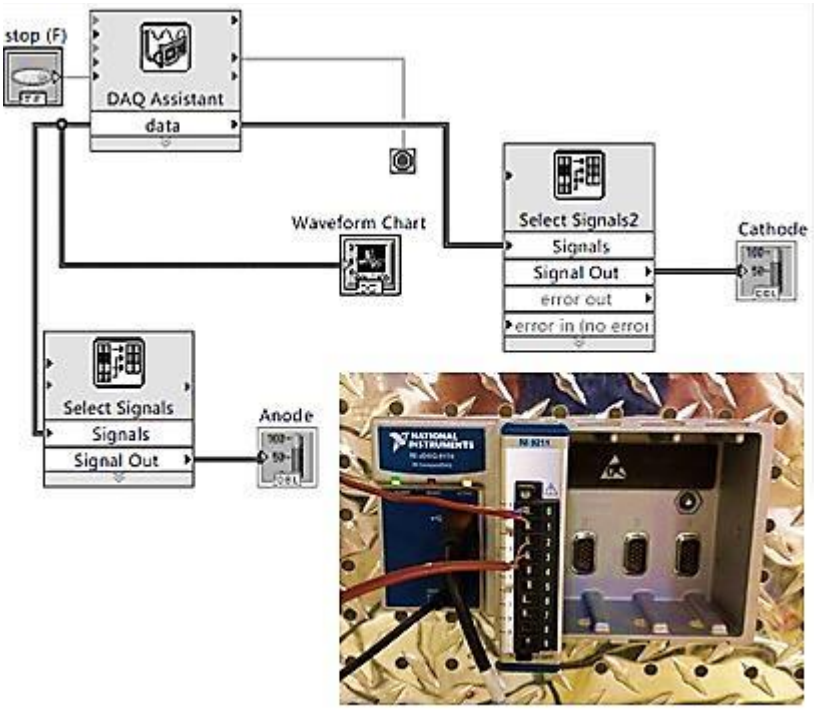

Figure 4.4 Temperature measurement system, DAQ system and designed block diagram.

The hydrogen production rate is continuously measured using an ABB advance optima continuous gas analyzer, AO2020 series. Advance Optima is based on analyzer modules that are available for performing measurements using different techniques. All analyzer modules have uniform electrical, gas and mechanical interfaces. This allows a

uniformly integrated analyzer system to be created. The analyzer systems differ only in their selection of analyzer modules. The Caldos 25 thermal conductivity analyzer module is utilized to measure thermo conductive components in a sample gas. This module has been designed to calculate a volumetric ratio of H_2 to N_2 with high precision. Internal components of the hydrogen analyzer are depicted in Figure 4.5.

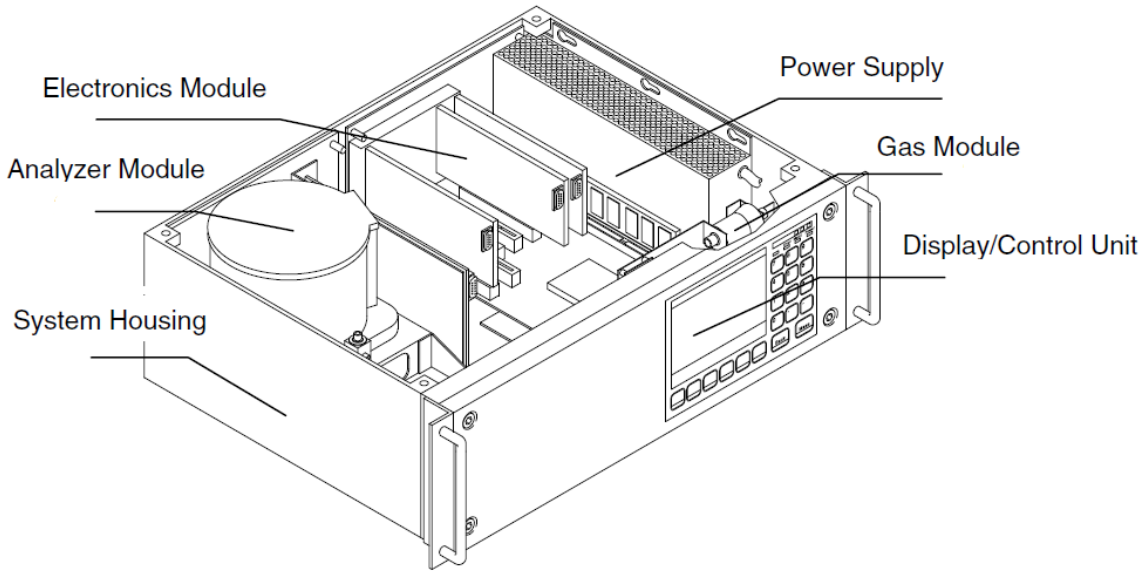

Figure 4.5 Device arrangement of the hydrogen analyzer.

The Caldos 25 thermal conductivity analyzer module is used to measure H_2 in N_2 or air. The measurement principle is primarily suited to measure a gas component in a binary or quasi-binary gas mixture relative to thermal conductivity [146]. The sample gas, which requires being analyzed, flows over two opposed temperature-sensitive resistor wires in the sample chamber. With the sample chamber resistor wires, the two resistor wires exposed to the reference gas, which is N_2, form a bridge circuit. The bridge circuit is powered by a constant current source to that the resistor wires are at a specified temperature. The bridge circuit is in equilibrium when the sample gas has the same

quantitative composition as the reference gas. Even slight differences in the thermal conductivity of sample gas and reference gas disturb the temperature-dependent bridge balance and give rise to a bridge diagonal voltage that is proportional to the concentration of the sample component [146]. A schematic picture of the measurement principle is illustrated in Figure 4.6. The measurement unit is located in a thermostat chamber so that measured values are extensively free from variations in ambient temperature.

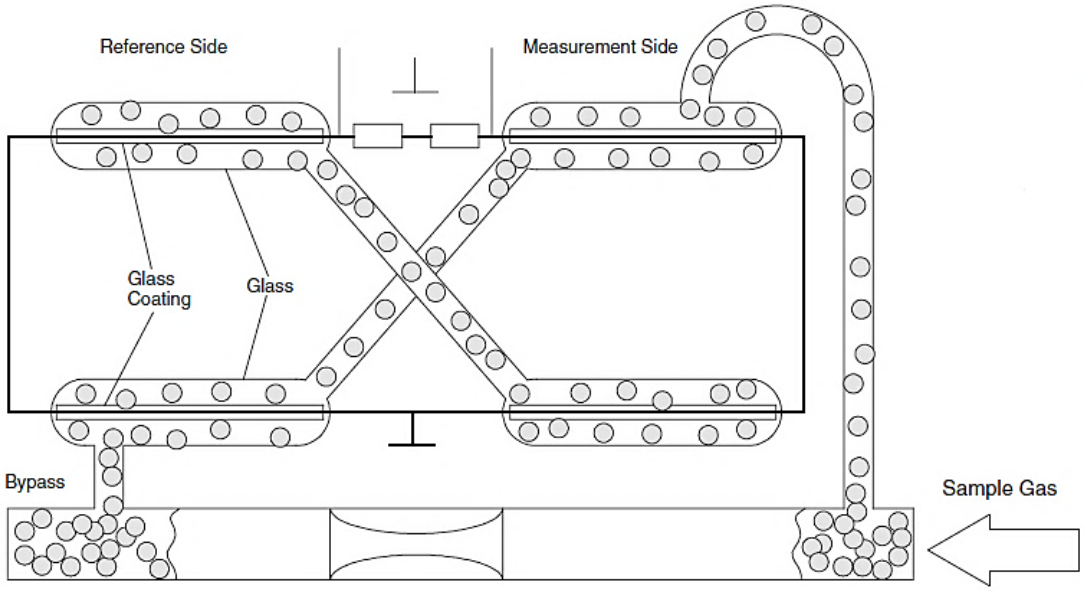

Figure 4.6 Schematic picture of the H_2 analyzer; measurement principle.

Moreover, the Caldos is not sensitive to variations is sample gas pressure, no pressure correction is required. Since, there is a possibility of having HCl vapor accompany the produced H_2 gas to the analyzer, the sample cell is made of glass to permit measurement of highly corrosive gases. The H_2 analyzer is shown in Figure 4.7. The acceptable flow rate range for the H_2 analyzer is between 0.17L.min^{-1} to 1.5L.min^{-1} and it requires 1.5 hours to warm up. Accuracy of the measurements is ±0.025% [146].

Figure 4.7 Hydrogen analyzer in the CuCl electrolysis experiment.

In order to minimize the amount of HCl vapor escaping from the system, chilled water at 3˚C is supplied to the reflux condensers (Ace Glass 300mm coiled condenser) mounted on the top of each container. The anolyte and catholyte solutions are pumped into a 25cm^2 PEM electrolysis cell by Electrochem with a flow rate range of 0.1L.min^{-1} to 0.5L.min^{-1}. The electrolysis cell has a serpentine flow pattern with PTFE fittings. The membrane electrode assembly (MEA) is a Nafion-117 HYDRion catalyzed membrane by Ion Power Inc. which is originally designed for water electrolysis [147]. Performance and compatibility of this membrane for CuCl electrolysis have been tested and confirmed [88]. Figure 4.8 depicts the CuCl electrolysis cell.

Hydrogen production in the cell is driven by an applied current density in a range of 0.1A.cm^{-2} to 0.5A.cm^{-2} using Gamry's Reference 3000 potentiostat and coupled 30K power booster [148]. The potentiostat is capable to apply current up to 3A which could be boosted up to 30A with the coupled power booster. Linear sweep voltammetry (LSV) and Galvanostatic method are used to obtain the experimental decomposition potential and

detect the cell voltage for applied current densities. LSV is an electrochemical method which the current at a working electrode is measured while the potential is swept linearly in time between the working electrode and a reference electrode [149]. Voltage measurement is performed with a zero offset error of 1mV and gain error of 0.2%. The total error in a voltage measurement can be as high as 3mV for a 1 volt signal. It should be noticed that the Oxidation of Cu^{+} to Cu^{++} is registered for the potential at which the Cu^{+} begins to be oxidized. The potentiostat and power booster is depicted in Figure 4.9.

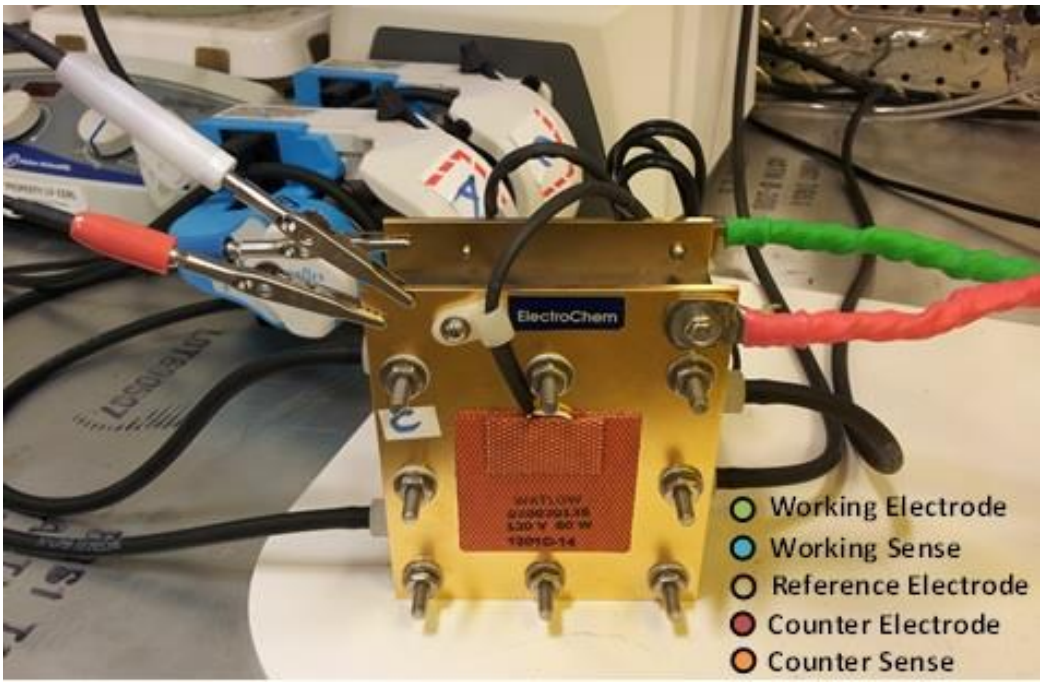

Figure 4.8 The CuCl electrolysis cell.

During the operation of the electrolysis cell, copper species may cross over the membrane from the anolyte into the catholyte which can negatively affect the cell performance by increasing the cell voltage. The cell potential requires to be kept as low as possible to reduce energy consumption of the electrolyser. In this case, in order to

quantify the amount copper crossover, the measurement of copper species concentration in catholyte after each experiment is conducted.

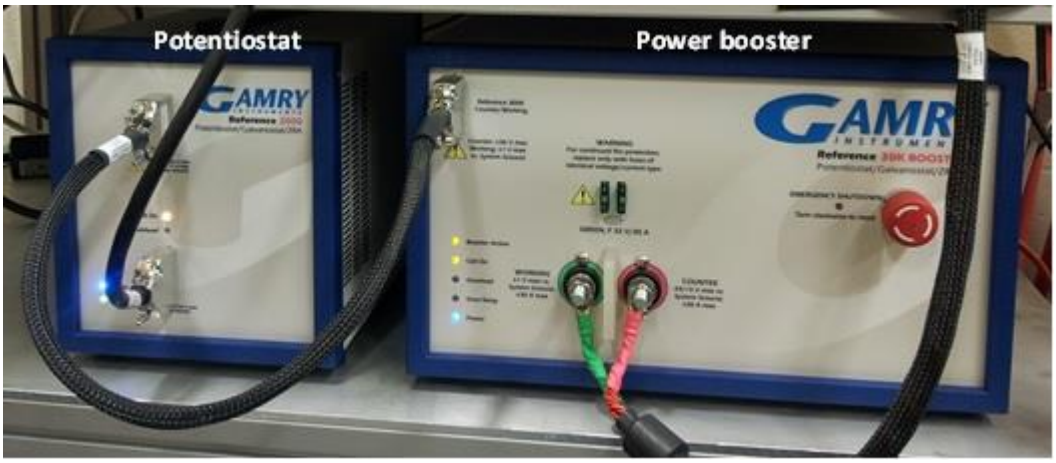

Figure 4.9 Potentiostat and power booster in the CuCl electrolysis experiment.

Total copper presence in the catholyte is measured by Pocket Colorimeter II Analysis System from HACH® with an accuracy of ±0.04 $mg.L^{-1}$ and a range of 0.04 to 5.00$mg.L^{-1}$. The copper colorimeter is calibrated first with use a 4.00$mg.L^{-1}$ copper standard solution. It should be considered that pH level of the sample is important and must be in the range of 4 to 6. So, 2N NaOH solution is added to the catholyte samples to increase their pH levels. Figure 4.10 depicts the Pocket Colorimeter II Analysis System.

In experiments, both anolyte and catholyte are recycled to the cell while the cell voltage is constantly monitored. The waste anolyte solution is then collected in a separate container which is finally supplied to the crystallization process. Two containers of DI water are used for start-up and shut-down purposes to completely wash inside the cell and process lines before and after each experiment. A start-up process consists of preparation of solutions and calibration of measurement devices. The solution flow rate, HCl and

CuCl concentrations, current density, and temperature are operational factors that are changed for each experiment. The cell potentials and hydrogen production rates are measured at different operating conditions.

Figure 4.10 Pocket colorimeter copper analysis system.

4.2 Experimental errors and measurement uncertainties

In all experimental tests even the most carefully calibrated instruments have errors associated with the measurements. The accuracy of a measurement demonstrates the closeness of agreement between an experimentally determined value of a quantity and its true value. Error is the difference between the true value and its experimentally measured value. The 100% accurate results indicate that errors in the measurements are close to zero. In practice, the estimation of error in the measurements is named uncertainty [150].

Estimation of an uncertainty (U) in a given measurement is made at a 95% confidence level. It means that the true value is expected to be within the $\pm U$ interval around the mean 95 times out of 100 [150].

The total error in a measurement is composed of two components of bias and precision error. Errors contributes to the scatter of the data are classified as a precision errors otherwise they are bias errors [151]. In a multiple measurement, the bias error gives the difference between the mean value of the readings and the true value of that variable. In measuring some variables using a single instrument, the bias errors are considered as fixed or constant errors which cannot be determined statistically. The uncertainty estimate for the bias error is called the bias limit [151]. Precision errors are because of limitations on repeatability of the measurement system which are estimated statistically. The uncertainty estimate of the precision error is called the precision limit.

In every experimental test, measuring the value of individual variable is affected by various error sources. The effects of these errors are acknowledged as bias and precision errors in the measured values. These errors then propagate through the equation to calculate the response variable and generating the bias and precision errors in the experimental results [151]. The total uncertainty in the result, Y, is the root-sum-square (RSS) of the bias and precision errors of the measurements and is calculated as below,

$$U_Y^{\,2} = B_Y^{\,2} + P_Y^{\,2} \tag{4.1}$$

where B_Y and P_Y are the bias and precision errors of the result, Y, respectively. B_Y is calculated as follows:

$$B_Y{}^2 = \sum_{i=1}^{m} \xi_i{}^2 B_i{}^2 + 2\sum_{i}^{m-1} \sum_{k=i+1}^{m} \xi_i \xi_k B_{ik} \tag{4.2}$$

where B_i is the bias error in variable X_i, B_{ik} is the correlated bias error in dependent variables X_i and X_k where L is the number of correlated bias errors for measurement of variables X_i and X_k, and ξ is the sensitivity coefficient.

$$B_{ik} = \sum_{p=1}^{L} (B_i)(B_k) \tag{4.3}$$

$$\xi_i = \frac{\partial Y}{\partial X_i} \tag{4.4}$$

The precision error of the result is estimated by the below equation where P_i is the precision error in variable X_i which is estimated as double the standard deviation, S, of the measured values. [151].

$$P_Y{}^2 = \sum_{i=1}^{m} (\xi_i P_i)^2 \tag{4.5}$$

The standard deviation is the commonly used measure of the dispersion of data around the mean which is defined as the square root of the variance. The variance in measurement is determined as the sum of the squared deviations from the mean, divided by number of data minus one. $\overline{X}$ is the mean value of a set of n measurements.

$$S = \sqrt{\frac{\sum_{i=1}^{m} (X_i - \overline{X})^2}{n-1}} \tag{4.6}$$

As shown in Table 4.1, the measuring devices used in the CuCl electrolysis experiment have a relatively high accuracy and low bias error associated with their operation. This information is used to estimate the propagation of bias and precision errors through the equation to calculate the cell potential. It is important to mention that the relative bias error is taken as the ratio of bias error to the corresponding reference value. Consistent operating conditions are maintained during the uncertainty analysis.

Table 4.1 Accuracy and relative error for the measurement devices.

Variable	Measurment device	Accuracy	Device range	Reference value	Relative bias error	Relative precision eror
Temperature	Omega Type-T Thermocouple	± 1˚C	−200˚C to 350˚C	60˚C	0.016	0.005
Current density	Gamry's Reference 3000 potentiostat	± 0.007 A	±3 A	3 A	0.0023	0.0013
Cell potential	Gamry's Reference 3000 potentiostat	± 0.003 V	±15 V	0.7 V	0.0042	0.0006
Hydrogen concentration	Caldos 25 thermal conductivity analyzer	± 0.025%	0 to 20%	10%	0.00125	0.001
Hydrogen flowrate	Omega direct read flow meter FL-2500 Series	±0.065 L	0.1 to 1.3 $L.min^{-1}$	0.5 $L.min^{-1}$	0.13	0.034
Copper concentration	Hach pocket colorimeter II	± 0.04 $mg.L^{-1}$	0.04 to 5 $mg.L^{-1}$	5 $mg.L^{-1}$	0.008	0.022

Chapter 5: Model Development and Analysis

5.1 Process integration of hydrolysis and electrolysis processes

5.1.1 Methodology

The proposed methodology for the integration of hydrolysis and electrolysis processes of the Cu-Cl cycle is using intermediate system consisting of Heat Recovery Steam Generator (HRSG) and a separation process. In HRSG, HCl and steam mixture from hydrolysis at 400˚C is condensed to dilute HCl acid at 90˚C and then fed into the separation process which concentrated HCl acid is produced for the electrolysis reaction. The heat of condensation is utilized to generate excess high temperature steam required for the hydrolysis reaction. Figure 5.1 demonstrates schematic model of the proposed integrated system.

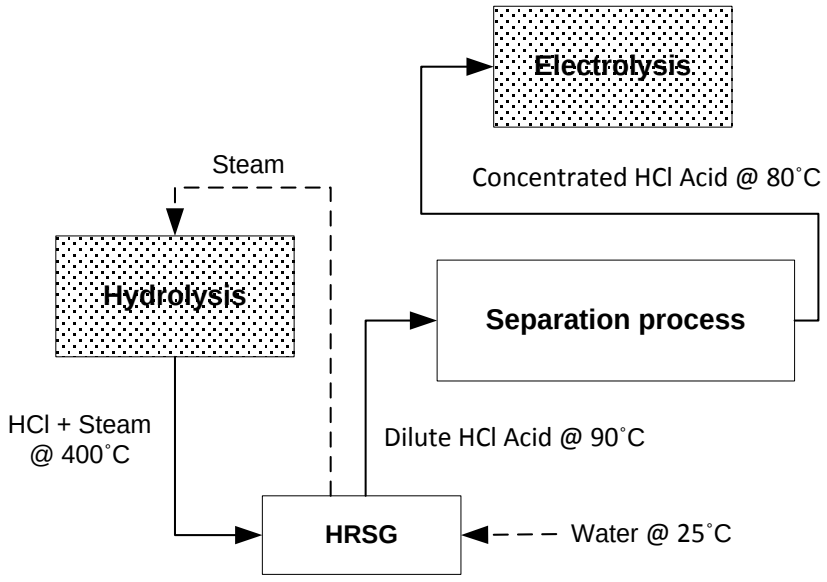

Figure 5.1 Schematic model of the proposed integrated system.

The separation process, as depicted in Figure 5.2, is comprised of rectification and absorption columns. A well-established method to concentrate HCl-H_2O mixture is a distillation process which requires a reduction of the temperature to below the vaporization temperature of the mixture [152]. The system of HCl and water mixture displays a maximum azeotrope at the boiling temperature of 108.6˚C, for a system pressure of 101kPa and HCl concentration of 20.2wt% or 11.3mol% [153]. If the acid concentration is lower than the azeotrope mixture, the acid can be concentrated only up to the azeotropic point. Further concentration needs special and complex procedures. If the concentration is above the azeotropic point, distillation process could generate almost dry HCl gas which could be further absorbed into water to make desired HCl acid concentration.

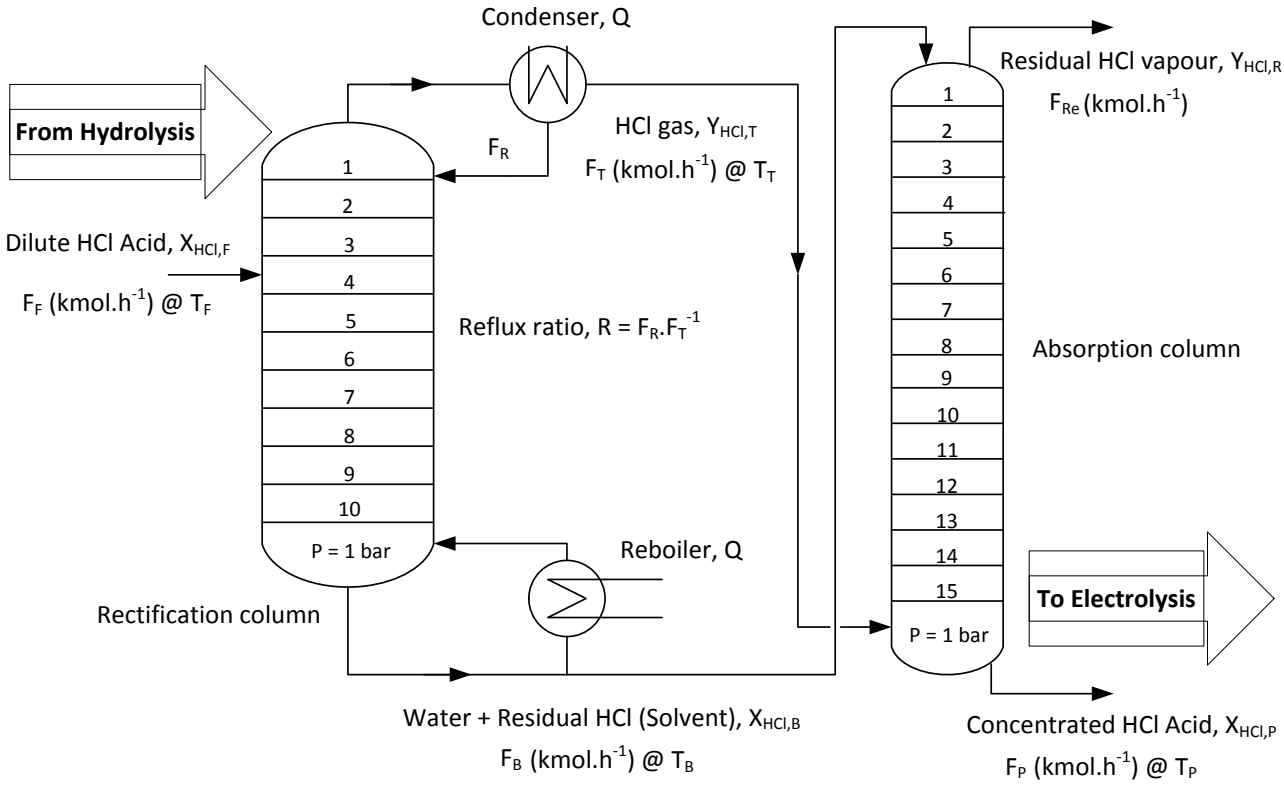

Figure 5.2 Schematic diagram of the separation process.

In the proposed separation process, dilute HCl acid with the concentration of 13.5mol% is fed into the rectification column where dry HCl gas is produced on the top of the column. The mixture of water and residual HCl at azeotropic concentration leaves the bottom of the column and is used as a solvent instead of water in the absorption process. Dry HCl gas temperature is 70˚C in the absorption column where the solvent is at 80˚C. Concentrated HCl acid leaves the column at 22mol% and temperature of 80˚C which is absolutely appropriate for the electrolysis reaction.

In the binary system of HCl and water, the basis of the separation is that the vapor phase is richer in HCl which is the more volatile component than the liquid. This enrichment is characterized by vapor-liquid phase equilibrium (VLE) [72]. Therefore, analysis of the VLE diagram is the starting point to predict the feasibility, thermodynamic possibility, and limitation of the separation which caused by the nature of the mixture. Figure 5.3 depicts the VLE phase diagram of HCl and H_2O mixture. The absorption of HCl in water behaves exothermic. It means that the boiling state is usually achieved for high concentration levels of HCl in the gas phase [152].

As illustrated in Figure 5.3, the boiling temperature is dependant to the acid concentration. The maximum temperature is achieved at the azeotropic point and reduces in almost linear way for higher concentration levels of HCl. It should be mentioned here that solubility processes with regard to potential chemical reactions are not considered. The equilibrium diagram of HCl and water mixture is the key to design the absorption process under boiling condition. As shown in Figure 5.4, HCl is hardly volatile in low concentration levels. It indicates that the gas phase is almost free of HCl in low-concentrated mixture.

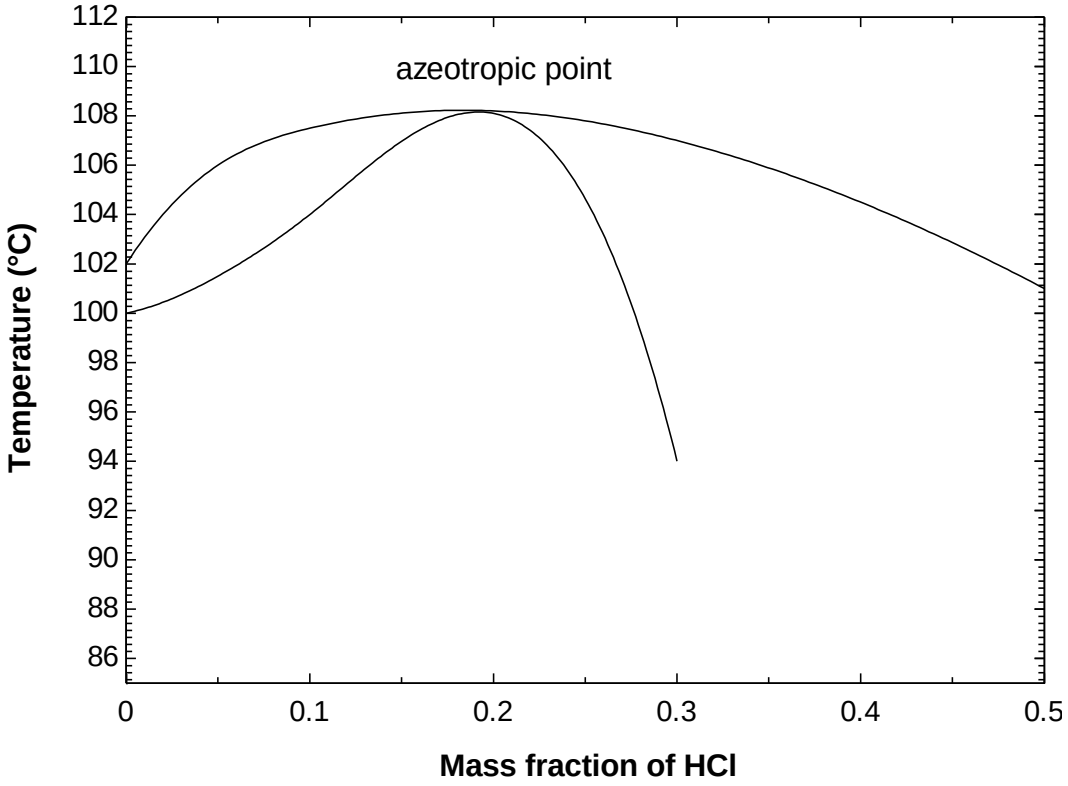

Figure 5.3 VLE phase diagram of HCl and water mixture.

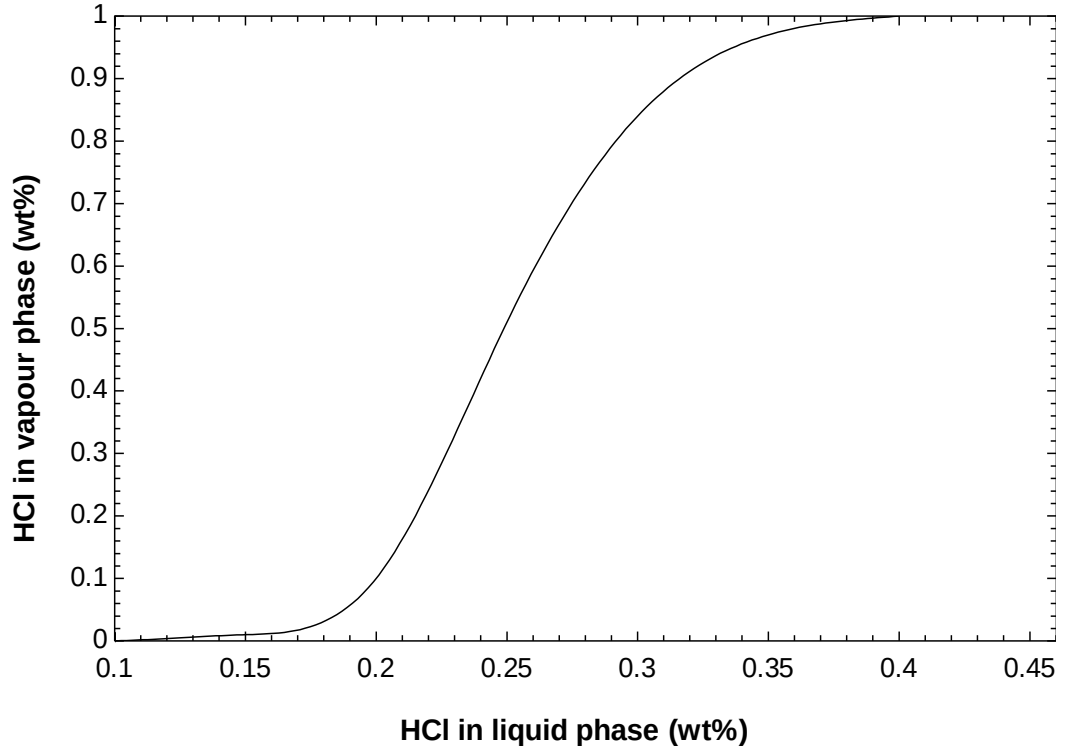

Figure 5.4 Equilibrium diagram of HCl and water mixture.

The same condition is expected at the azeotropic point but the volatility of the HCl significantly increases beyond that. The gas phase practically consists of only HCl for a fluid concentration of 40wt% and above. Therefore, the HCl acid of 36wt% may only be produced if the concentration of HCl gas is greater than 97wt% with reference to the gas moisture content.

The other key parameter to design the absorption process is a solvent flow rate that defines the concentration of the produced HCl acid for a known feed composition. Typically, the removal of absorption energy is performed at the column head when using water as a solvent to achieve higher concentration. In the proposed absorption process, using mixture of HCl and water at the azeotropic point as a solvent eliminates the necessity of such a cooling process. The degree of enrichment or the ease of separation is measured with the relative volatility between a pair of components. The relative volatility of most mixtures changes with temperature, pressure and composition. The more deviates from unity, the easier it is to separate the components of a mixture. At an azeotropic point, the relative volatility of the azeotrope-forming components equals to one and it is impossible further enrichment of the vapor [154]. Although the activity coefficient is unity for ideal solutions, for majority of chemical systems like HCl and H_2O mixture as a non-ideal system deviates and is strongly correlated to the composition. In order to consider this non-ideality, activity models should be used instead of equation of states, which is mainly used for ideal systems, to predict activity coefficients of the components in the liquid phase. Details of the property modeling and calculation are discussed in the following section.

5.1.2 Model development and simulation

The separation of mixtures by distillation is based on difference in volatility between the components. The higher the relative volatility results in the easier separation process. One of the most important steps to model and simulate the rectification and absorption processes is equilibrium-stage modelling. The schematic diagram of the equilibrium stage for a distillation column is shown in Figure 5.5. Liquid from the stage above and vapor from the stage below are brought into contact together counter-currently. Part of the condensed vapor is returned to the top of the column from the condenser to provide liquid flow above the feed point. Also, part of liquid at the bottom of the column is vaporized in the reboiler and returned back to provide the vapor flow. The column is hypothetically divided into two regions based upon the feed stream location. More volatile components are stripped from the liquid in the section below the feed and cause their concentration increases on the upper section of the column. Since the top product is required as a vapor, only the specific amount of vapor condensed to provide the liquid flow to the column. The condensed liquid flow is named the reflux flow and the condenser is referred to as a partial condenser. In a partial condenser, the reflux is in equilibrium with the vapor leaving the condenser.

The simulation of columns is performed by simultaneous calculation for all stages. It is assumed that vapor and liquid streams leaving the stage are in equilibrium with each other. The total material balance for stage *j* is expressed as below [155]:

$$V_{j+1} + L_{j-1} + F_j - (1 + R_j^{Vap})V_j - (1 + R_j^{Li})L_j = 0 \qquad (5.1)$$

where *V*, *L*, and *F* are the vapor, liquid, and feed molar flow rates respectively.

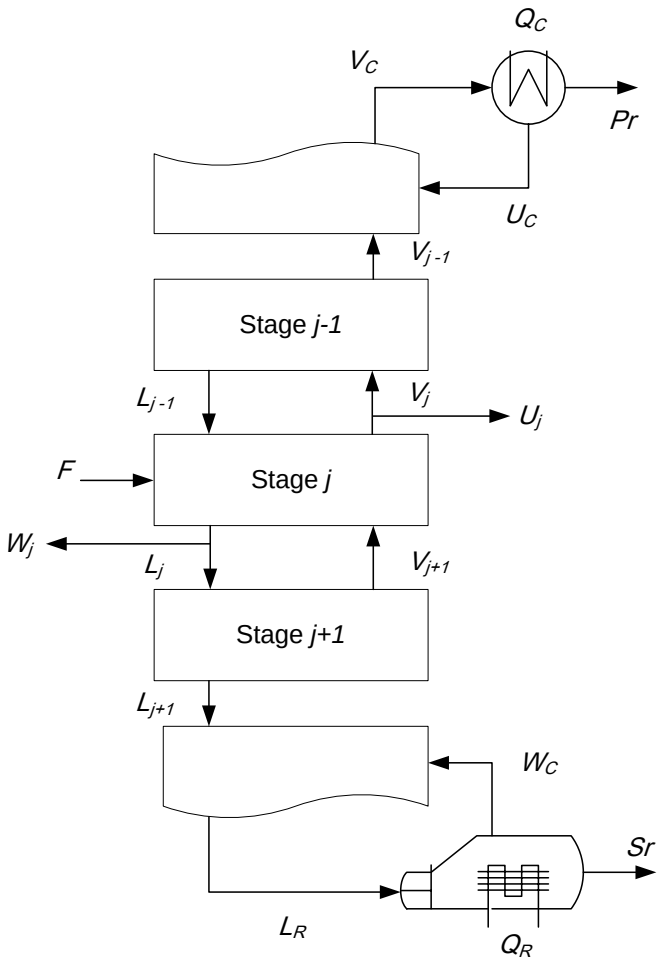

Figure 5.5 Equilibrium stage representation of a multistage column.

Here, R_j^{Vap} and R_j^{Li} are the ratio of the sidestream flow to the inter-stage flow as follows:

$$R_j^{Vap} = \frac{U_j}{V_j} \tag{5.2}$$

$$R_j^{Li} = \frac{W_j}{L_j} \tag{5.3}$$

where W and U are vapor and liquid sidestream flow rates. The component material balance is written as

$$V_{j+1}y_{i,j+1} + L_{j-1}x_{i,j-1} + F_j z_{i,j} - (1+R_j^{Vap})V_j y_{i,j} - (1+R_j^{Li})L_j x_{i,j} = 0 \quad (5.4)$$

where y and x are vapor-phase and liquid-phase mole fractions, and z is the feed composition. In the simulation, it is assumed that there is no sidestream flow except for the condenser and reboiler. The quantity of produced vapor that is being condensed and returned to the top of the rectification column is an important factor to be specified. The first stage R_j^{Vap} on the top the column is defined as the reflux ratio. Increasing the reflux ratio requires higher amount of heating duty which corresponds to the higher operation cost but reduces the number of stage required. Reflux ratio is one of the most important parameter in the operation of a distillation column that is needed to be carefully specified. Furthermore, the location of the feed point has a significant influence on the number of stage required and the column operation subsequently. In general, the feed stream should enter the column at the point that the feed composition matches the vapor and liquid streams in the column. In the simulated columns, pressure drop is assumed to be zero in all stages and stage efficiency is considered 1.0. Moreover, the mole fraction of the components is forced to sum to unity:

$$\sum_{i=1}^{n} x_{i,j} = 1, \ \sum_{i=1}^{n} y_{i,j} = 1, \ \sum_{i=1}^{n} z_{i,j} = 1 \quad (5.5)$$

The enthalpy balance equation is written as below [155], where h is the molar enthalpy and $\dot{Q}$ is the stage heat flow rate:

$$V_{j+1}h_{j+1}^{Vap} + L_{j-1}h_{j-1}^{Li} + F_j h_j^{Fe} - (1+R_j^{Vap})V_j h_j^{Vap} - (1+R_j^{Li})L_j h_j^{Li} - \dot{Q}_j = 0 \quad (5.6)$$

In the rectification process, the separation agent is energy. So, the energy balance equation should take into account the enthalpies of all entering and exiting streams and the energy duties of reboiler and condenser. It is assumed that the system operates adiabatically and there is no heat loss to the surroundings. The energy balance equation is written as follows:

$$Fh_{Fe} + \dot{Q}_R = Srh_{sl} + Prh_{pr} + \dot{Q}_C \tag{5.7}$$

where *F*, *Sr*, and *Pr* are molar flow rates of the feed, bottom product which is a solvent for absorption process, and top product respectively, *h* is the molar enthalpy, $\dot{Q}_R$ and $\dot{Q}_C$ are energy flow requirements in reboiler and condenser. It should be noticed that at the constant pressure, the stage temperature and therefore molar enthalpies are functions of the vapor and liquid compositions. The HRSG unit is simulated as a shell and tube heat exchanger at the steady state condition and without heat loss to surrounding. The heat exchanger is considered to have no pressure drop. The heat exchanger calculations are based on energy balances for the hot and cold streams. The fundamental equations for heat transfer across a surface are given by:

$$\dot{Q}_h = U_h A \Delta T_{LMTD} = \dot{n}_{shell} c_{p,shell} (t_2 - t_1) = \dot{n}_{tube} c_{p,tube} (T_1 - T_2) \tag{5.8}$$

where $\dot{Q}_h$ is the heat flow rate in a heat exchanger, $\dot{n}$ is a molar flow rate, c_p is the molar heat capacity at constant pressure, U_h is the overall heat transfer coefficient, and *A* is heat transfer area. *T* represents the inlet and outlet temperatures of a hot stream, which is the HCl and water mixture, and *t* symbolizes the inlet and outlet temperatures of a cold

stream, which is water to be vaporized. ΔT_{LMTD} is the log mean temperature difference (LMTD) for counter current flow and is calculated with the following equation:

$$\Delta T_{LMTD} = \frac{(T_1 - t_2) - (T_2 - t_1)}{\ln \frac{T_1 - t_2}{T_2 - t_1}} \tag{5.9}$$

The HRSG unit is considered to have a shell with two tube passes. The heat transfer coefficient and the surface area are often combined for convenience into a single variable referred to as *UA*. Minimum approach temperature is considered 10˚C [56].

The next step to simulate the HRSG unit and the separation system is property modelling and calculations. The key properties that are required to calculate mass and heat balance equations are fugacity and enthalpy. The fugacity of a real gas is an effective pressure which replaces the system mechanical pressure in accurate chemical equilibrium calculations [72]. The impact of property calculation on the simulation result is great and needs careful consideration. Applied thermodynamics provides two methods for representing the fugacity from the phase equilibrium relationship in terms of measurable state variables, the equation-of-state method and the activity coefficient method. In non-ideal systems like HCl and water mixture which the liquid fugacity of each component is not directly proportional to the mole fraction of the component, using activity coefficient method is appropriate. In the activity coefficient method:

$$f_i^{Vap} = \varphi_i^{Vap} y_i P \tag{5.10}$$

$$f_i^{Li} = x_i \gamma_i f_i^{*,Li} \tag{5.11}$$

where f_i^{Vap} and f_i^{Li} are the fugacity of component *i* in the vapor and liquid phase respectively, φ_i^{Vap} is the fugacity coefficient which for a vapor at moderate pressure is equal to unity [72], *P* is a pressure, x_i is the mole fraction of component *i* in the liquid phase, γ_i is the activity coefficient, and $f_i^{*,Li}$ is the liquid fugacity of pure component *i* at the mixture temperature. As it was mentioned earlier, the greater γ_i deviates from unity, the more non-ideal the mixture. For a mixture of HCl and H_2O, the activity coefficient is smaller than unity which could be interpreted as strong attraction between unlike molecules. In the activity coefficient method, the vapor enthalpy is calculated as follows:

$$h^{Vap} = h^{ig} + (h^{Vap} - h^{ig}) \tag{5.12}$$

Here, h^{Vap} is the vapor molar enthalpy, and h^{ig} is the molar ideal gas enthalpy which is calculated by the equation (5.13), where y_i is the mole fraction of component *i* in vapor phase, $c_{p,i}^{ig}$ is the ideal gas molar heat capacity, $\overline{\Delta h_{f\,i}}^{ig}$ is standard enthalpy of formation for ideal gas at the reference temperature and pressure of 25˚C and 101kPa respectively. Liquid mixture enthalpy is defined as follows:

$$h^{ig} = \sum y_i \left[\overline{\Delta h_{f\,i}}^{ig} + \int_{T^{ref}}^{T} c_{p,i}^{ig}(T)dT \right] \tag{5.13}$$

$$h^{Li} = \sum x_i \left(h_i^{*,Vap} - \Delta h_{Vap,i}^{*} \right) + h^{E,Li} \tag{5.14}$$

where $h_i^{*,Vap}$ is the pure component vapor enthalpy at *T* and vapor pressure, $\Delta h_{Vap,i}^{*}$ is the molar enthalpy of vaporization of component *i*, and $h^{E,Li}$ is excess liquid molar enthalpy

which is related to the activity coefficient with the below expression, where R is the universal gas constant:

$$h^{E,Li} = -RT^2 \sum_i x_i \frac{\partial \ln \gamma_i}{\partial T} \tag{5.15}$$

In simulation of the proposed integrated system using Aspen HYSYS, the NRTL (Non-Random-Two-Liquid) equation is an appropriate option to represent VLE, LLE (liquid-liquid equilibrium) behaviour of non-ideal HCl and water mixture. This equation contains adjustable temperature dependant and independent parameters to estimate binary coefficients of the mixture components. Accurate consideration of the HCl and water mixture reveals the fact that HCl in water instantly breaks up into positive H^+ ions and an equal number of Cl^- ions. That solution conducts electricity and fits the definition of electrolyte [152]. Ions are components which do not participate directly in vapor-liquid equilibrium. However, ions influence activity coefficients of the other species by interactions [156]. For example, addition of an electrolyte to a solution reduces its vapor pressure. It means that in the electrolyte solution of HCl and water, a larger variety of interactions and phenomena exist than in non-electrolyte solutions. Besides physical and chemical molecule-molecule interactions, ionic reactions and interactions could influence the simulation results. Consequently, electrolyte activity coefficient models like Electrolyte NRTL (ENRTL) which is chosen for this simulation, is more accurate than non-electrolyte activity coefficient models.

Figures 5.6 and 5.7 present the simulated process flow diagram (PFD) of separation process consisting of rectification and absorption columns and HRSG unit in Aspen HYSYS. All calculations are based on the production of 1kmol.h^{-1} HCl gas in the

rectification column which then fed into the absorption process. Heat duties in the reboiler and condenser are calculated for different possible feed concentration to provide flexibility when getting integrated to the hydrolysis process.

Figure 5.8 depicts simulated PFD of the rectification process. The concentration of HCl acid in the absorption column is studied for different operating conditions to simplify analysis of the integration to electrolysis process. The amount of steam could be generated in HRSG unit is calculated and compared to the hydrolysis reaction requirement. The results are presented in the next chapter. All calculations are based on the property package and material data bank in Aspen HYSYS. The modelling and simulation of the HRSG is based on Peng-Robinson equation property package.

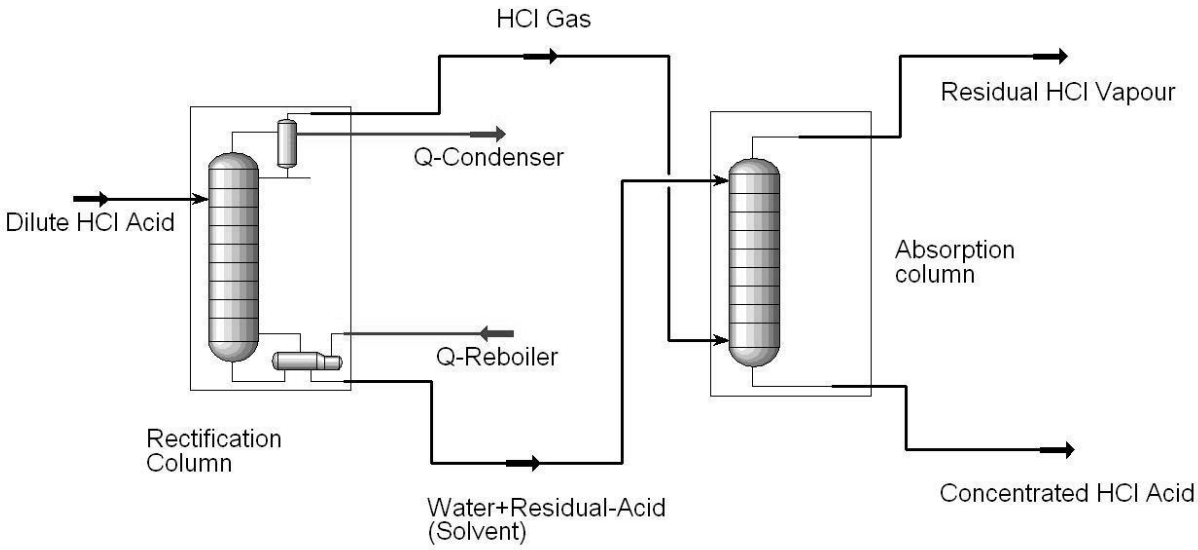

Figure 5.6 Simulated process flow diagram of the separation process.

Thermal efficiency of the CuCl cycle is very reliant on the amount of excess steam required for the hydrolysis reaction. Consequently, the amount of heat recovered in the HRSG could significantly help to improve the cycle energy efficiency.

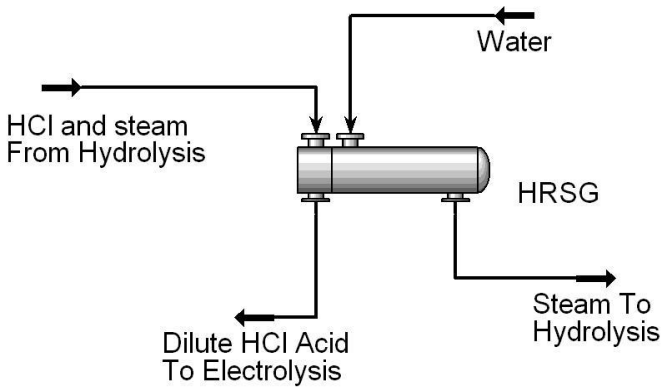

Figure 5.7 Simulated process flow diagram of HRSG.

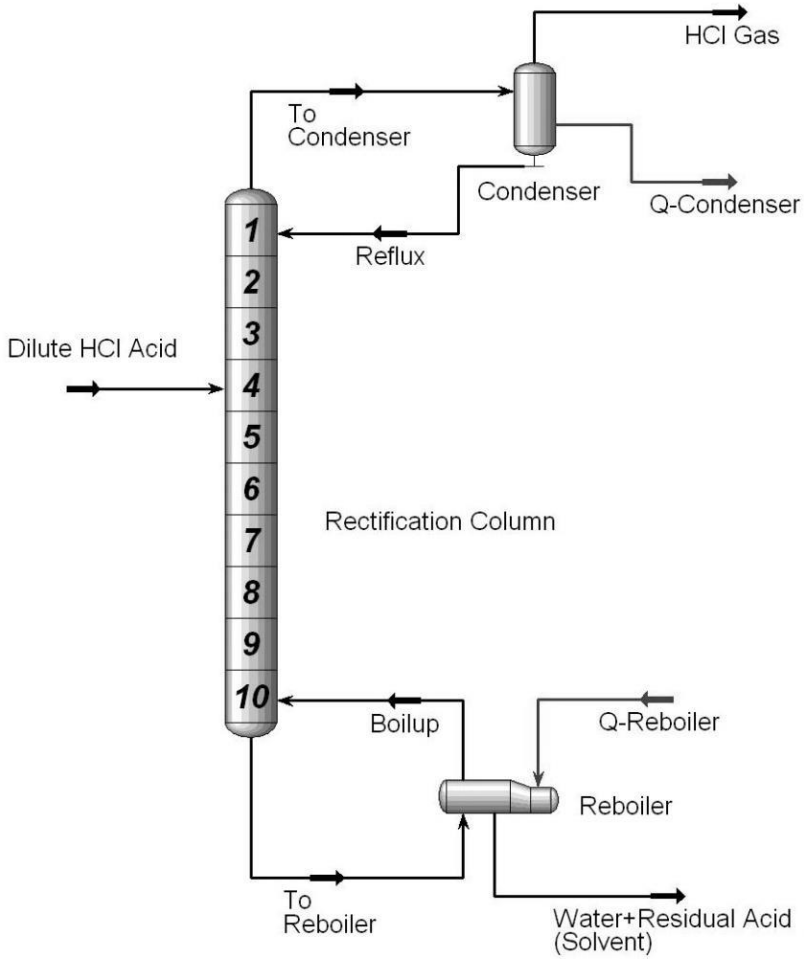

Figure 5.8 Simulated process flow diagram of the rectification process.

In order to quantify the effect of heat recovery on the cycle efficiency, heat requirements of the hydrolysis reaction and other processes should be estimated. Splitting water into hydrogen and oxygen requires sufficient energy to break the chemical bond of hydrogen and oxygen atoms. The minimum energy is equal to the enthalpy of formation of water which is 286 kJ.mol^{-1} at the standard condition [89]. Since, in the Cu-Cl cycle, a series of intermediate processes are required to split water, the energy required to split water will not completely dependent on the thermodynamic state alone and is also a function of each process. The energy efficiency of the Cu-Cl cycle is defined as below:

$$\eta_{Cu-Cl} = \frac{\overline{\Delta h_{f\ water}}}{(E^{m}_{in,heat} - E^{m}_{out,heat}) + E^{m}_{in,electricity}} \times 100 \tag{5.16}$$

where $\overline{\Delta h_{f\ water}}$ is the formation enthalpy of water in kJ.mol^{-1}, $E^{m}_{in,heat}$ and $E^{m}_{in,electricity}$ are the total heat required in the cycle and the electrical energy required in the electrolysis process per mole of hydrogen produced, respectively. $E^{m}_{out,heat}$ represents the sum of heat released internally within the cycle either by exothermic reactions or cooling processes. In order to calculate $E^{m}_{in,heat}$ and $E^{m}_{out,heat}$, the input and output heat for each process should be determined separately. The heat and electricity requirement of the 4-step Cu-Cl cycle are shown in Table 5.1 [89]. The percentage of heat loss to environment is assumed to be zero. In the hydrolysis reaction, the heat required to supply steam can be calculated as follows:

$$E^{m}_{in,steam} = n_{H_2O}\, \overline{\Delta h_{f\ water}}\Big|_{25^{\circ}C}^{400^{\circ}C} \tag{5.17}$$

where $E^{m}_{in,steam}$ is the heat required to generate steam at 400˚C from water at 25˚C per mole of hydrogen produced which is 57.61 kJ.mol^{-1} and n_{H_2O} is the mole of water.

Table 5.1 Heat and electricity requirements of the 4-step Cu-Cl cycle.

$E^{m}_{in,heat}$ Heat input (kJ.mol^{-1}H$_2$)	$E^{m}_{out,heat}$ Heat Output (kJ.mol^{-1}H$_2$)	$E^{m}_{in,electricity}$ Electricity input (kJ.mol^{-1}H$_2$)
1478.3	232	62.6

In the simulation of the separation system, heat flow rates of the rebolier and condenser are required to be minimized. The variables required to be specified in the column operation are characterized as either design variables or optimization variables. Design variables such as temperature, pressure, and flow rate of the feed stream are assumed constant based on the simulation assumptions. Moreover, the purity of produced HCl gas in the rectification column and the HCl concentration of the produced acid at the bottom of the absorption column are specified. On the contrary, optimization variables must arbitrarily be assigned different values which are subject to change from the base case to the optimal design. This procedure needs an iterative algorithm to calculate the reboiler and condenser heat duties for different set of values for the optimization variables. In this simulation, reflux ratio, number of stages in the column, solvent flow rate, solvent composition, location and composition of the feed stream are optimization variables. The optimization procedure using Aspen HYSYS requires setting the number of trays in both columns. But short-cut design analysis in the software provides the opportunity of analyzing the variation of reboiler heat duty as a function of reflux ratio. This facilitates the calculation of the optimum tray number and the feed location.

Selecting optimum feed location is critical to maximizing distillation column performance. Inappropriate selection of the feed location decreases the degree of separation at the same reflux ratio. An optimum feed location is the section of a distillation column where column internal liquid composition is similar to the feed stream composition. In this case, the optimization algorithm minimizes the composition gradient between feed stream and distillation internal fluids to find the optimal location. Reflux ratio has a significant impact on the reboiler and condenser heat flow rates and defines the purity of distillate.

5.2 Factorial design of the CuCl electrolysis operation

In industry, many engineers are facing the problems of dealing with the system analysis and how to determine the effects of various factors on the system outputs. Factorial design is an effective method to determine the influence of multiple dependent variables on desired independent variables or responses. Factorial design can reduce the number of experiments with the evaluation of multiple factors simultaneously. Moreover, it can be utilized to include the analysis of both main effects and interaction effects on the response variables. Although factorial design can only give relative values, it is a useful method to design experiments in both laboratory and industrial settings. Factorial design works well when interactions between variables are strong and important and where every variable contributes significantly. Optimization of experiments with the factorial design can lead to useful savings of scientific resources.

In the statistical analysis, a full factorial design is a series of experiments consisting of two or more factors, each with discrete possible values or levels, which

experimental units take into account for all possible combinations of these levels across all factors [157]. Such an experiment allows analysis of the effect of each factor as well as the effects of interactions between factors on the response variable. If the number of combinations in a full factorial design is too high to be logistically and economically feasible, a fractional factorial design is preferred in which some of the possible combinations are not considered. In a two-level factorial design, a 2^k factorial experiment is usually designed from a 2^{k-1} factorial experiment and 2^{k-1} replications which is a very reliable way of assessing experimental error [157].

The other useful extension of two-level fractional factorial designs is to incorporate center points into the factorial structure. Adding center points permits a statistical check for the accuracy of the fitness. The average response value from the actual center points is compared to the estimated value that comes from averaging all factorial points. If there is curvature of the response surface in the region of the design, the actual center point value will be either higher or lower than predicted by the factorial design points. Curvature of the surface may indicate that the design is in the region of an optimum [158].

In the CuCl electrolysis experiments, HCl and CuCl concentrations, solution flow rates, current densities and temperatures are treated as the main operation factors, and the cell voltage is considered as a response variable. The hydrogen production rate is measured for each experiment and compared with a theoretical production rate. A total numbers of 51 experiments are conducted including three replications and one center point. A period of 3 hours for each test confirms a stable operation.

A factorial model is composed of a list of coefficients multiplied by the associated factor levels as follows:

$$\mathrm{Y} = \theta_0 + \theta_1 \mathrm{A} + \theta_2 \mathrm{B} + \theta_3 \mathrm{C} + \theta_{12} \mathrm{AB} + \theta_{13} \mathrm{AC} + \ldots \quad (5.18)$$

where θ_n is the coefficient associated with factor n, and the letters, A, B, C, ... represent the factors in the model. Combinations of factors such as AB represent an interaction between the individual factors in that term [27]. Three-factor interactions are not considered is the model since the effects are negligible.

In order to calculate the theoretical amount of H_2 is produced in the electrolysis process, the amount of transferred electrons is correlated to the mole of hydrogen produced. The coulomb (C) is the unit of electric charge transported by a steady current of one ampere (A) in one second:

$$Q_C = It_s \quad (5.19)$$

where Q_C is the charge transported, I is the constant current density, and t_s is time in second. It should be mentioned that a coulomb is a charge quantity, not a particle quantity. 6.24×10^{18} electrons have one coulomb total charge. Theoretically, for two transported electrons, one hydrogen molecule is produced. Using the Avogadro constant which is defined as the number of molecules in one mole of a given substance, 6.022×10^{23} mol^{-1}, the mole of produced hydrogen is calculated [159]. The calculated value is then compared with the measured value in the experiment and the H_2 production ratio is then estimated.

$$H_2 \text{ production ratio} = \frac{\text{Experimental hydrogen production}}{\text{Theoretical hydrogen production}} \times 100 \quad (5.20)$$

In the CuCl electrolysis, factors A, B, C, D, and E represent HCl concentration, flow rate, temperature, current density, and CuCl concentration respectively. Y represents the response variable which is the cell potential. The factorial model is evaluated by analysis of variance (ANOVA) using a partial sums of squares (SS) to develop an explanation and confirm accuracy of the observed data. The results from ANOVA quantify the effect of factors and their interactions on the response variable. ANOVA is a statistical process for analysing the amount of variance that is contributed to a sample by different factors. It was initially introduced in 1925, for the case of equal numbers of observations for each level of a factor [160]. In probability theory and statistics, the variance is a measure of how far a set of numbers is spread out which describes how far the numbers are positioned from the mean or expected value [161]. When data is unbalanced, there are different ways to calculate the sums of squares for ANOVA. There are different types of ANOVA have been defined but, the focus here is on the partial SS method, which is explained below.

In order to simplify the explanation, a model is considered to include two factors A and B. Therefore, there are two main effects, and an interaction, AB. So, the full model is represented by SS(A, B, AB). As an example, SS(A, B) represents the model with no interaction effect and SS(B, AB) shows the model that does not include effects from factor A. The influence of particular factor including its interaction effects can be tested by examining the differences between models. The partial SS method tests for the presence of a main effect after the other main effect and interaction [160]. This approach

is therefore valid in the presence of significant interactions. In this method, SS(A | B, AB), which is the sum of squares for the main effect A after the main effect B and interaction, is tested and then SS(B | A, AB), which is the sum of squares for the main effect B after the main effect A and interaction, is examined and compared.

$$SS(A \mid B, AB) = SS(A, B, AB) - SS(B, AB) \tag{5.21}$$

$$SS(B \mid A, AB) = SS(A, B, AB) - SS(A, AB) \tag{5.22}$$

The partial sum of squares is also called deleted sum of squares because the value of the SS for each parameter is calculated as the difference between the residual SS (RESS) when the parameter is included or not [160]. It is the best way to calculate SS for unbalanced data. RSS is a measure of the discrepancy between the data and an estimation model which is defined as below:

$$\mathrm{RESS} = \sum_{i=1}^{n} (y_i - f(x_i))^2 \tag{5.23}$$

where y_i is the measured value of the variable i and $f(x_i)$ is its predicted value by the fitted model. An experimental design summary which includes design, factor, and response information are given in Table 5.2. The response variable, cell potential, varies from 0.53V to 1.44V which is less than the decomposition potential of water electrolysis. In the water electrolysis, hydrogen production starts at 1.65V which is experimentally measured with the same test bench. This confirms that the rate of produced hydrogen corresponds solely to the oxidation of CuCl.

Table 5.2 Summary of experimental conditions for CuCl electrolysis.

Factor	Name	Units	Minimum	Maximum	Mean	Std. Dev.
A	HCl Concentration	Molar	6	10	8	1.940
B	Flowrate	L min^{-1}	0.1	0.5	0.3	0.194
C	Temperature	C	25	60	42.5	16.977
D	Current Density	A cm^{-2}	0.1	0.5	0.3	0.194
E	CuCl Concentration	Molar	0.5	1	0.75	0.243
Response	Name	Units	Obs	Minimum	Maximum	Mean
Y	Cell Potential	V	51	0.53	1.40	0.972
Std. Dev.	0.288					

5.3 Modeling and simulation of a gasification process in an IGCC power generation system

5.3.1 Thermodynamic modeling of a gasification process

The chemistry of gasification is complex since there are several processes occurring simultaneously. In order to develop a gasification model, the chemical formula of feedstock is considered as $CH_aO_bN_c$ and the general gasification reaction is defined as below in equation (5.24), where a, b, and c represent the number of atoms of hydrogen, oxygen, and nitrogen per number of atom of carbon respectively. The composition of feedstock, which is obtained by ultimate analysis of the Illions #6 coal, is based on Texaco gasification process [162] as shown in Table 5.3.

$$CH_aO_bN_c + mH2O + w(O_2 + 3.76N_2) = n_{H_2}H_2 + n_{CO}CO + n_{CO_2}CO_2 + n_{H_2O}H_2O + n_{CH_4}CH_4 + (\frac{c}{2} + 3.76w)N_2 \quad (5.24)$$

The initial stages of gasification are partial oxidation and pyrolysis which occur in the absence of oxygen. Partial oxidation occurs when a carbonaceous fuel reacts with less than the stoichiometric amount of oxygen. Once all of the oxygen is consumed, the high operating temperature of the gasifier devolatilizes the volatile components of the feedstock. These processes result in a two-phase system consisting of a gas phase and a carbon-based solid phase known as char. The main components of syngas, CO and H_2, are then produced by steam reforming of the carbon-based char. If the temperature of the gasifier is high enough, all the char can be converted to CO and H_2 and the 'water-gas' reaction, as stated in equation (5.26), reaches completion.

Table 5.3 Composition of the gasification feedstock.

Feed composition	wt%
Moisture	11.12
Carbon	63.75
Hydrogen	4.50
Nitrogen	1.25
Oxygen	6.88
Chlorine	0.29
Sulfur	2.51
Ash	9.70

The most desired product of a gasification process is usually hydrogen. In the final stage of gasification, steam reforming of CO produces H_2 according to the 'water-gas shift' reaction, as written in equation (5.26). Unlike partial oxidation and steam reforming, the water-gas shift reaction does not convert all reactants into products. The extent of reaction is determined by its equilibrium point, which is a function of

temperature and steam concentration. The partial oxidation, water-gas, and water-gas shift reactions are shown in equations (5.25), (5.26), and (5.27), respectively. Some methane often produced in the gasification process with the reaction shown in equation (5.28). However, it is not considered in the calculation since coexists in relatively small quantity in comparison to H_2 and CO_2. All inputs on the left-hand side of the below equations are defined at 25˚C:

$$C + O_2 \rightarrow CO_2 \ , \quad \Delta H° = -390 \text{ kJ} \tag{5.25}$$

$$C + H_2O \rightarrow CO + H_2 \ , \quad \Delta H° = +130 \text{ kJ} \tag{5.26}$$

$$CO + H_2O \longleftrightarrow CO_2 + H_2 \ , \quad \Delta H° = -42 \text{ kJ} \tag{5.27}$$

$$C + 2H_2 \longleftrightarrow CH_4 \ , \quad \Delta H° = -71 \text{ kJ} \tag{5.28}$$

Here, $\Delta H°$ is the enthalpy of reaction for 1 mole of the pure substance, at a temperature of 25°C, and a pressure of 1 atmosphere [72]. If $\Delta H°$ is positive, the reaction is endothermic and requires heat to be absorbed by the system since the reaction products have a greater enthalpy than the reactants. In the contrary, if $\Delta H°$ is negative, the reaction is exothermic and is achieved by the generation of heat. In the above equations, the one-sided arrows indicate that the reactions are irreversible in the forward direction. The double-sided arrows indicate that the reaction can precede in either the forward or reverse direction. Equilibrium is reached when the rate of change of the forward and reverse reactions are equal.

Gasification is modeled as a thermodynamic system at chemical equilibrium. Solving reaction equilibrium together with the mass and energy balances gives the desired equilibrium composition and the system temperature. In practice, a gasifier is a

dynamic system where both chemical equilibrium and reaction kinetics both have a role. It is assumed that all processes occur at a steady-state condition, potential and kinetic energy changes are negligible, H_2, CO, and CO_2 are the main product gases of the gasification process and considered ideal, the gasifer is isothermal at an equilibrium state, and the syngas at the gasifier outlet is at the gasification temperature. Since the produced gases are assumed ideal, their enthalpy is only a function of temperature. The environment and reference state is considered at 25°C and 1bar. The resident time in the gasifier is sufficient to operate the gasifier under the equilibrium mode. The chemical equilibrium constant *K* of reaction (5.27) is defined as follows:

$$K = \exp\left(\frac{-\Delta G}{RT}\right) \tag{5.29}$$

$$\Delta G = \Delta H - T\Delta S \tag{5.30}$$

where ΔG denotes the Gibbs free energy change of reaction (5.27) while *R* and *T* are the universal gas constant and the gasifier temperature, respectively. The Gibbs free energy change is calculated as per equation (5.30), where ΔH and ΔS denote the change in enthalpy and entropy of the water-gas shift reaction, respectively. The equilibrium constant of a chemical reaction depends on the Gibbs free energy change and the reaction temperature. The Gibbs free energy change of a reaction is a thermodynamic function that measures the difference in energy between products and reactants. When ΔG is positive, the reverse reaction is spontaneous. The forward reaction is spontaneous when ΔG is negative and when it is zero, the system has reached an equilibrium state.

$$\Delta H = \Delta H_{ref} + \int \Delta C_p dT \tag{5.31}$$

$$\Delta S = \Delta S_{ref} + \int \frac{\Delta C_p}{T} dT \tag{5.32}$$

Here, ΔH_{ref} and ΔS_{ref} are the change in enthalpy and entropy of reaction (5.27) at reference conditions, 25°C and atmospheric pressure, respectively. If the change in heat capacity ΔC_p is assumed to be constant, then equations (5.31) and (5.32) can be rewritten as follows:

$$\Delta H = \Delta H_{ref} + \Delta C_p (T - T_{ref}) \tag{5.33}$$

$$\Delta S = \Delta S_{ref} + \Delta C_p \ln\left(\frac{T}{T_{ref}}\right) \tag{5.34}$$

where T and T_{ref} is the gasification and thermodynamic reference temperatures respectively. The change in the reference molar enthalpy and entropy and the change in heat capacity are calculated as follows:

$$\Delta h_{ref} = \overline{\Delta h_f}_{\,CO_2} + \overline{\Delta h_f}_{\,H_2} - \overline{\Delta h_f}_{\,CO} - \overline{\Delta h_f}_{\,H_2O} \tag{5.35}$$

$$\Delta s_{ref} = s^o{}_{CO_2} + s^o{}_{H_2} - s^o{}_{CO} - s^o{}_{H_2O} \tag{5.36}$$

$$\Delta c_P = c_{P\,CO_2} + c_{P\,H_2} - c_{P\,CO} - c_{P\,H_2O} \tag{5.37}$$

Here, $\overline{\Delta h_f}$ and s^o denote the standard enthalpy of formation and standard molar entropy for chemical species respectively. Similarly, c_p denotes the molar heat capacity of chemical species at constant pressure. The ideal gas enthalpy formation and standard molar entropy of for CO_2, H_2, CO, and H_2O are listed in Table 5.4 [163].

Table 5.4 Standard enthalpy of formation and standard molar entropy at 25°C.

Substance	Standard enthalpy of formation, $\overline{\Delta h_f}$ (kJ kmol^{-1})	Standard molar entropy, s^o (kJ kmol^{-1}K^{-1})
CO	−110,525	197.653
CO_2	−393,509	213.795
H_2O	−241,818	188.833
H_2	0	130.684
C(s)	0	5.74
O_2	0	205.138
N_2	0	191.61

The standard enthalpy of formation of a substance is the change of enthalpy from the formation of one mole of the compound from its elements, with all substances in their standard states. All elements in their standard states such as hydrogen, oxygen, nitrogen, and solid carbon in the form of graphite have a standard enthalpy of formation of zero, as there is no change involved in their formation. Standard molar entropy is the entropy content of one mole of substance and unlike standard enthalpies of formation has an absolute value at the room temperature. The molar heat capacity at constant pressure of the ideal gases in kJ.kmol^{-1}.K^{-1} are calculated by the below polynomial equations with the good estimation for the range of 26°C to 3220°C [164] where β is the temperature in Kelvin divided by 100:

$$H_2: c_p = 56.5 - 702.7\beta^{-0.75} + 1165\beta^{-1} - 560.7\beta^{-1.5} \quad (5.38)$$

$$O_2: c_p = 37.4 + 0.02\beta^{1.5} - 178.5\beta^{-1.5} + 236.8\beta^{-2} \quad (5.39)$$

$$N_2: c_p = 39 - 512.7\beta^{-1.5} + 1702.7\beta^{-2} - 820.4\beta^{-3} \quad (5.40)$$

$$CO_2: c_p = -3.73 + 30.5\beta^{0.5} - 4.1\beta + 0.02\beta^2 \quad (5.41)$$

$$CO: c_p = 69.1 - 0.7\beta^{0.75} - 200.77\beta^{-0.5} + 176.7\beta^{-0.75} \quad (5.42)$$

$$H_2O: c_p = 143.05 - 183.5\beta^{0.25} + 82.7\beta^{0.5} - 3.69\beta \quad (5.43)$$

Equations (5.29) to (5.37) show that the equilibrium constant only depends on the reaction temperature. The gasification temperature is one of the key variables in this analysis. The equilibrium constant of a reaction can be calculated based on the Gibbs free energy change and temperature as per equation (5.29), and by the relative concentration of each molecule at equilibrium:

$$K_3 = \frac{a_{CO_2}\ a_{H_2}}{a_{CO}\ a_{H_2O}} \quad (5.44)$$

where a_i denotes the activity of chemical species i. For an ideal gas, the activity could be represented by the partial pressure P_i. Similarly, partial pressures could be represented in terms of the mole fraction, v_i, of species i and the total pressure P_{tot}:

$$K = \frac{P_{CO_2}\ P_{H_2}}{P_{CO}\ P_{H_2O}} \quad (5.45)$$

$$K = \frac{(v_{CO_2} P_{tot})\ (v_{H_2} P_{tot})}{(v_{CO}\ P_{tot})\ (v_{H_2O}\ P_{tot})} \quad (5.46)$$

$$K = \frac{v_{CO_2}\ v_{H_2}}{v_{CO}\ v_{H_2O}} \quad (5.47)$$

Equation (5.47) indicates that the value of the equilibrium constant will determine the ratio of products to reactants. The formation of products is favoured over reactants If

$K > 1$ while the opposite reaction is dominant if $K < 1$. The mole fraction of the reaction components is determined by calculating the relative amount of the gas at equilibrium:

$$v_i = \frac{n_{i,eq}}{n_{tot,eq}} \tag{5.48}$$

$$n_{tot,eq} = \sum_{i=1}^{N} n_{i,eq} \tag{5.49}$$

where $n_{i,eq}$ and $n_{tot,eq}$ are the number of moles of species i and the total number of moles at equilibrium, respectively. The number of moles of a molecule at equilibrium depends on the initial number of moles and the reaction network. An Initial Change Equilibrium (ICE) chart is used to predict the equilibrium concentration as shown in Table 5.5. Since reactions (5.25) and (5.26) are assumed to react completely, the equilibrium concentration of C and O_2 are zero. The equilibrium concentrations of the other species are based on initial values and the extent of chemical reactions X.

In Table 5.5, the extent of chemical reaction X refers to the amount of reactant moles that are consumed in the reaction. For the partial oxidation reaction or equation (5.25), X_1 is equal to the initial amount of O_2 because all of the oxygen reacts with carbon. For the water-gas reaction or equation (5.26), X_2 is equal to the remaining amount of carbon, which is assumed to react completely. It means

$$X_1 = n_{O_2,0} \tag{5.50}$$

$$X_2 = n_{C,0} - n_{O_2,0} \tag{5.51}$$

Equations (5.47) to (5.51) are used to solve for X_3 and express it as a function of other variables as follows:

$$X_3 = \frac{-b + \sqrt{b^2 - 4ac}}{2a} \tag{5.52}$$

where

$$a = 1 - k_3 \tag{5.53}$$

$$b = X_1 + X_2 + K_3 n_{H_2O,0} \tag{5.54}$$

$$c = X_1 X_2 - K_3 n_{H_2O,0} X_2 + K_3 {X_2}^2 \tag{5.55}$$

Once X_1, X_2, and X_3 are specified, the syngas composition can be predicted based on the correlations provided in Table 5.5.

$$y_{CO} = \frac{X_2 - X_3}{n_{H_2O,0} + X_1 + X_2} \tag{5.56}$$

$$y_{H_2O} = \frac{n_{H_2O,0} - X_2 - X_3}{n_{H_2O,0} + X_1 + X_2} \tag{5.57}$$

$$y_{H_2} = \frac{X_2 + X_3}{n_{H_2O,0} + X_1 + X_2} \tag{5.58}$$

$$y_{CO_2} = \frac{X_1 + X_3}{n_{H_2O,0} + X_1 + X_2} \tag{5.59}$$

The thermodynamic model in equations (5.29) to (5.59) is solved simultaneously to predict the equilibrium composition of the produced syngas based on the temperature of the gasifier and the amount of input oxygen and steam.

Table 5.5 ICE chart for the gasification reactions.

Molecule	I	C	E
C	$n_{C,0}$	$-X_1 - X_2$	0
O_2	$n_{O_2,0}$	$-X_1$	0
CO	0	$+X_2 - X_3$	$X_2 - X_3$
H_2O	$n_{H_2O,0}$	$-X_2 - X_3$	$n_{H_2O,0} - X_2 - X_3$
H_2	0	$+X_2 + X_3$	$X_2 + X_3$
CO_2	0	$+X_1 + X_3$	$X_1 + X_3$
Total	$n_{C,0} + n_{O_2,0} + n_{H_2O,0}$	$-X_1$	$n_{H_2O,0} + X_1 + X_2$

For a gasification process at a steady-state condition as depicted in Figure 5.9, mass flow into the gasifier is equal to the gasifier outlet mass flow. Thus, the mass balance is determined from the following equation, where *N* and *M* are the total numbers of inlet and outlet streams, respectively.

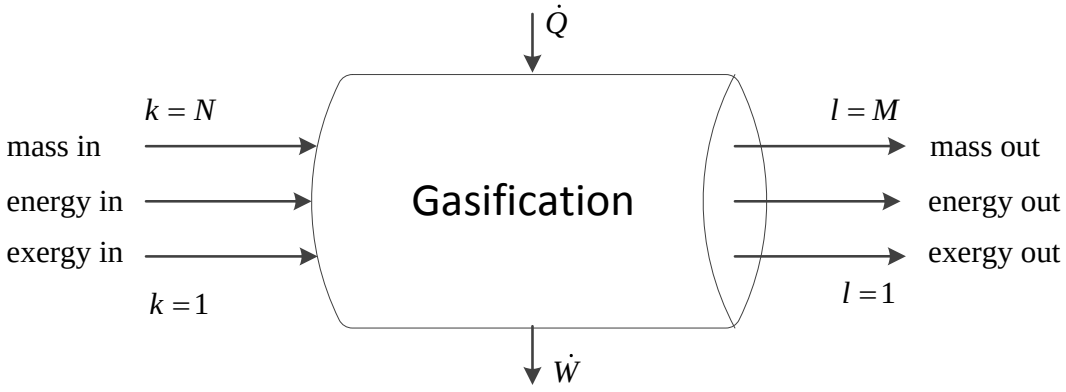

Figure 5.9 Schematic diagram of a steady-state gasification process.

$$\sum_{k}^{N} \dot{m}_{in} = \sum_{l}^{M} \dot{m}_{out} \tag{5.60}$$

The mass flow rate is calculated in terms of the molar flow rate and substituted into the mass balance equation, where *MW* is the molecular weight.

$$\sum_{k}^{N} \dot{n}_k MW_k = \sum_{l}^{M} \dot{n}_l MW_l \tag{5.61}$$

The energy balance equation can be written as follows, where $\dot{Q}$ and $\dot{W}$ are the net heat and work rates (power) crossing the gasifier boundary, respectively:

$$\sum_{k}^{N} \dot{m}_k h_k^m + \dot{Q} = \sum_{l}^{M} \dot{m}_l h_l^m + \dot{W} \tag{5.62}$$

The energy flows of the fuel entering the gasification process are calculated in terms of the lower heating vale (LHV). The LHV is obtained by subtracting the latent heat of vaporization of the water vapor formed in the combustion process from the higher heating value (HHV) of the fuel. The HHV value of the fuel is considered 27.1 $MJ.kg^{-1}$ based on Texaco gasification process.

$$\dot{E}_{fuel} = \dot{m}_{fuel} \mathrm{LHV}_{fuel} \tag{5.63}$$

The exergy balance equation can be represented in the following form using exergy values of all streams entering and leaving the gasifier. The main difference between the exergy and energy balance equation is that exergy is not conserved. It means that the exergy leaving the gasifier will always be less than the exergy inflow. The difference between all entering exergy streams and the exiting streams is called the rate of exergy destruction, $\dot{E}x_{des}$. Exergy destruction represents the internal exergy loss in the gasification process as a result of thermodynamic irreversibilities. The losses of exergy which regarded as an available work are due to entropy generation during fluid flow, heat and mass transfer, and chemical reaction.

$$\sum_{k}^{N} \dot{E}x_{in} + \left(1 - \frac{T_0}{T}\right)\dot{Q} = \sum_{l}^{M} \dot{E}x_{out} + \dot{W} + \dot{E}x_{des} \tag{5.64}$$

The exergy content of the gasification inlet and outlet streams are divided into two major components. The physical exergy is calculated by enthalpy and entropy data where h and s are the specific enthalpy and entropy of a stream at a given temperature and pressure, h_0 and s_0 are specific enthalpy and entropy at the reference state, respectively:

$$\dot{E}x_k = \dot{E}x_{ch,k} + \dot{E}x_{ph,k} \tag{5.65}$$

$$\dot{E}x_{ph,k} = \dot{m}\left[\left(h_k - h_0\right) - T_0\left(s_k - s_0\right)\right] \tag{5.66}$$

The chemical exergy of a mixture is determined by the composition and concentration of its components:

$$Ex_{ch,k} = \sum_{k}(x_k Ex^{o}_{ch,k}) + RT_0 \sum_{k}(x_k \ln x_k) \tag{5.67}$$

The standard chemical exergy of a chemical substance, Ex^{o}_{ch}, is defined as the maximum work that can be obtained when the considered system is brought into reaction with reference substances present in the environment. Defining the exergy reference environment is one of the most vital parts of analyzing chemical exergy [165]. In general, the environment is defined as the composition of air at 25°C and the pressure of 101kPa. The values of standard chemical exergy of some substance are listed in Table 5.6.

In general, the chemical exergy of solid fuels are calculated based on the below statistical correlation for different oxygen and hydrogen to carbon ratios [143]:

$$Ex_{ch,\,fuel} = \lambda \mathrm{LHV}_{fuel} \tag{5.68}$$

for $\frac{O}{C} \le 0.5$,

$$\lambda = 1.0438 + 0.0158\frac{H}{C} + 0.0813\frac{O}{C} \tag{5.69}$$

and for $0.5 \le \frac{O}{C} \le 2$,

$$\lambda = \frac{1.0414 + 0.0177(\frac{H}{C}) - 0.3328(\frac{O}{C})\left[1 + 0.0537(\frac{H}{C})\right]}{1 - 0.4021(\frac{O}{C})} \tag{5.70}$$

The LHV value of a fuel is the amount of heat released during its complete combustion. The syngas heating value on a molar basis is calculated as the sum of the heat of combustion, at 25°C and 1atm, multiplied by the mole fraction for each component in a syngas.

Table 5.6 Standard chemical exergy of some substances [163].

Substance	Ex_{ch}^{o} (kJ kmol^{-1})
CO	275,430
CO_2	20,141
H_2O	11,710
C(s)	410,260
H_2	238,500
O_2	3,900
N_2	720

The exergy efficiency of the gasification process is defined as the ratio between useful exergy outputs to the necessary exergy input to the gasifier. It can be expressed in the following manner, where *Ex* is the exergy flow rate of the inlet and outlet streams:

$$\psi = \frac{\dot{E}x_{syngas}}{\dot{E}x_{fuel} + \dot{E}x_{steam} + \dot{E}x_{air}} \tag{5.71}$$

5.3.2 Simulation of the gasification process in an IGCC power plant

In this section, a process simulation tool, Aspen HYSYS, is used to develop a predictive model for a gasification process and its exegetic efficiency. The tool is used to analyze the performance of a gasification process in various operating conditions. Process integration analysis with the Cu-Cl cycle is performed for calculating the external heat required in the hydrolysis process. Process data of an industrial Texaco gasification process [160] and gas cooling unit are used as a reference base case. The integration with a Cu-Cl cycle is based on its individual process energy requirements [89].

The main concept of integration is that the oxygen produced in the Cu-Cl cycle is used instead of air in the gasification process and the heat provided for steam generation by the syngas cooling unit of the IGCC power plant is used to provide part of the external heat required for the Cu-Cl cycle in the hydrolysis reaction. The IGCC process model is developed based on the configuration of a Texaco gasifier with an integrated cooling system. The IGCC simulation model is comprised of two main parts: gasification subsystem and combined cycle subsystem consists of a gas and steam turbines. In the gasification unit, which is the main focus of this study, the produced syngas is cooled down from the gasification temperature to the temperature around 230°C and then passes through a gas scrubber and a cleaning process. Figure 5.10 shows that the gas cooling section of a gasification process could be effectively coupled with the hydrolysis reaction of the Cu-Cl cycle using a heat recovery steam generator unit.

In the original design of the IGCC by Texaco, the syngas cooling section of the gasification unit supplies part of the steam requirement of the combined cycle subsystem to generate electricity. Small modification to the steam cycle in IGCC could redirect part of the produced steam in the gas cooling process to the hydrolysis reaction at 400°C. This modification is illustrated to have minor effects on the IGCC overall efficiency [7]. The influence of heat recovery in the hydrolysis reaction of the Cu-Cl cycle is analyzed in the next chapter. Figure 5.11 depicts a process flow diagram of the simulated gasification process.

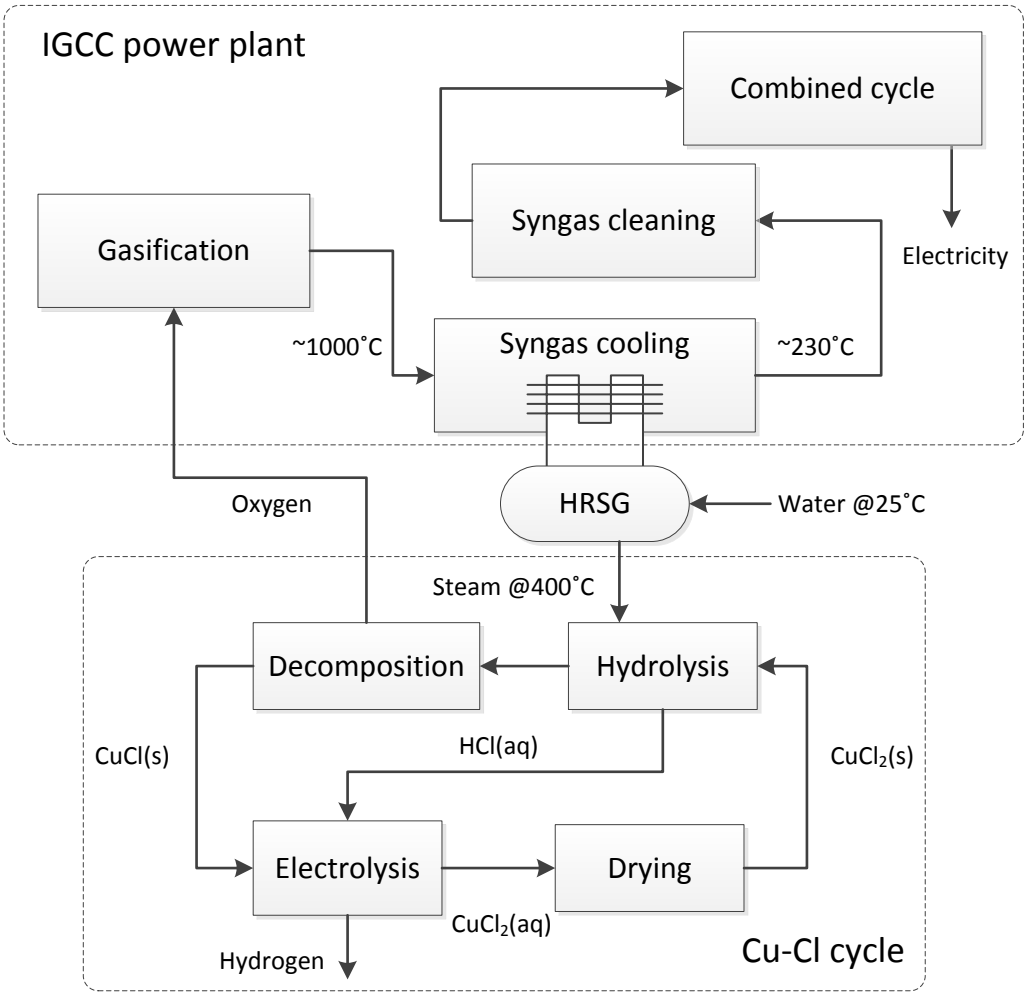

Figure 5.10 Schematic diagram of an integrated IGCC and the Cu-Cl cycle.

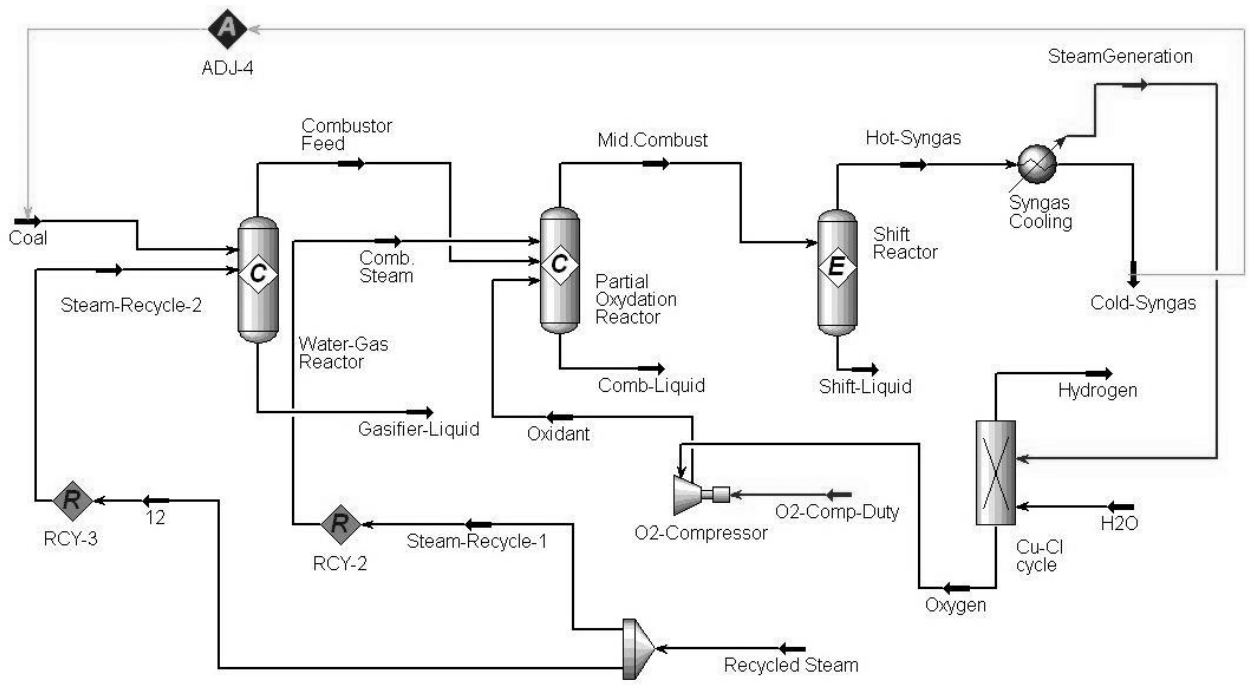

Figure 5.11 Simulation flow sheet of the gasification process.

The production of synthesis gas is an important part of the overall process of IGCC. The conversion of coal into syngas is modeled by two conversion reactions and an equilibrium reaction. The ratio of H_2 to CO defines the suitable application of the syngas. This ratio represents the stoichiometric amounts of the reactants in the gasification process. In a typical syngas process, two reactors are needed. This model requires three reactors since the conversion and equilibrium reactions cannot be placed in the same reaction set in Aspen HYSYS, and thus cannot be placed in the same reactor. The gasification reactions are separated into two conversion reactors and an equilibrium reactor. Coal is reformed in the first conversion reactor (reformer) when combined with steam. Oxygen is added to the second reactor at a controlled flow rate, such that the desired ratio of H_2 to CO in the synthesis gas is attained. The addition of steam to the second reactor serves the dual purpose of maintaining the reactor temperature and

adjusting the syngas composition. The gasification process is simulated for 1kmol.s^{-1} of feedstock. Sensitivity analysis is conducted to investigate the effects of operation factors such as equivalence ratio, gasification temperature, and steam to carbon ratio on the exergy efficiency and the syngas composition.

Chapter 6: Results and Discussion

In this chapter, results of modeling, simulation and experimental work are presented. Predictions of the theoretical modeling related to the integration of the hydrolysis and electrolysis processes, as well as process integration of the Cu-Cl cycle with a gasification system are validated by comparison against previous research and works in literature and information abstained from related industries, which all have been cited accordingly. Results and trends in the experimental analysis of the electrolysis process are verified through comparison between predicted and measured data. It is also validated with results from other experimental investigations, which have been cited on the previous chapters.

6.1 Process integration of hydrolysis and electrolysis processes

An effective integration of the hydrolysis and electrolysis processes of the Cu-Cl cycle of hydrogen production is one of the main objectives of this thesis. The proposed methodology introduces an intermediate system including HRSG unit, to provide excess steam required for the hydrolysis reaction, and separation system consisting of rectification and absorption column to recover dry HCl gas and produce concentrated HCl acid for the electrolysis reaction. There is no general solution since the effects of parameter variations provide different possibilities. But the main simulation criteria are to minimize energy required for the separation process, providing concentrated 22mol% HCl acid to the electrolysis from dilute 13.5mol% HCl acid coming from the hydrolysis,

and generating high temperature steam for the hydrolysis reaction which could significantly increase thermal efficiency of the Cu-Cl cycle.

In HRSG, HCl and steam mixture from hydrolysis at 400˚C is condensed to dilute HCl acid at 90˚C and then fed into the separation process which concentrated HCl acid is produced for the electrolysis reaction. In the separation system, dilute HCl acid with the concentration of 13.5mol% is fed into the rectification column where dry HCl gas is produced on the top of the column. The mixture of water and residual HCl at azeotropic concentration leaves the bottom of the column and is used as a solvent instead of water in the absorption process. Dry HCl gas temperature is 70˚C in the absorption column where the solvent is at 80˚C. Concentrated HCl acid leaves the column at 22mol% and temperature of 80˚C which is absolutely appropriate for the electrolysis reaction.

In simulation of the rectification column, see Figure 5.2, HCl gas flow rate, F_T, and the reflux ratio, R, should be specified to calculate reboiler and condenser heat flows, $\dot{Q}_R$ and $\dot{Q}_C$, in addition to concentration, mass, and temperature profiles. The column operates at ambient pressure and the feed stage is 4. In order to analyze and compare the effects of column configuration on the simulation, the results are presented for columns with different number of stages. Figures 6.1 and 6.2 depict the effects of the reflux ratio and HCl gas flow rate on HCl concentration of the top and bottom products for a column with 10 and 15 stages respectively. The feed flow rate is specified to be 18kmol.h^{-1} with HCl concentration of 13.5mol% and the temperature of 90˚C.

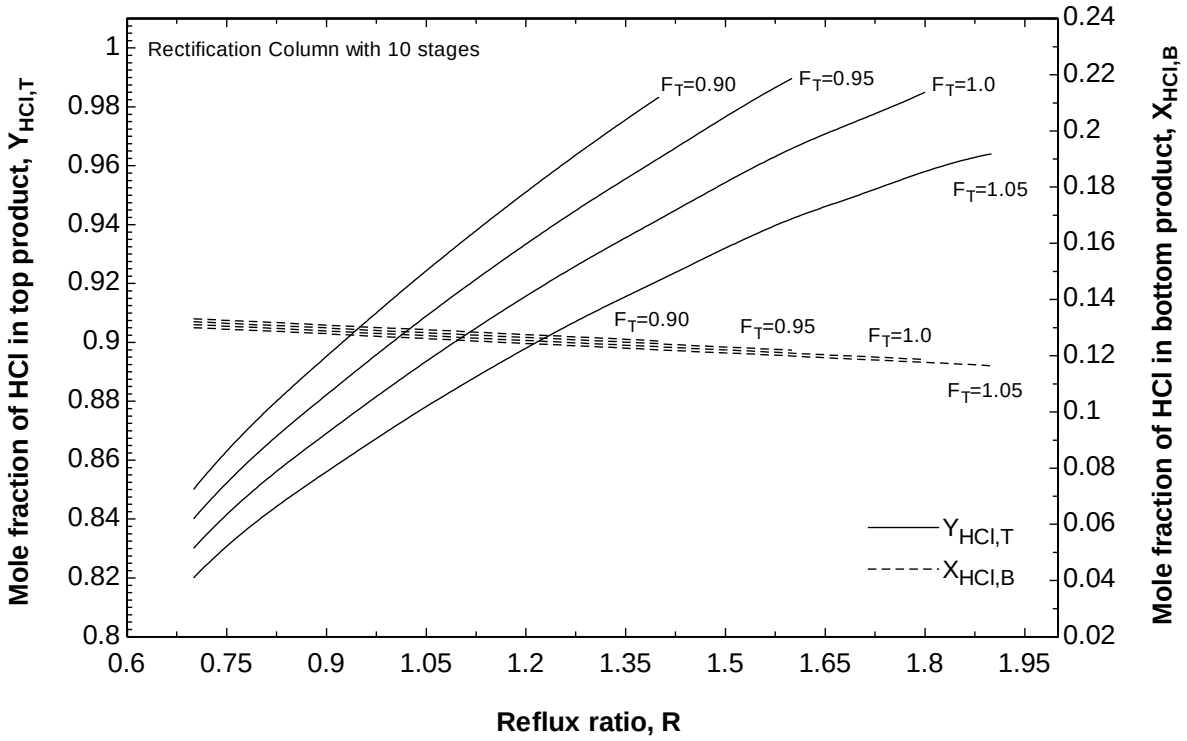

Figure 6.1 Influence of the reflux ratio and HCl gas flow rate on the concentration of products, column with 10 stages.

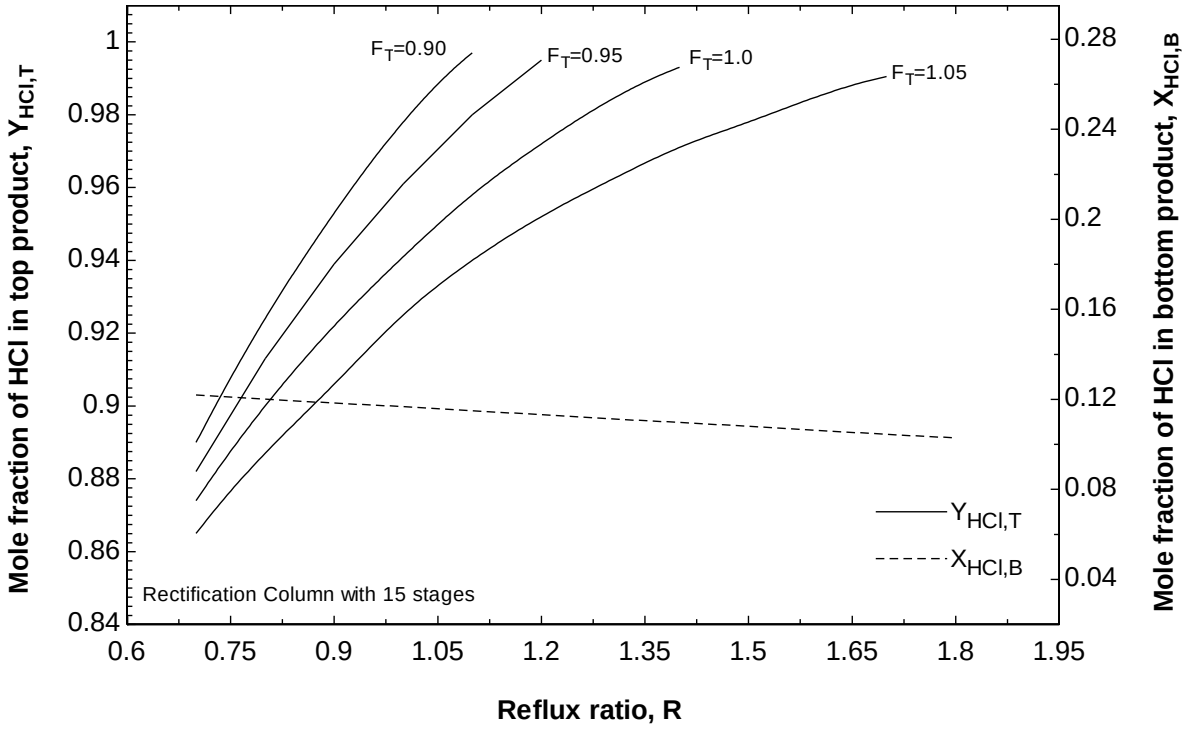

Figure 6.2 Influence of the reflux ratio and HCl gas flow rate on the concentration of products, column with 15 stages.

It is shown that with increasing the reflux ratio and number of stages, the purity of produced HCl gas, the top product, considerably improves. These parameters apply small effect on the concentration of the bottom product which is at the azeotropic concentration. It should be considered that increasing the number of stages requires higher capital investment that necessitate trade-offs. Moreover, in the constant reflux ratio, the lower the flow rates of produced HCl gas, the higher its purity.

Figures 6.3 and 6.4 illustrate the effect of feed composition on the heat flows in the reboiler and condenser respectively at different reflux ratios for 10 stage rectification column. Results are demonstrated based on the top product HCl concentration of 98mol%. Increasing the mole fraction of HCl in the feed stream decreases the heat flow requirements in both reboiler and condenser. It means that if the hydrolysis reaction provides higher concentration of HCl, considerable amount of energy would be saved in the separation process. But, this is not preferable for the hydrolysis reaction which would increase the amount of required excess steam and decrease the cycle overall efficiency. It can be concluded that the energy requirement of the separation process needs to be traded off with the steam requirement of the hydrolysis reaction for specific HCl concentration. In Figures 6.3 and 6.4, it is also shown that the lower the reflux ratio for the specific feed composition results in lower heat duties of the reboiler and condenser. This effect is more significant in condenser operation.

Figure 6.5 presents the effect of reflux ratio on the temperature of the top and bottom products for different location of the feed stage. Figure 6.6 shows the effects of reflux ratio and location of the feed stage on the HCl concentration of the top and bottom products. The feed HCl concentration is considered to be 13.5mol% for both cases.

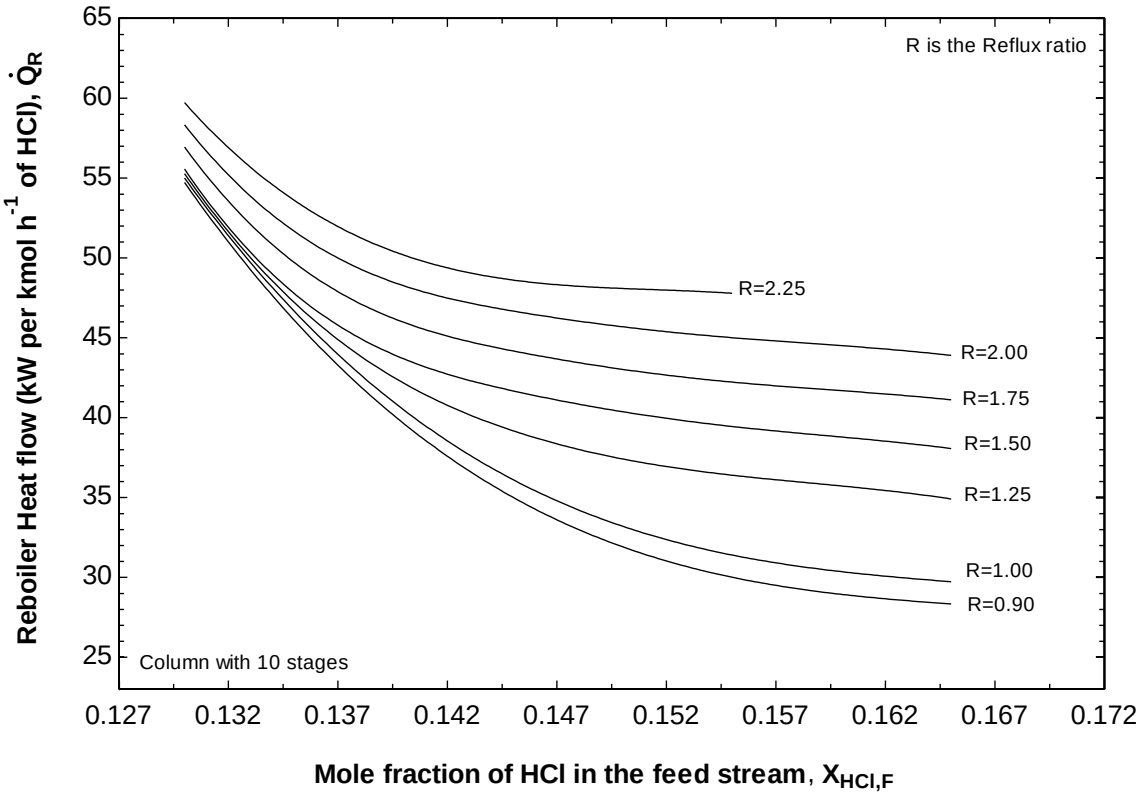

Figure 6.3 Influence of the feed composition and reflux ratio on the reboiler heat flow.

It is revealed that the optimum choice of the feed stage enables reduction of the reflux ratio to achieve a maximum concentration of top product, when other parameters remain constant. So, careful selection of the feed stage could results in reduction of the energy requirements of the separation process.

In the absorption column, see Figure 5.2, solvent composition and flow rate has a greatest effect on the composition and flow rate of the produced HCl acid. Figure 6.7 depicts the influence of the solvent composition on HCl concentration of the top and bottom of the absorption column with 15 stages. The operating pressure is 101kPa. The HCl gas concentration is 98mol% and the solvent flow rate is assumed 7kmol.h^{-1}. The HCl gas and solvent temperature is considered 70˚C and 80˚C respectively.

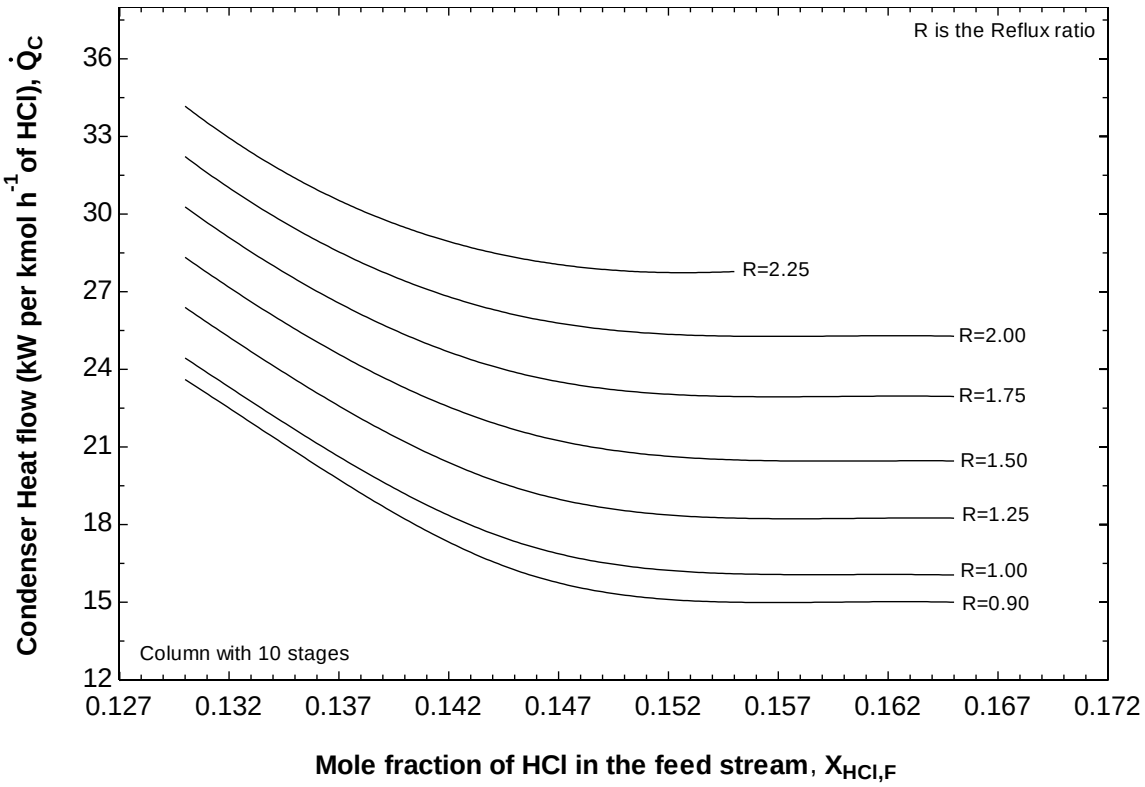

Figure 6.4 Influence of the feed composition and reflux ratio on the condenser heat flow.

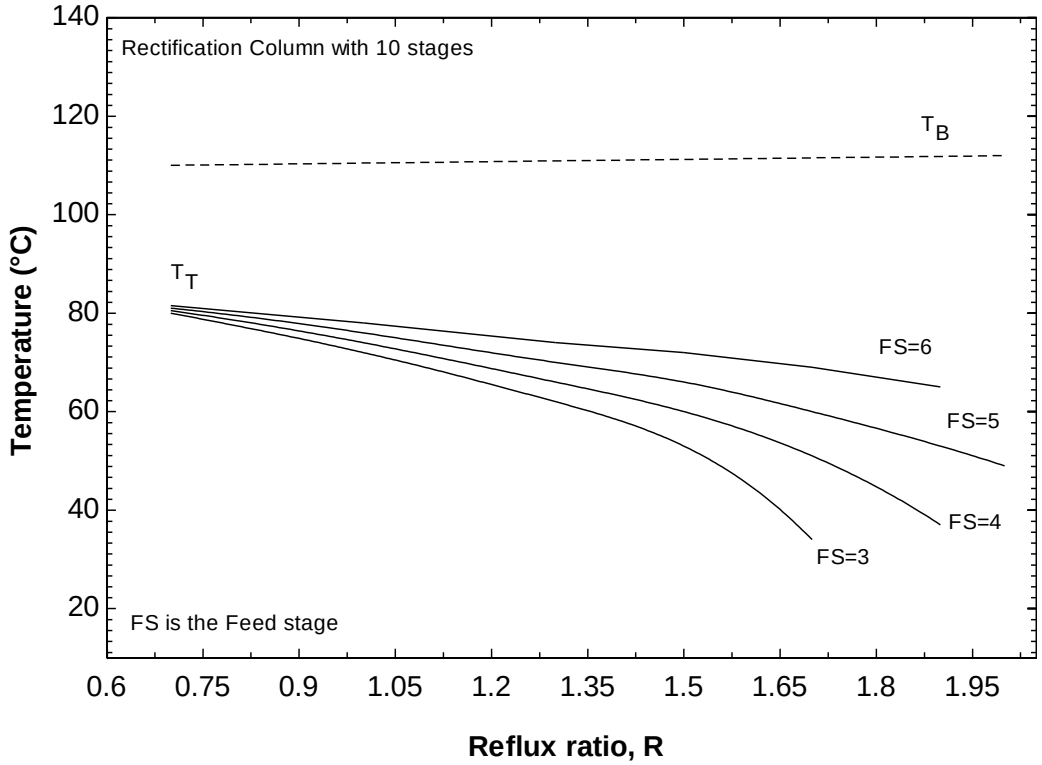

Figure 6.5 Effects of reflux ratio and location of the feed stage on the temperature of products.

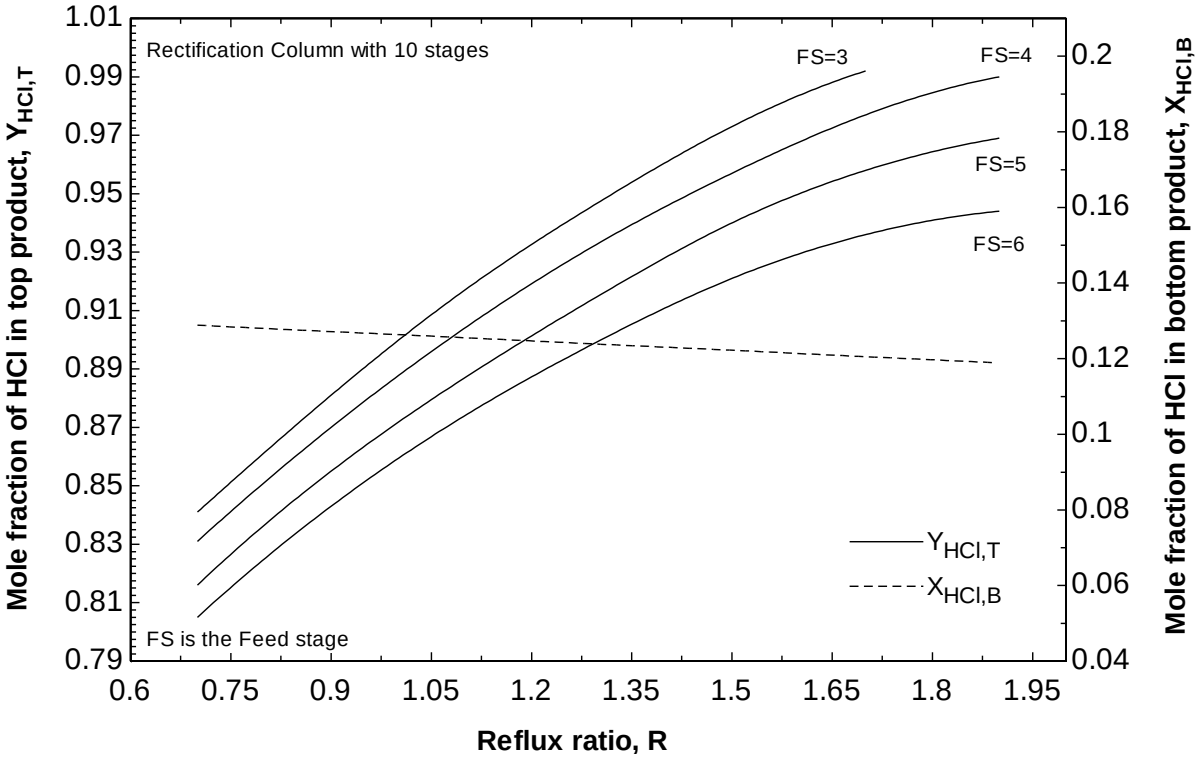

Figure 6.6 Effects of reflux ratio and location of the feed stage on the composition of products.

Figure 6.8 demonstrates the same analysis for a column with 8 stages. An improvement of the absorption process could be achieved by increasing the number of stages. This reduces the residual HCl concentration in the top product and simultaneously increases concentration of the produced acid. It is also revealed that the higher the HCl concentration of the solvent, the higher concentration of the produced acid. It denotes that using HCl acid at the azeotropic concentration instead of water would significantly increases the concentration of produced HCl acid which is beneficial for the electrolysis reaction. In other word, the results confirm the importance and effectiveness of the rectification and absorption integration to fulfill the requirements of the electrolysis process.

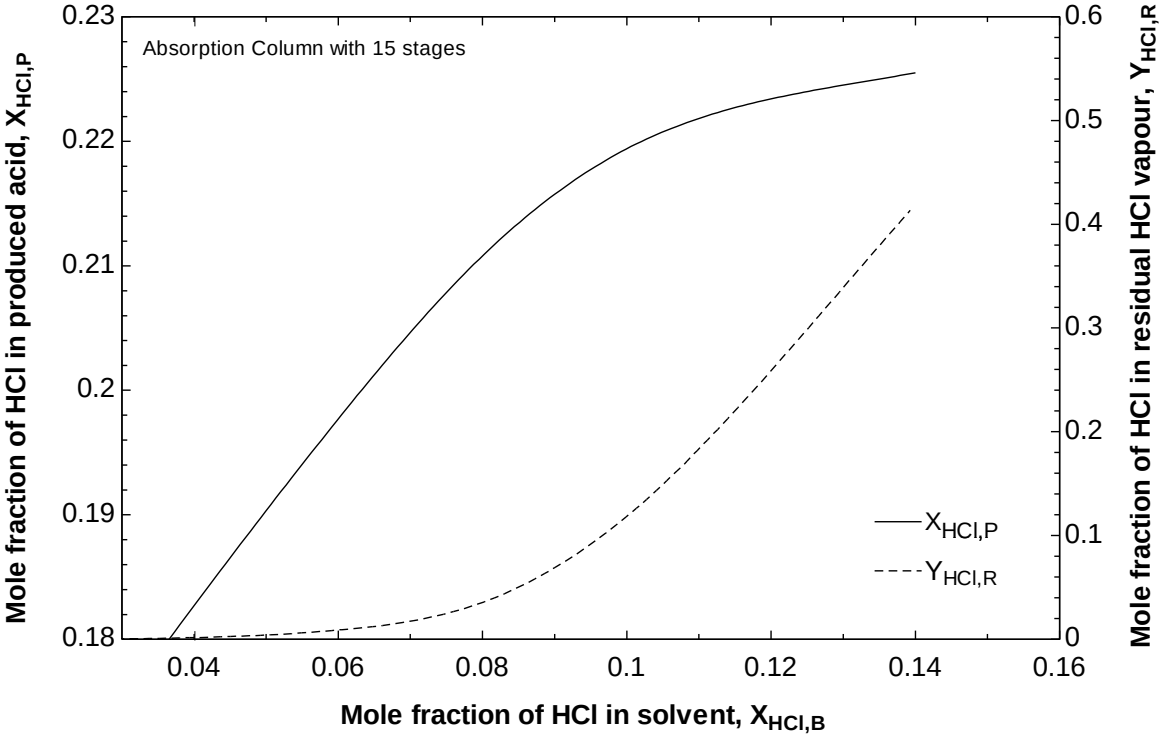

Figure 6.7 Influence of the solvent composition on the composition of products, column with 15 stages.

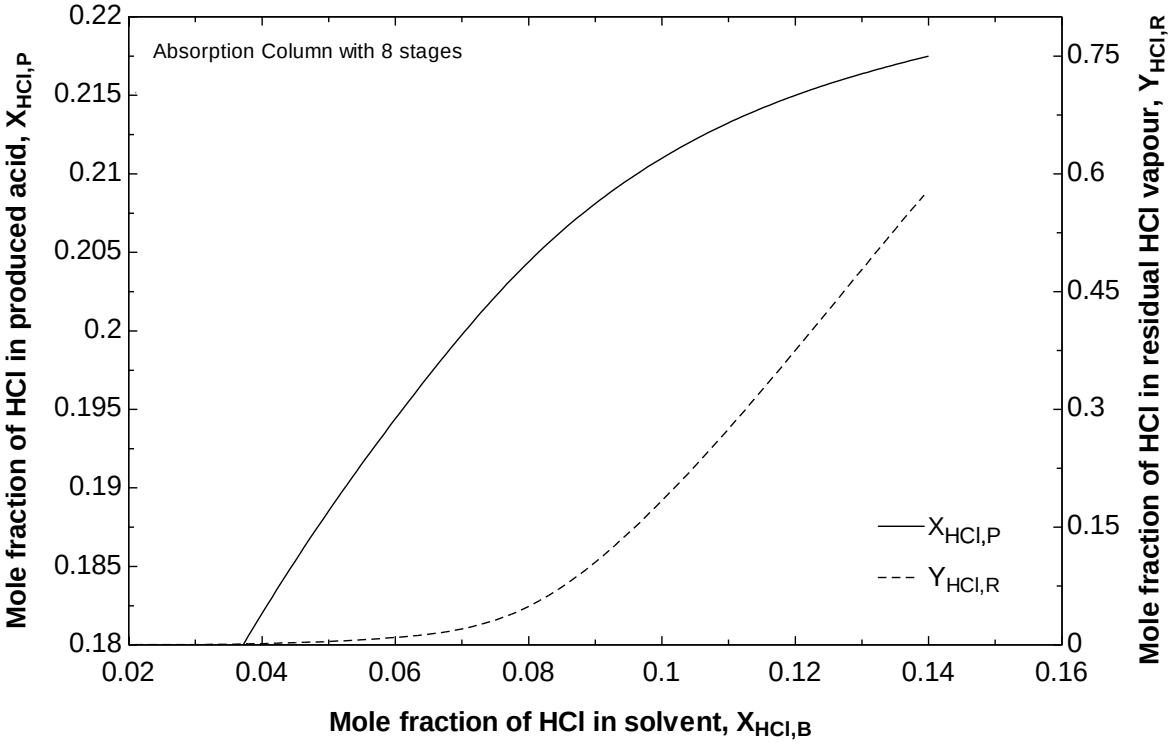

Figure 6.8 Influence of the solvent composition on the composition of products, column with 8 stages.

Figure 6.9 shows variation of the flow rate and concentration of produced HCl acid with the solvent flow rate at the constant HCl gas flow rate of 1kmol.h^{-1}. It is illustrated that with an increment in the solvent flow rate the amount of produced HCl acid increase and in contrary the acid concentration is reduced. The optimum solvent to gas ratio is found to be 7:1 for feasible operation of the absorption process. Solvent temperature is a key factor to control the residual HCl vapor flow rate as shown in Figure 6.10. In the absorption process with the solvent to feed ratio of 7, an increment of the solvent temperature corresponds to increase in the residual HCl vapor flow rate. The HCl acid flow rate shows opposite correlation.

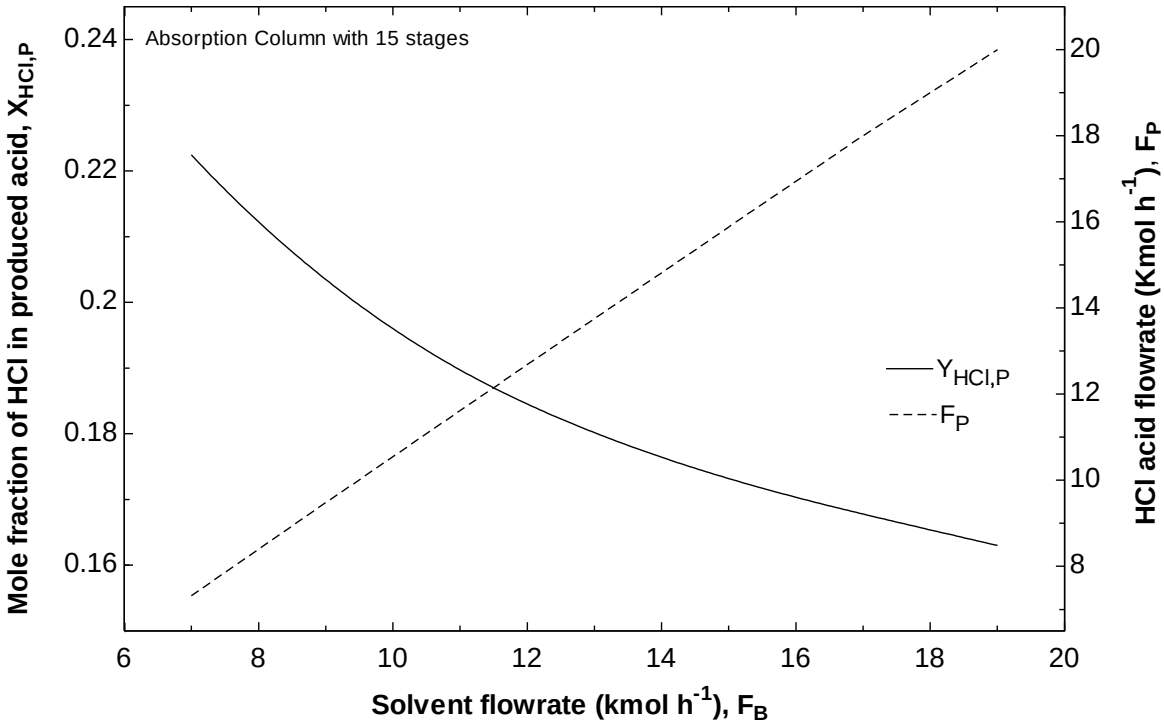

Figure 6.9 Variation of the produced acid flow rate and concentration with the solvent flow rate.

The influence of the HCl gas (feed) temperature on the composition of the HCl acid and residual HCl vapor is depicted in Figure 6.11. It is found that feed temperature doesn't change the HCl acid composition but considerably increases the mole fraction of HCl on the top of the column. Consequently, it is preferable to operate the absorption column at lower temperatures. As it was mentioned before, production of HCl gas in the rectification process under the specified operating condition requires 18kmol.h^{-1} of dilute HCl solution fed into the column. Based on the calculation of HRSG unit and the stoichiometry of the hydrolysis reaction, the proposed integrated system could satisfy excess steam requirement of the hydrolysis reaction up to 14 times of its stoichiometric value. On the other hand, the produced 7kmol.h^{-1} HCl acid with the concentration of 22mol% leads to 0.8 kmol.h^{-1} hydrogen production in the electrolysis process.

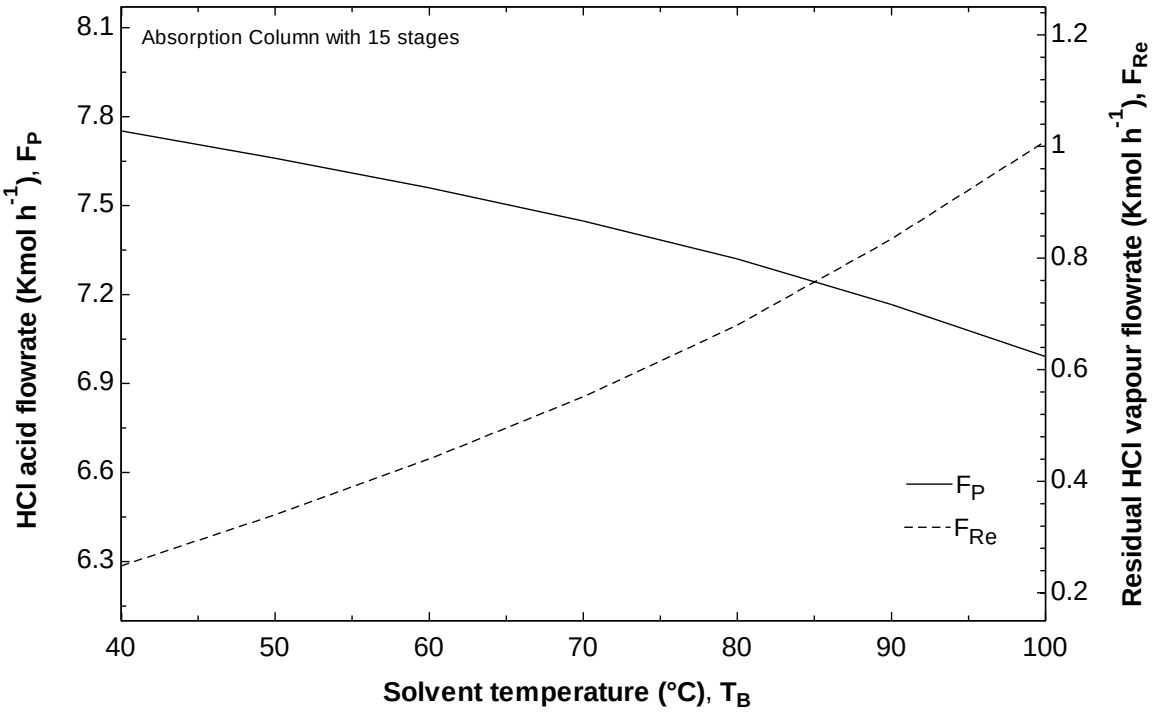

Figure 6.10 Influence of the solvent temperature on the production flow rate.

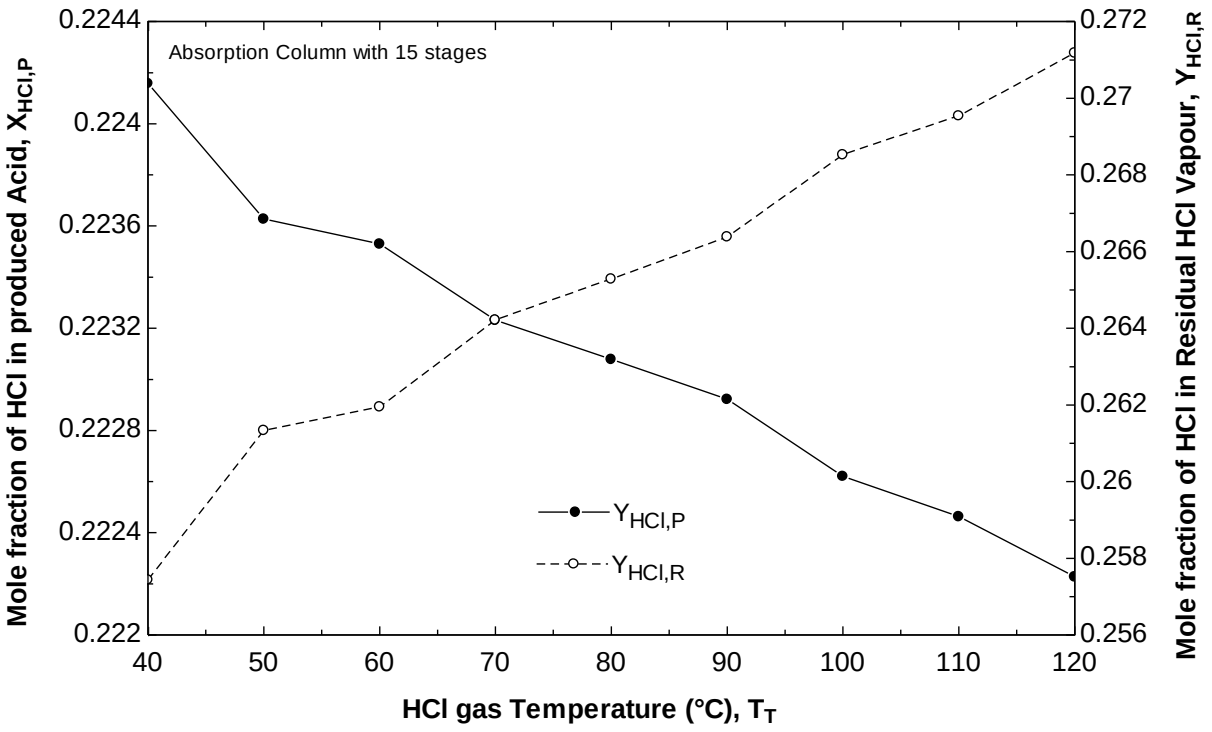

Figure 6.11 Effects of the HCl gas temperature on the composition of products.

It is mentioned earlier that the energy efficiency of the Cu-Cl cycle is highly dependent to the amount of steam recovered for the hydrolysis process. It means that the cycle performance is very sensitive to amount of steam could be generated in HRSG unit of the proposed integrated separation system. Figure 6.12 illustrates the dependency of the Cu-Cl cycle thermal efficiency to the amount of heat recovered in the HRSG unit to generate high pressure steam at the hydrolysis temperature, 400˚C. The proposed integrated system could satisfy excess steam requirement of the hydrolysis reaction up to 14 times of its stoichiometric value. This would increase the cycle thermal efficiency up to 75% comparing to the cycle efficiency of 22.8% when no excess steam recovered. This estimation is based on the calculation of extra steam required in the hydrolysis reaction and information presented in Table 5.1.

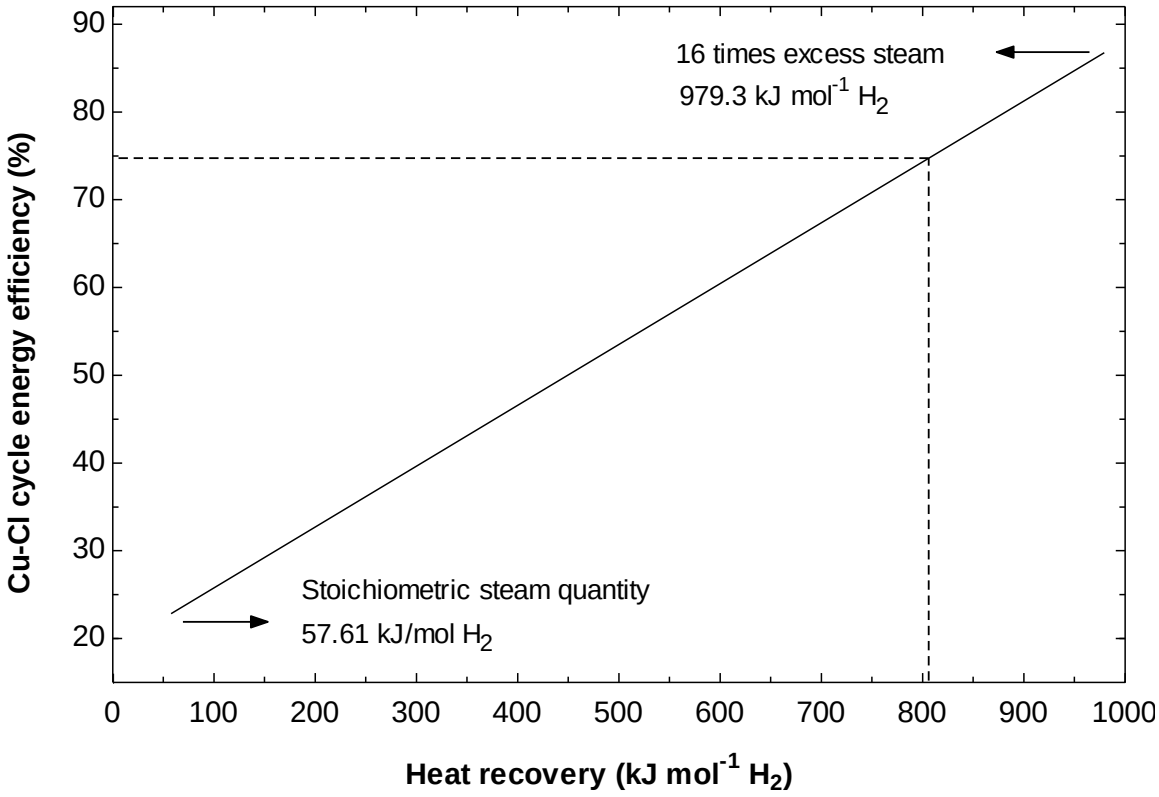

Figure 6.12 Heat recovery steam generation for the hydrolysis process.

It is a point of interest to analyze the separation process of HCl and water mixture where the HCl concentration is below the azeotropic point. In the hydrolysis process of the Cu-Cl cycle, when the produced HCl acid is below the azeotropic point, the rectification process requires addition of an ingredient as an entrainer, or solvent, to change the relative volatility of HCl and water. The relative volatility is changed by alteration of the activity coefficients and causes the azeotrope point moved or eliminated. $CaCl_2$, which is recommended in literature, is chosen as the extractive agent in the rectification process to increase the relative volatility of HCl to water. Figure 6.13 depicts phase equilibrium of HCl and water mixture for addition of different amount of $CaCl_2$ as an entrainer. As it is shown, in order to achieve higher HCl concentration on the top of

the column and decrease the amount of HCl in the bottom product, the concentration of $CaCl_2$ should considered about 44wt% of the feed flow. This results in the best desired solution which completely eliminates the azeotropic point.

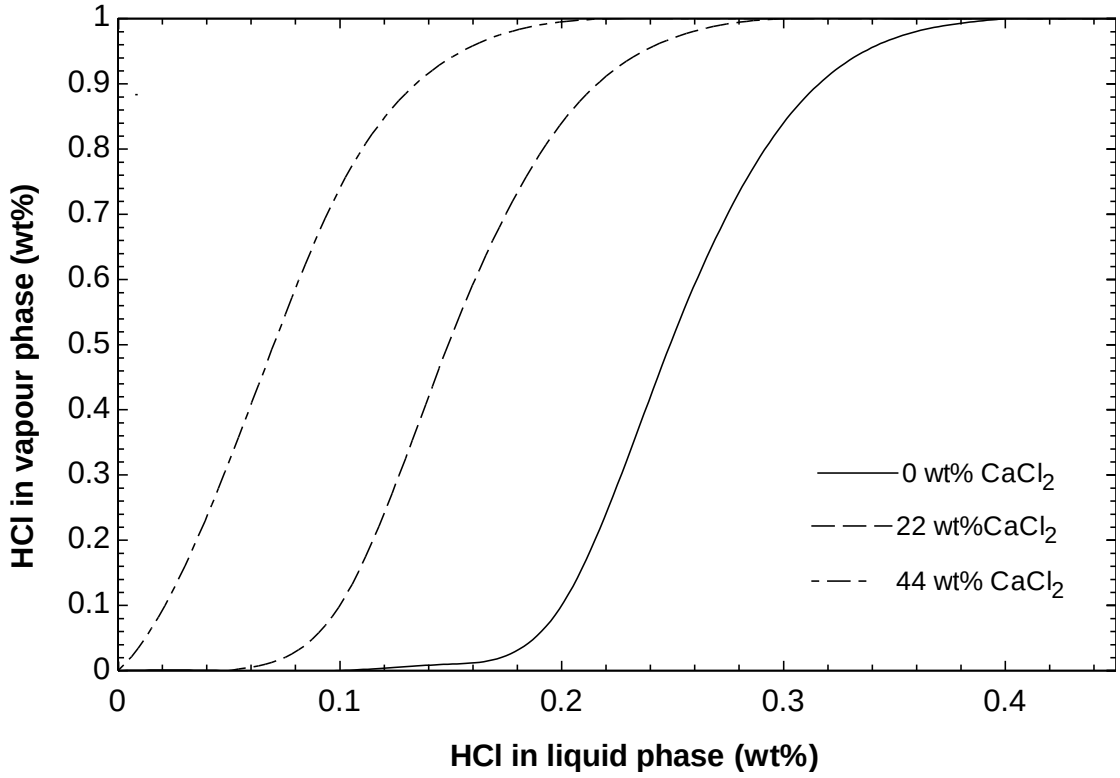

Figure 6.13 Phase equilibrium of HCl and water mixture with addition of $CaCl_2$.

Increasing $CaCl_2$ concentration has a drawback of escalating the energy requirements in the rectification process. Figures 6.14 and 6.15 depict variation of the reboiler and condenser heat flows with $CaCl_2$ concentration respectively. Increasing the concentration of $CaCl_2$ extends the energy requirements in both reboiler and condenser which also increased with an increment in the reflux ratio. It means the higher HCl concentration produced in the hydrolysis reaction of the Cu-Cl cycle results in the lower energy required in the separation process. It is beneficial to have HCl produced in the

hydrolysis process with a concentration above the azeotropic point to eliminate extra energy demand in the rectification process. In the case of using $CaCl_2$ as an extractive agent, it is recommended that the reflux ratio is operated in a lower value, so the entrainer concentration should be manipulated to achieve desired concentration of products.

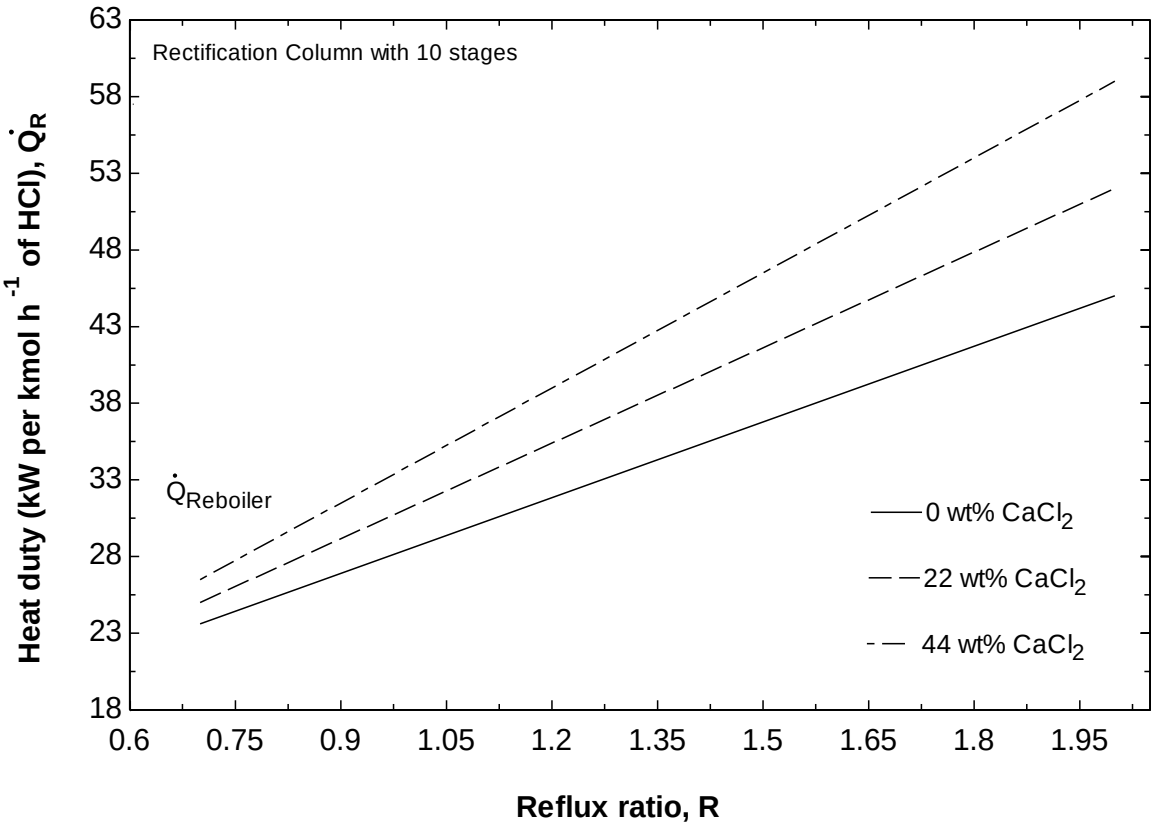

Figure 6.14 Variation of heat flows in the reboiler of the rectification process with $CaCl_2$ concentration.

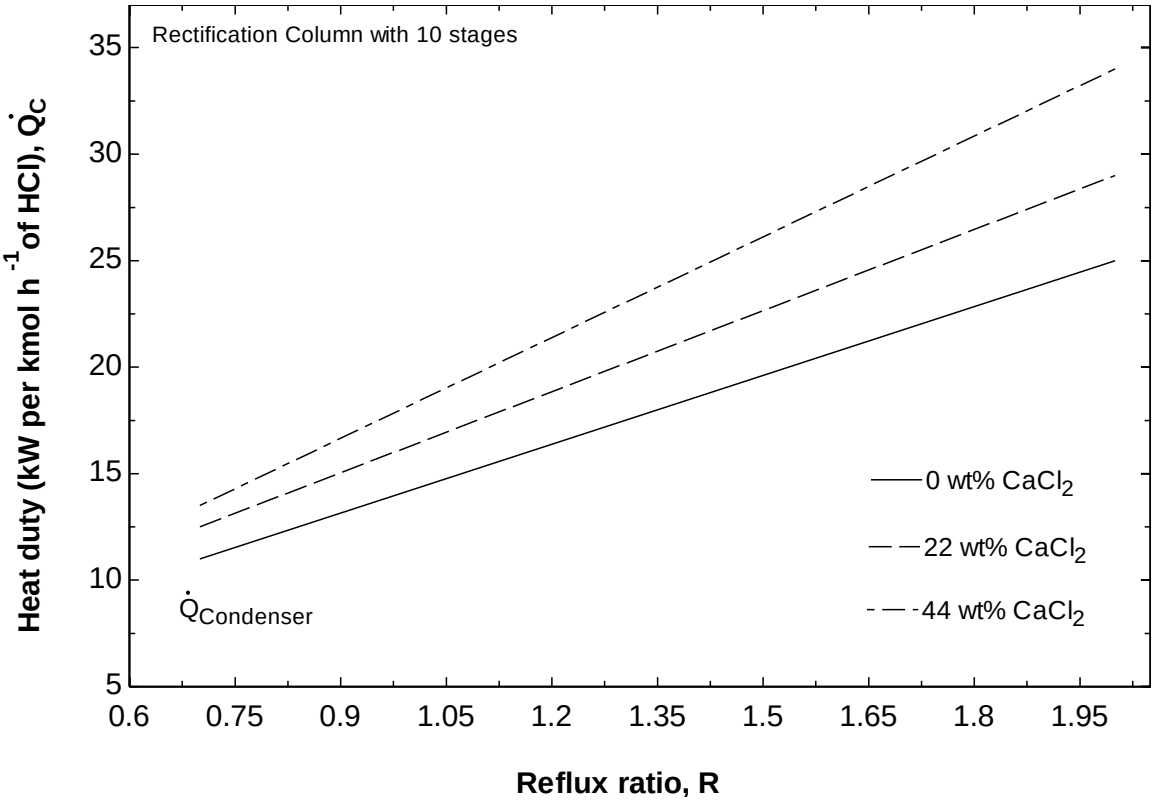

Figure 6.15 Variation of heat flows in the condenser of the rectification process with $CaCl_2$ concentration.

6.2 Experimental analysis of the CuCl electrolysis process

In the statistical modelling of the electrolysis process using factorial design analysis, the fraction of design space (FDS) graph, which is depicted in Figure 6.16, is a line graph showing the relationship between the volume of the design space, or area of interest, and the amount of prediction error. The curve indicates what fraction of the design space has a given prediction error or lower. In general, a lower and flatter FDS curve is preferable. The smaller standard mean error is more important than a flatter graph. A lower curve translates to a higher FDS space which indicates that the design has useful precision. Figure 6.17 which depicts the standard error of design graph is a plot showing the

standard error of prediction for areas in the design space. The standard error is defined as the standard deviation of the sampling distribution of a statistic [161]. The term may also be referred to an estimate of that standard deviation, acquired from a particular sample.

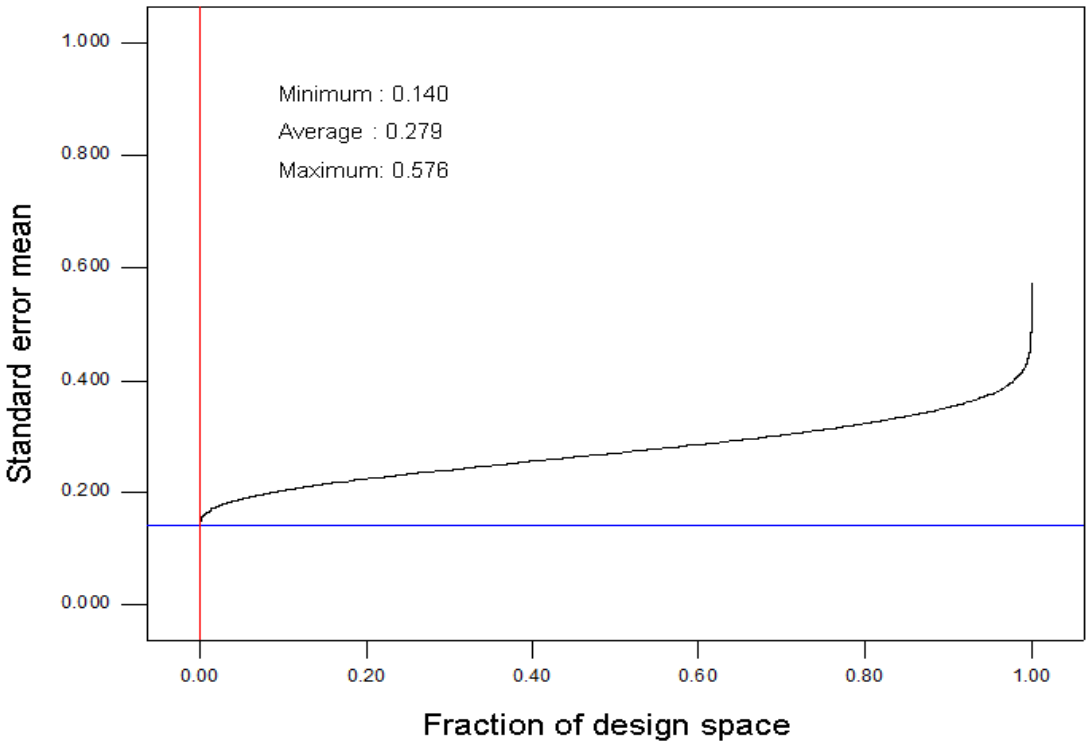

Figure 6.16 FDS results of the experiments for CuCl electrolysis process.

It is necessary to know that these values are reflective of the design only, not the response data. Generally, a standard error across the region of interest below 1.0 implies good accuracy in the modeling [158]. In other word, the lower standard error reflects the fact that less of the error in control factors will be transmitted to the selected response, which results in a more robust modelling process. The first step of analysis is to evaluate the significance of the effect of the operation factors on the cell voltage. As shown in Figure 6.18, the Pareto chart reveals that the applied current density followed by HCl concentration and flow rate have dominant effects on the cell voltage subsequently. It is

also illustrated that the combined impact of HCl concentration and current density is relatively larger than the CuCl concentration effect.

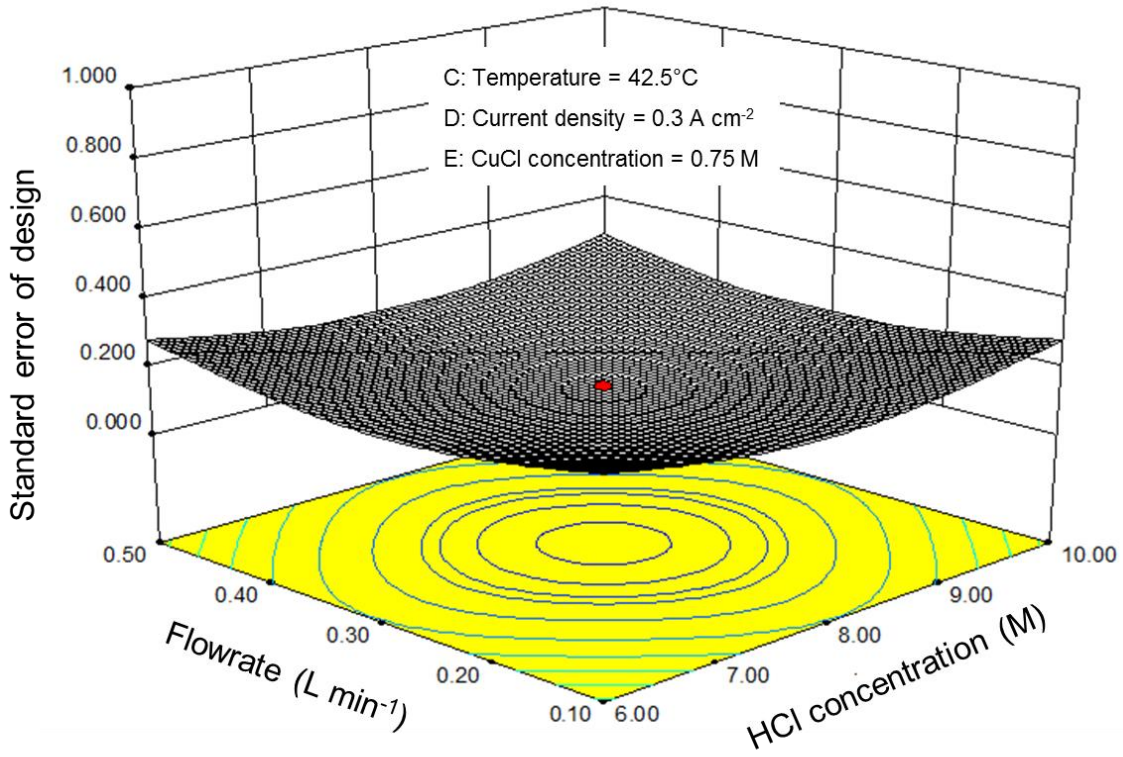

Figure 6.17 Experimental error of design for CuCl electrolysis process.

The t-value in Figure 6.18 is the score obtained when a t-test is performed. One of the most frequent applications of a t-test is a test of the null hypothesis that the difference between two responses measured on the same statistical unit has a mean value of zero. For example, suppose we measure the cell voltage before and after consideration of HCl concentration effects. If the HCl concentration has a significant effect on the cell voltage, the cell voltage is expected to be changed considerably. Otherwise, the HCl concentration is assumed as a null hypothesis. In statistical assumption of observed data, the null

hypothesis refers to a general circumstance that there is no relationship between two measured phenomena [166].

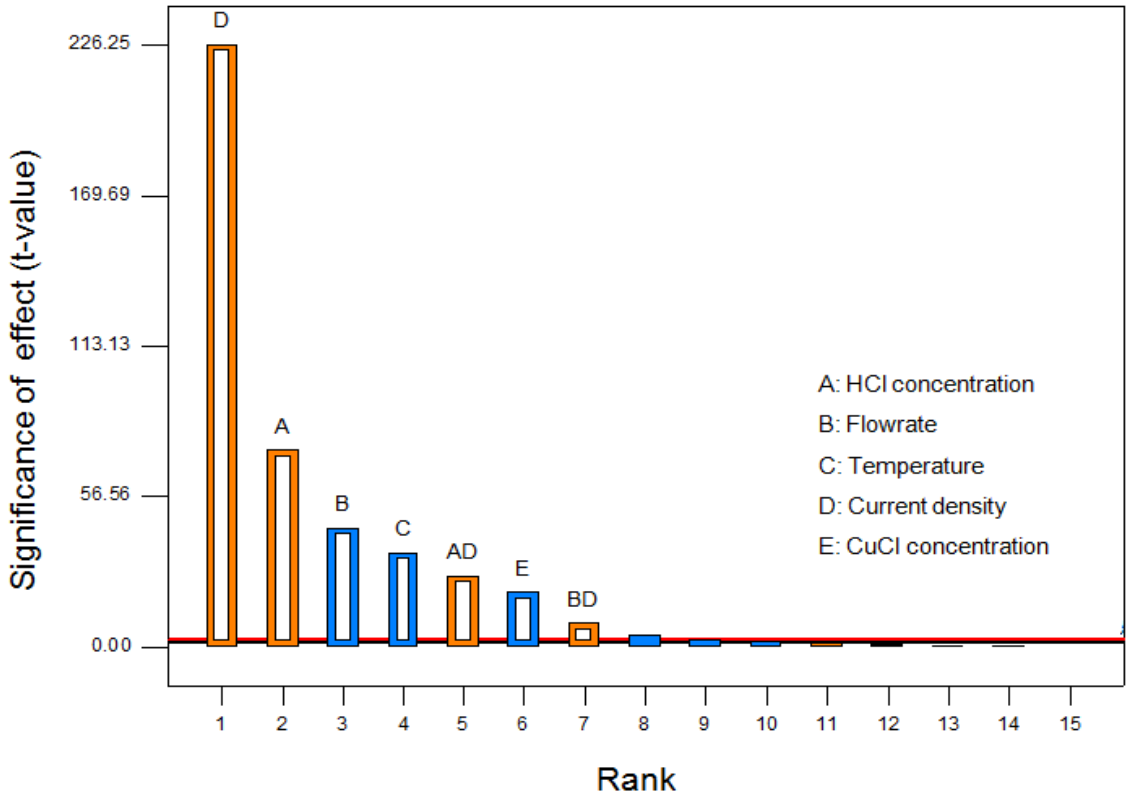

Figure 6.18 Pareto chart of the operation factors.

A normal probability plot is used to understand how operational factors influence the cell voltage. As illustrated in Figure 6.19, a plot of the ordered values of a sample versus the expected ordered values from the true population will be approximately a straight line. Therefore, if the effects represent a sample from a normal population, it is expected to be located on approximate straight lines on a normal probability plot of the effects. The factors which show up as outliers on the normal probability plot have significant impact on the response variable. The current density, HCl concentration, and their combinatory effect have a positive influence on the cell voltage and flow rate,

temperature, while CuCl concentration shows a negative effect. An increase in the value of a factor which has a positive effect results in an increment in the cell voltage and increase in the value of a factor which has a negative effect that drops the cell voltage.

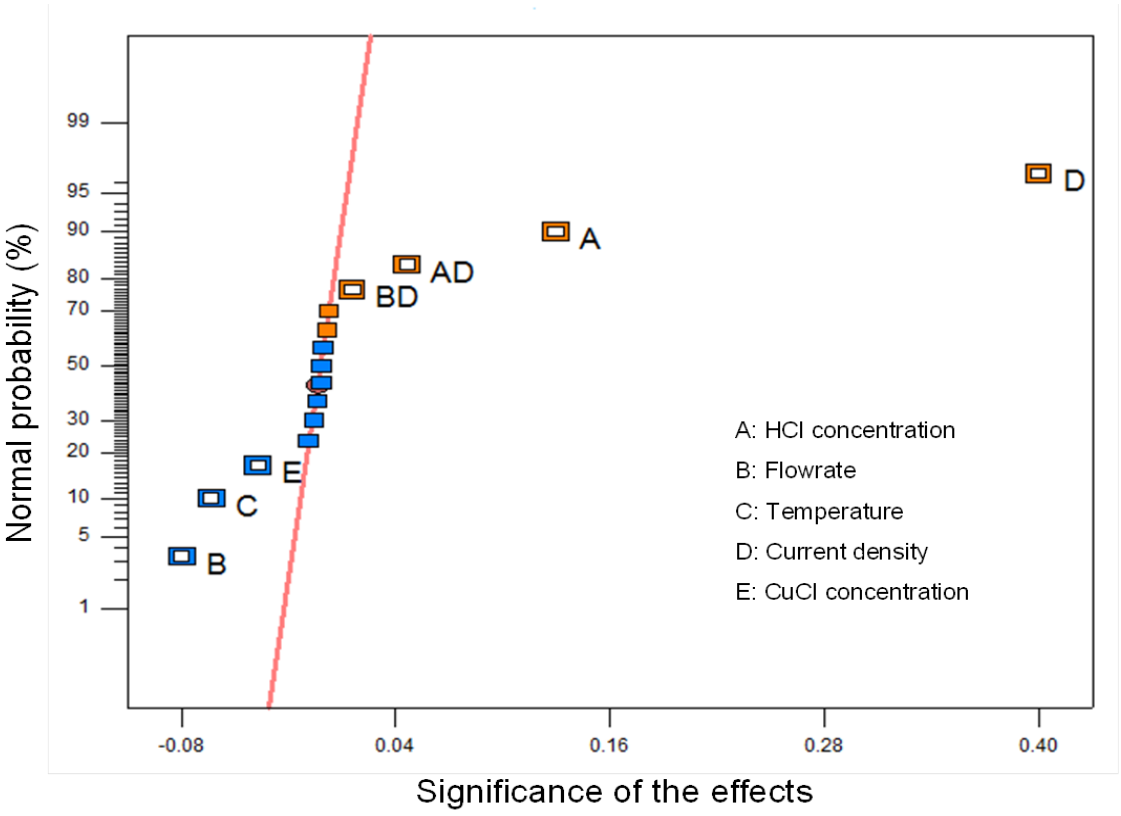

Figure 6.19 Normal probability plot of the operational factors.

In order to find a correlation between the operational factors and the response variable, a normal plot of residuals is analyzed to check the linearity of interactions. The normal probability plot indicates whether the residuals follow a normal distribution or don't follow a straight line. The residuals are calculated from the difference of actual versus predicted response. Figure 6.20 depicts the normal plot of residuals. It is shown that residuals clearly follow the s shape nonlinear pattern which indicates a completely nonlinear correlation between cell voltage and operating parameters.

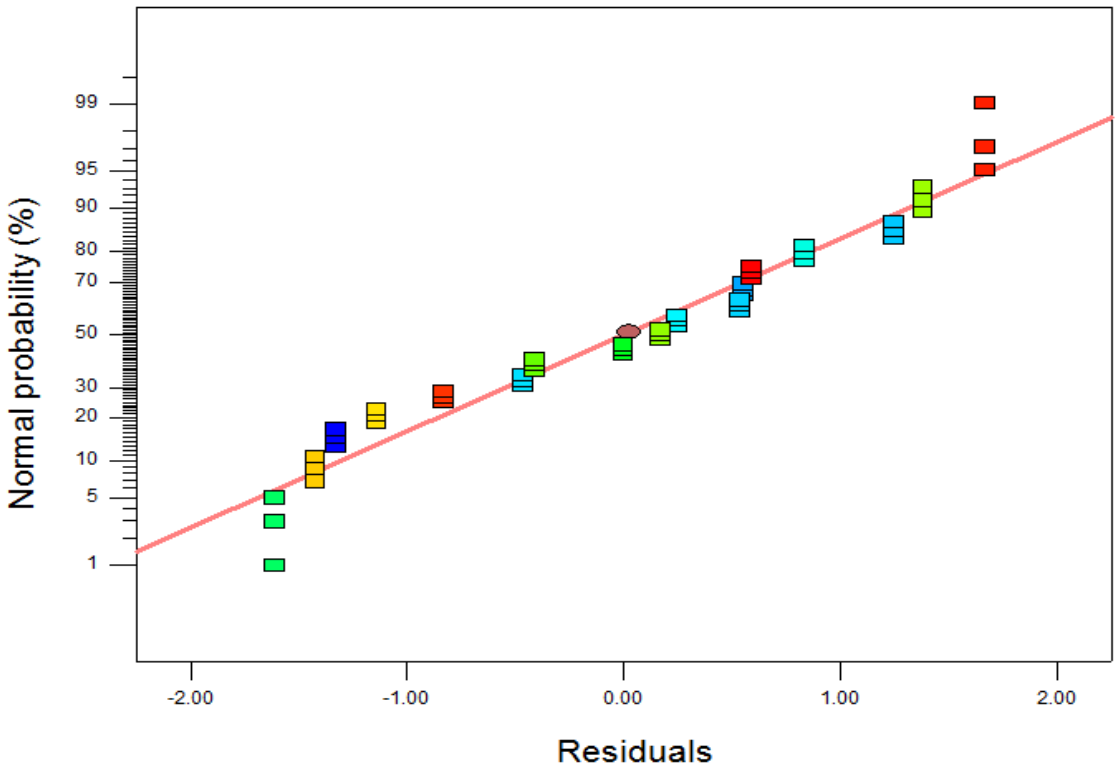

Figure 6.20 Normal probability plot of residuals.

The plot of the residuals versus the experimental run order is depicted in Figure 6.21. This figure allows checking for variables that may have hidden influence on the response during the experiment. The plot shows a random scatter which indicates that no time-related variable running in the background. Randomization provides insurance against trends spoiling the analysis.

The Box-Cox plot provides a guideline to select the correct power law transformation. As illustrated in Figure 6.22, the recommended transformation is 0.74 based on the best power value which is found at the minimum point of the curve generated by the natural log of the sum of squares of the residuals. The green line indicates the best power value, while the red lines indicate the 95% confidence interval surrounding it.

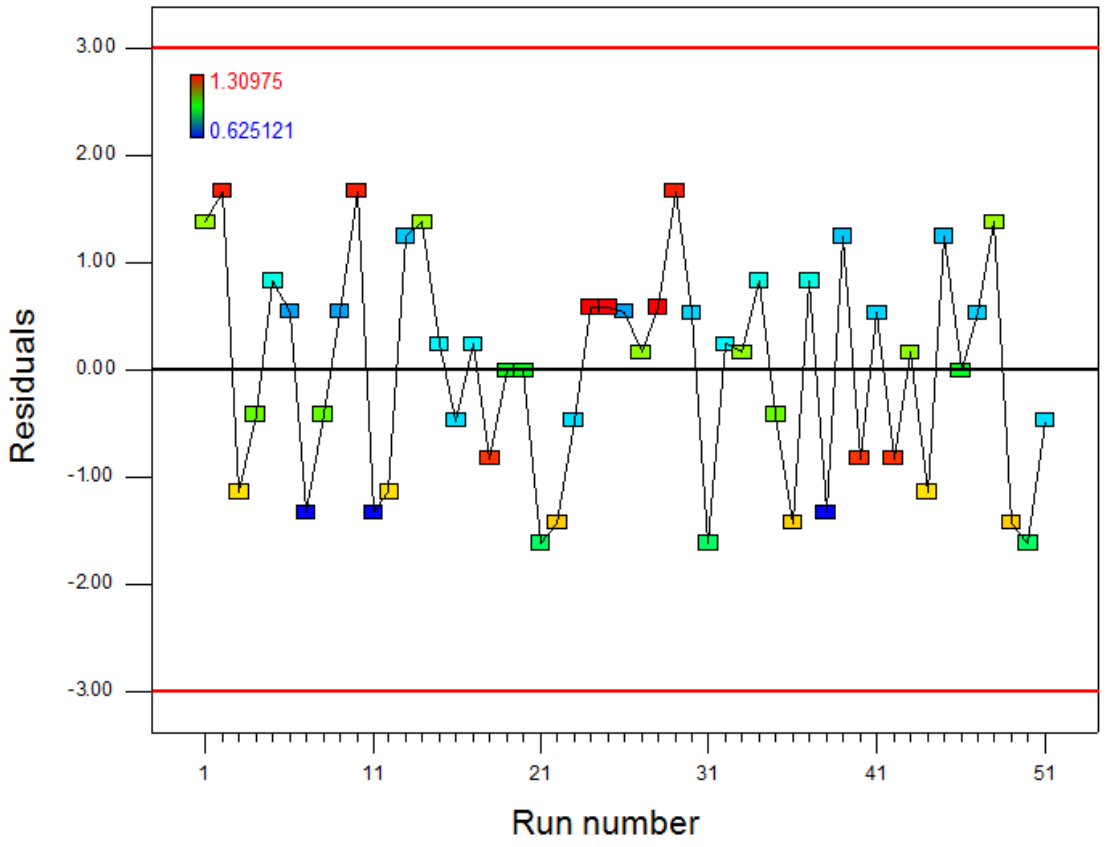

Figure 6.21 Residuals versus run numbers.

The resulting predictive model of the cell voltage is given as follows:

$$Y^{0.74} = 0.76 + (0.015)\text{A-}(0.26)\text{B-}(0.0018)\text{C+}(0.466)\text{D-}(0.0737)\text{E} \\ +(0.06)\text{AD+}(0.2)\text{BD} \tag{6.1}$$

where Y is the cell voltage and A, B, C, D, and E are HCl concentration, solution flow rate, temperature, current density, and CuCl concentration respectively. AD is the interaction effect of HCl concentration and current density on the cell voltage and BD is the interaction effect of flow rate and current density. As depicted in Figure 6.23, the graph of predicted response values versus the actual responses, which are experimentally measured, indicates good accuracy of the proposed model.

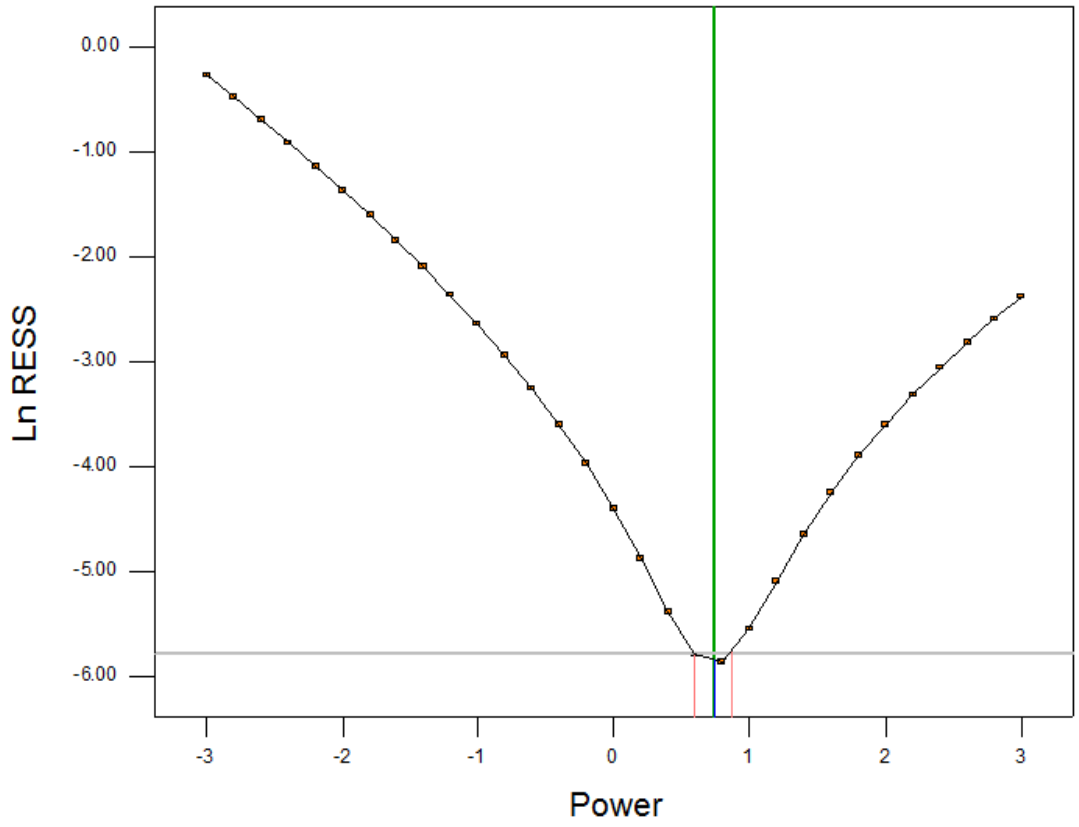

Figure 6.22 Box-Cox plot for power transform.

An ANOVA summary of the proposed model in the equation (6.1) is presented in Table 6.1. The model F-value of 4300.37 implies that it is significant. F-value is the result of F-test in which the accuracy of a statistical model that has been fitted to a data set is analyzed. F-tests are mainly utilized when the models have been fitted to the data using least squares. The best fit in the least-squares definition minimizes the sum of squared residuals which is the difference between an observed value and the fitted value provided by a model. There is only a 0.01% chance that the F-value could occur due to noise. The R-Squared coefficient of determination is a statistical measure of how well the regression line approximates the real data points. An R^2 of 1 indicates that the regression line perfectly fits the data. In the CuCl electrolysis model, The predicted R^2 of 0.9982 is

in reasonable agreement with the adjusted R^2 of 0.9983 and shows the high level of accuracy. An adequate precision measures the signal to noise ratio. A ratio higher than 4 is desirable [158]. The calculated ratio of 194.5 indicates an adequate signal. It means this model can be used to navigate the design space.

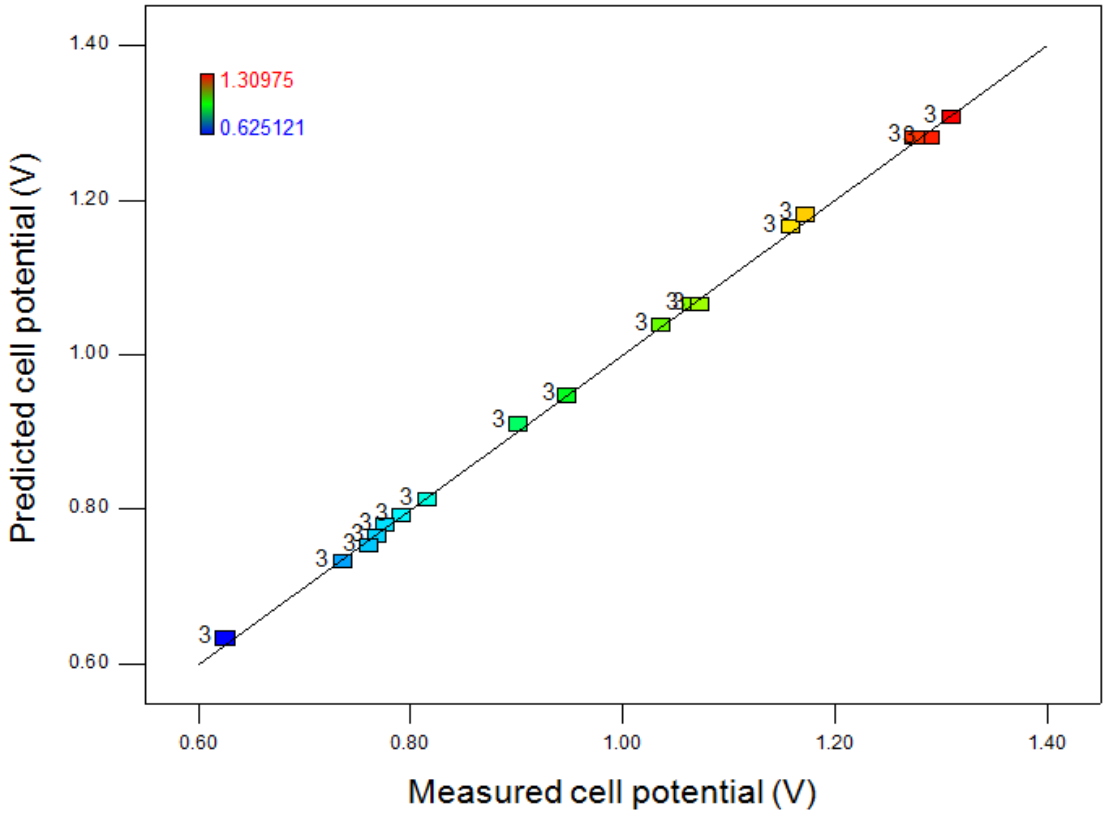

Figure 6.23 Model predictions versus actual (experimental) cell potential.

The error estimates shown in Table 6.1 are derived from replicated runs. The replication increases the precision of the response which is estimated by averaging results, but more importantly, provides an independent estimate of the experimental variability over the design space. The sum of squares due to pure error is the sum of squares of the differences between each observed value of the cell voltage and the average of all cell voltages corresponding to the same operating conditions. As shown in

Table 6.1, the observation is highly unlikely to be the result of random chance for the considered operation factors. The lack of fit value of about 0.0032 for the proposed model indicates the accuracy of predictions and reliability of the experimental study. When the p-value is less than the predefined significance level, which is often 0.05 or 0.01, indicating that the observed result would be highly unlikely under the null hypothesis [167]. The p-value is the probability of obtaining a test statistic assuming that the null hypothesis is true.

Table 6.1 ANOVA summary of the model parameters.

Source	Sum of Squares	df	Mean Square	F Value	p-value (Prob > F)
Model	2.303277	7	0.329040	4300.374	< 0.0001
A-HCl Concentration	0.205596	1	0.205596	2687.038	< 0.0001
B-Flowrate	0.075546	1	0.075546	987.344	< 0.0001
C-Temperature	0.047213	1	0.047213	617.048	< 0.0001
D-Current Density	1.928388	1	1.928388	25203.016	< 0.0001
E-CuCl Concentration	0.016327	1	0.016327	213.389	< 0.0001
AD	0.027062	1	0.027062	353.692	< 0.0001
BD	0.003144	1	0.003144	41.094	< 0.0001
Residual	0.003290	43	0.000077	R-Squared	0.998574
Lack of Fit	0.003290	9	0.000366	Adj. R-Squared	0.998341
Pure Error	0.000012	34	0.000004	Pred. R-Squared	0.998228
Total	2.306567	50		Adeq. Precision	194.501394

The influence of current density on the cell potential is depicted in Figure 6.24, where other operational factors remain constant. It is shown that the cell potential increases by the increment in the applied current density. Basically, in an electrolytic cell, the overpotential requires more energy than thermodynamically expected to drive a reaction. The overpotential refers to the voltage difference between a half-reaction's reduction potential which is thermodynamically determined and the potential at which the

reduction and oxidation (redox) is experimentally occurred. The Tafel equation in electrochemical kinetics correlates the rate of an electrochemical reaction to the overpotential which increases with increasing current density [168].

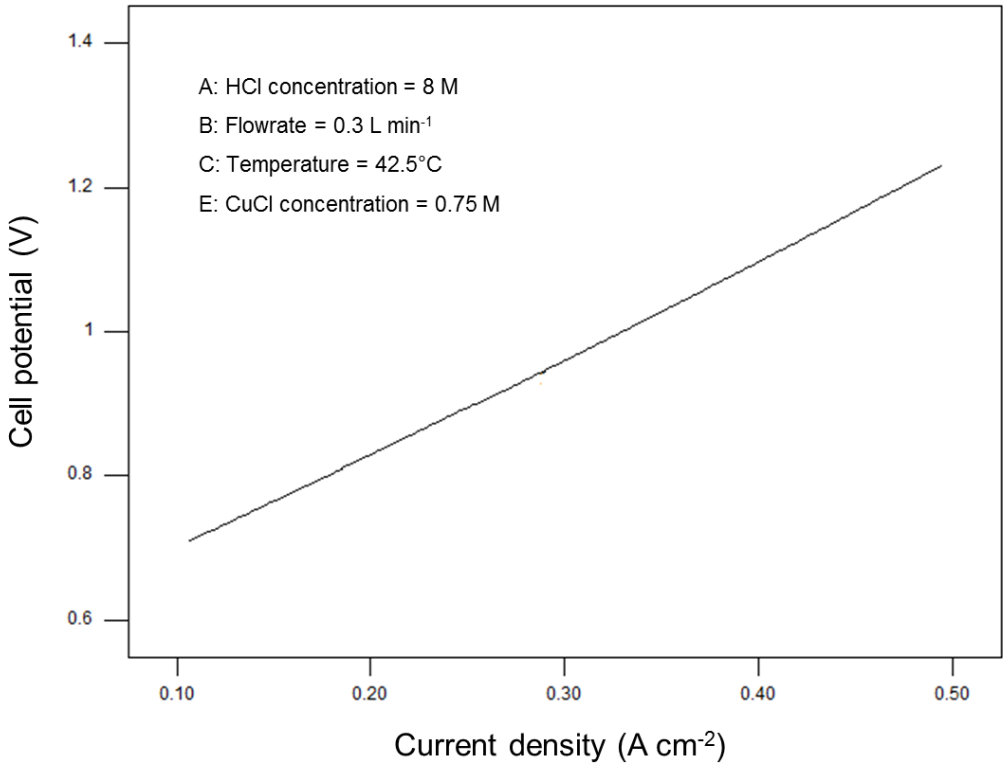

Figure 6.24 Influence of current density on the cell potential.

The variation of the cell potential with HCl concentration is illustrated in Figure 6.25. Since the current density and HCl concentration have a combined effect on the cell potential, Figures 6.26 and 6.27 provide a better understanding of these interactions. It should be explained that the cell voltage drops across the cell under specific current density due to the internal resistance of the cell. Ohmic losses within the cell, which has the main contribution to the total cell resistance, decrease with decreasing HCl concentration [94].

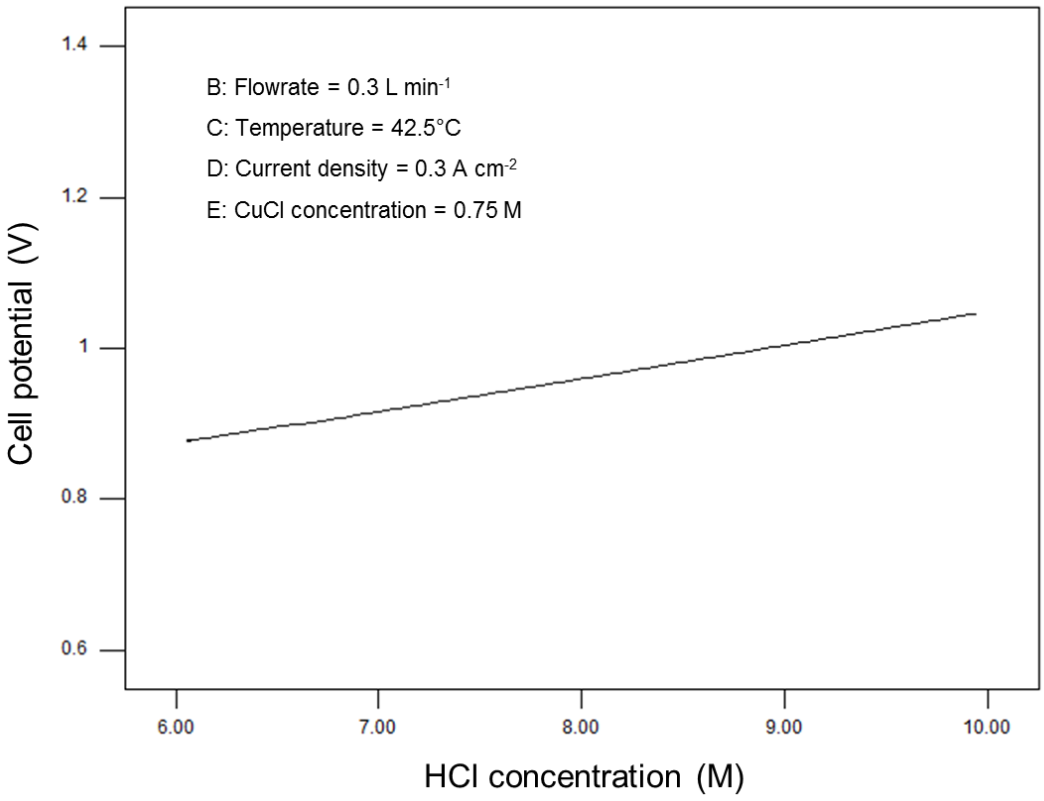

Figure 6.25 Influence of HCl concentration on the cell potential.

On the one hand, increasing the HCl concentration would potentially decrease the amount of copper species present in the catholyte [41]. Moreover, the higher HCl concentration would increase dissolution rate of solid CuCl in the anolyte. On the other hand, the higher HCl concentration results in the higher cell potential and the more complex operation of the electrolysis process. It is concluded that finding an optimum HCl concentration requires trade-offs and depends on the Cu-Cl cycle design criteria.

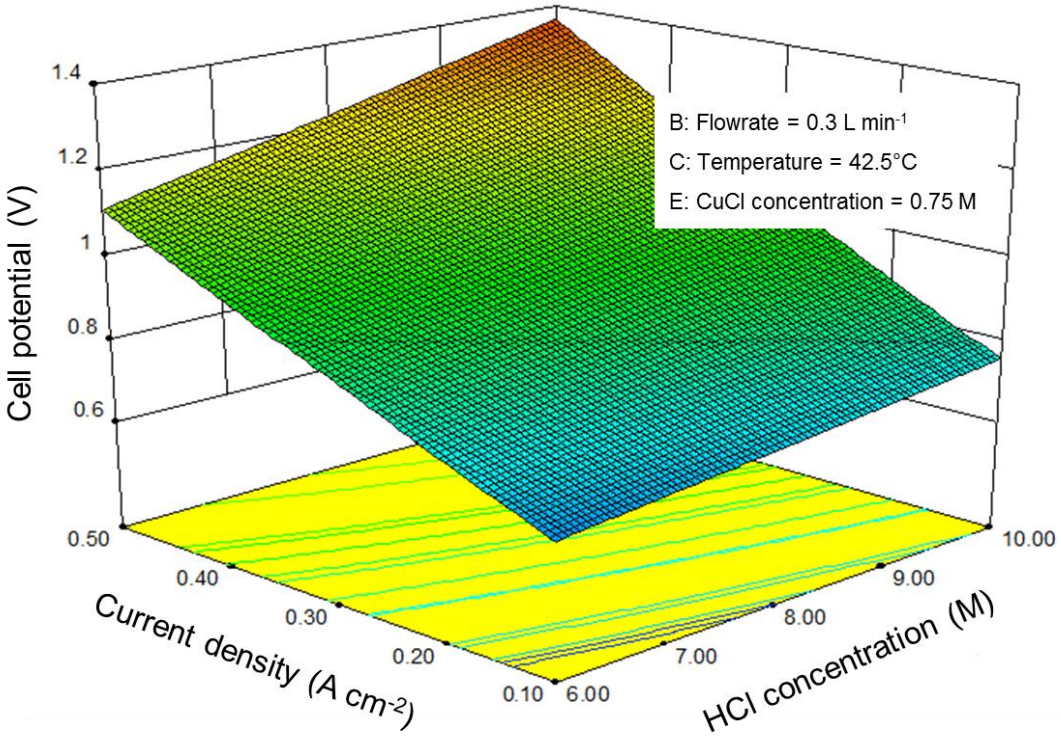

Figure 6.26 Effects of current density and HCl concentration on the cell voltage.

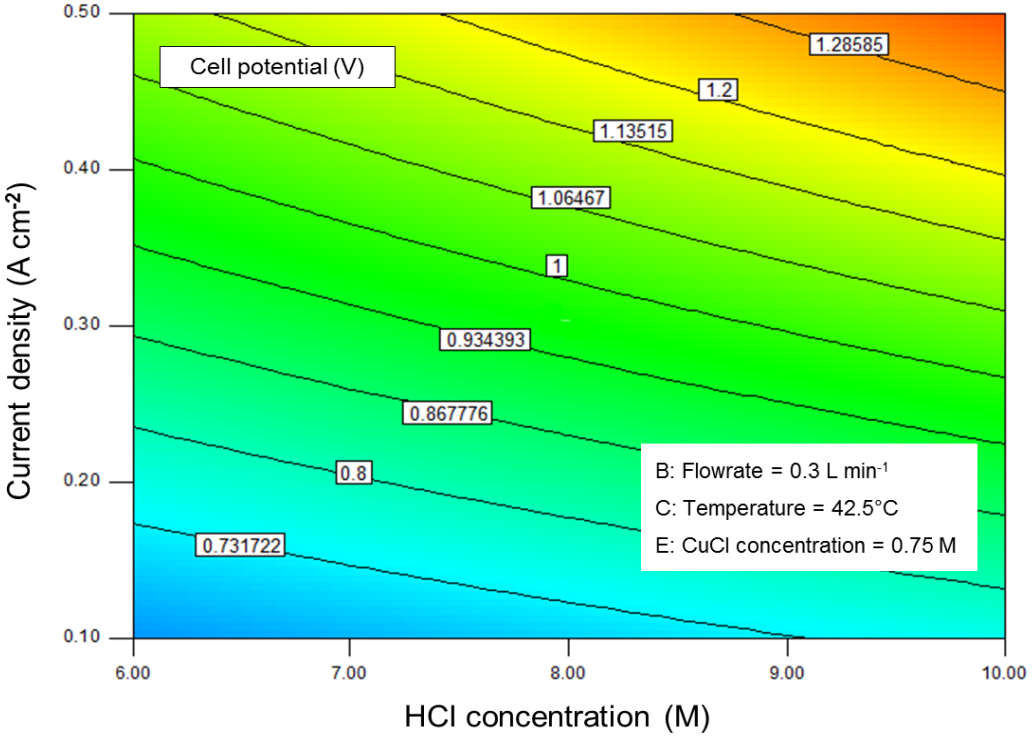

Figure 6.27 Effects of current density and HCl concentration on the cell voltage.

The influence of temperature and CuCl concentration on the cell voltage is shown in Figures 6.28 and 6.29 respectively. CuCl concentration has the lowest effect on the cell potential when other factors remain constant. A weak dependence of the cell potential on temperature, when it increases from 25˚C to 60˚C, indicates that the activation losses are relatively small. Activation losses are those losses associated with the initial significant voltage losses in low temperature fuel cells. These losses are basically representative of a loss of overall voltage at the expense of forcing the reaction to completion. Small activation losses imply that the electrochemical reactions are easy to start. In other word, addition of heat to the CuCl electrolysis process, which increases solution temperature, doesn't considerably reduce electricity requirement. Moreover, it increases the risks and complexity of the operation since HCl vapor could escape easily from the solution at elevated temperatures and it is extremely hazardous.

Figures 6.30 and 6.31 depict the combined effects of flow rate and current density on the cell potential. It is observed that increasing the flow rate decreases the cell voltage for a specific current density, where other operational factors are constant. The predictive model provides the ability to find the optimum operating conditions that correspond to the minimum cell potential. For the specific applied current density of $0.3A.cm^{-2}$, Figures 6.32 and 6.33 demonstrate how HCl concentration and flow rate could be altered to minimize the cell voltage. It is shown that for the HCl concentration of 6M and flow rate of $0.5L.min^{-1}$, the cell voltage could be minimized to 0.77V, where the operating temperature is 60˚C, respectively.

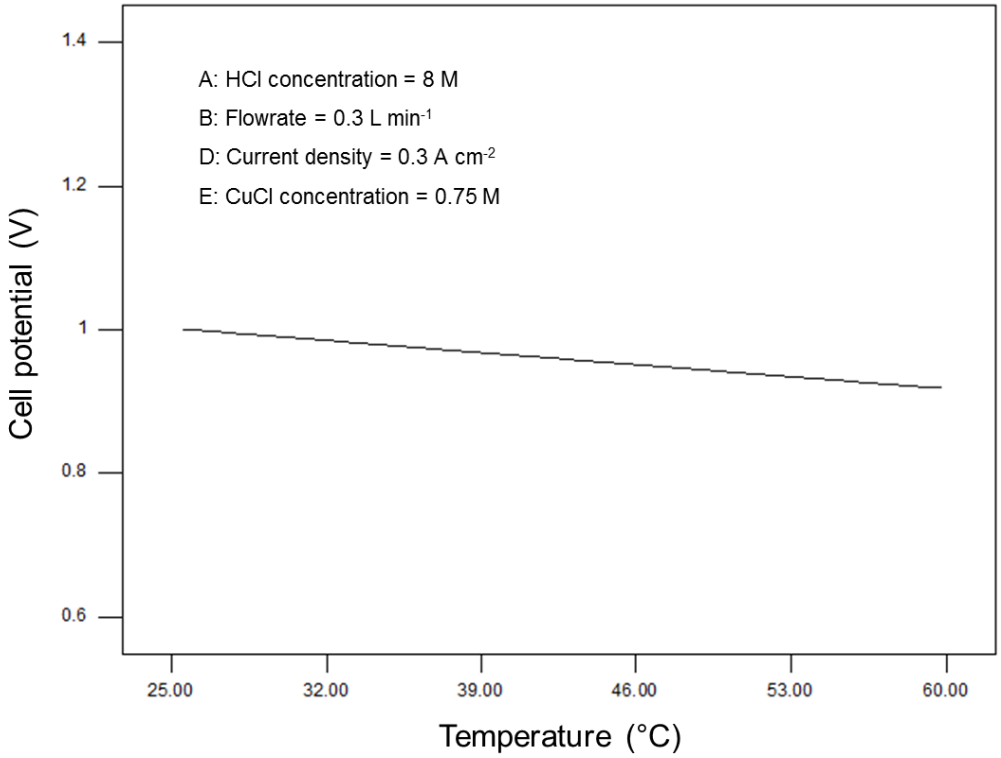

Figure 6.28 Influence of temperature on the cell potential.

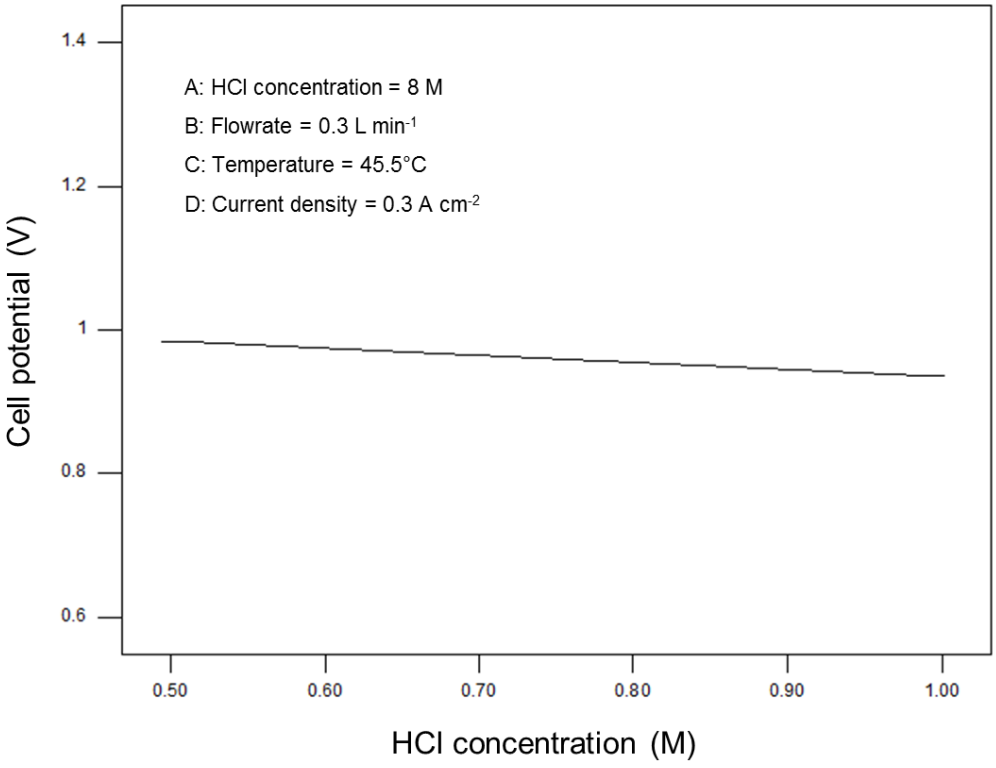

Figure 6.29 Influence of CuCl concentration on the cell potential.

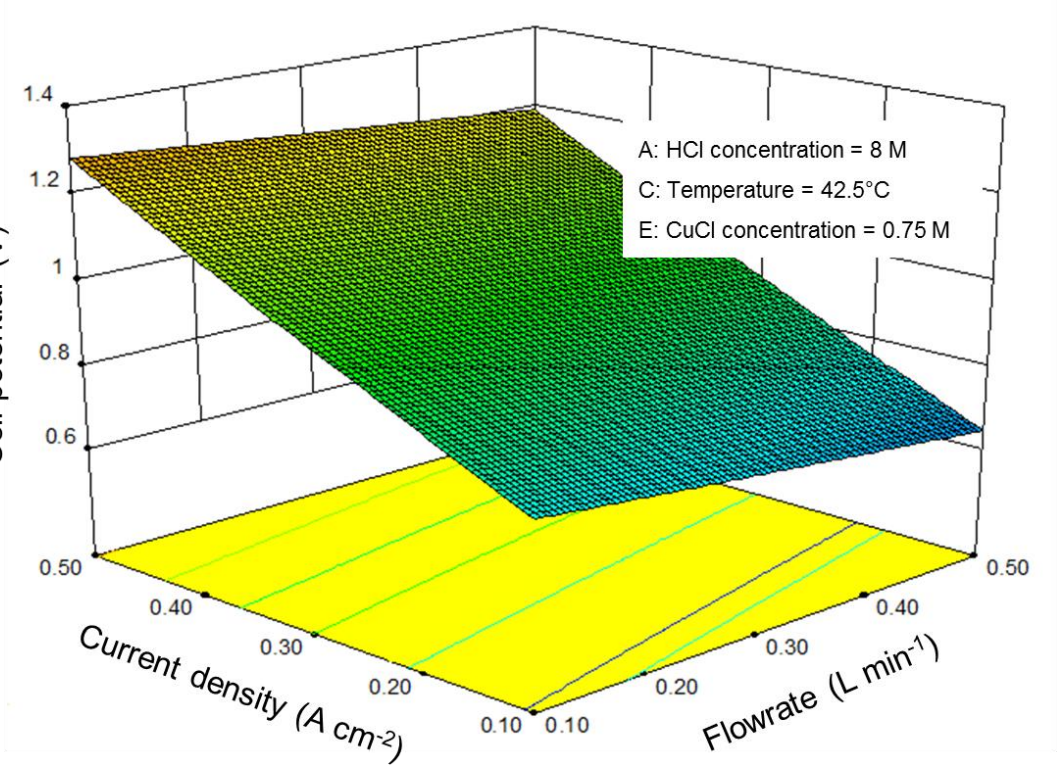

Figure 6.30 Influence of current density and flow arte on the cell voltage.

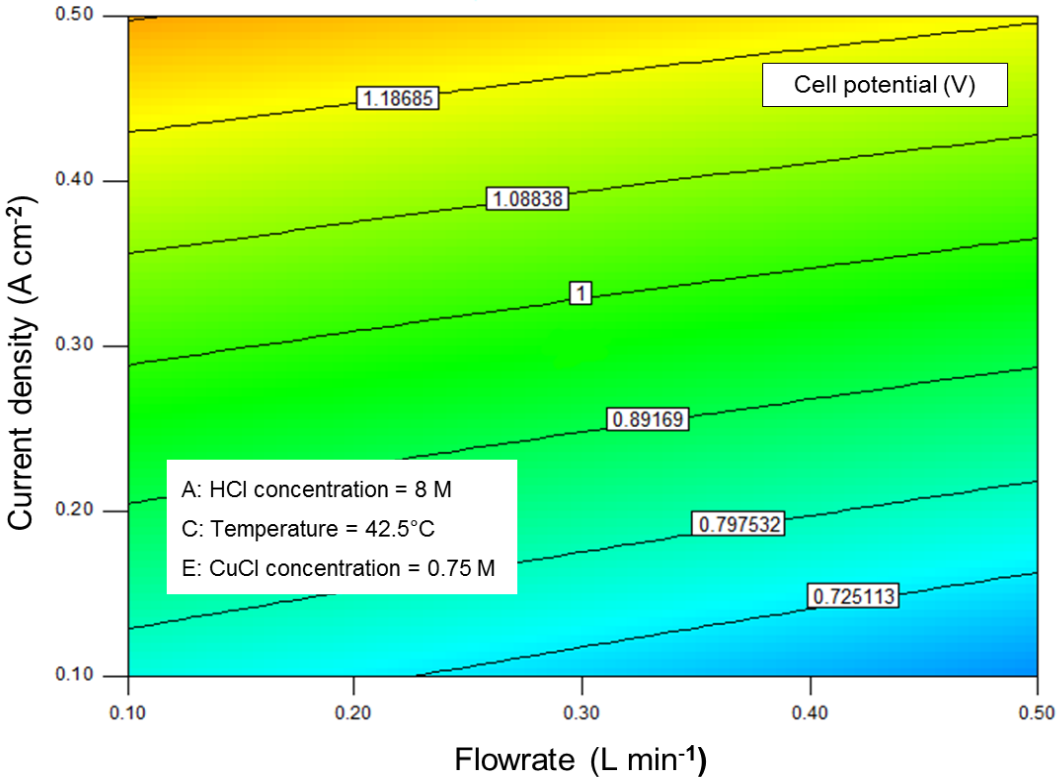

Figure 6.31Influence of current density and flow rate on the cell voltage.

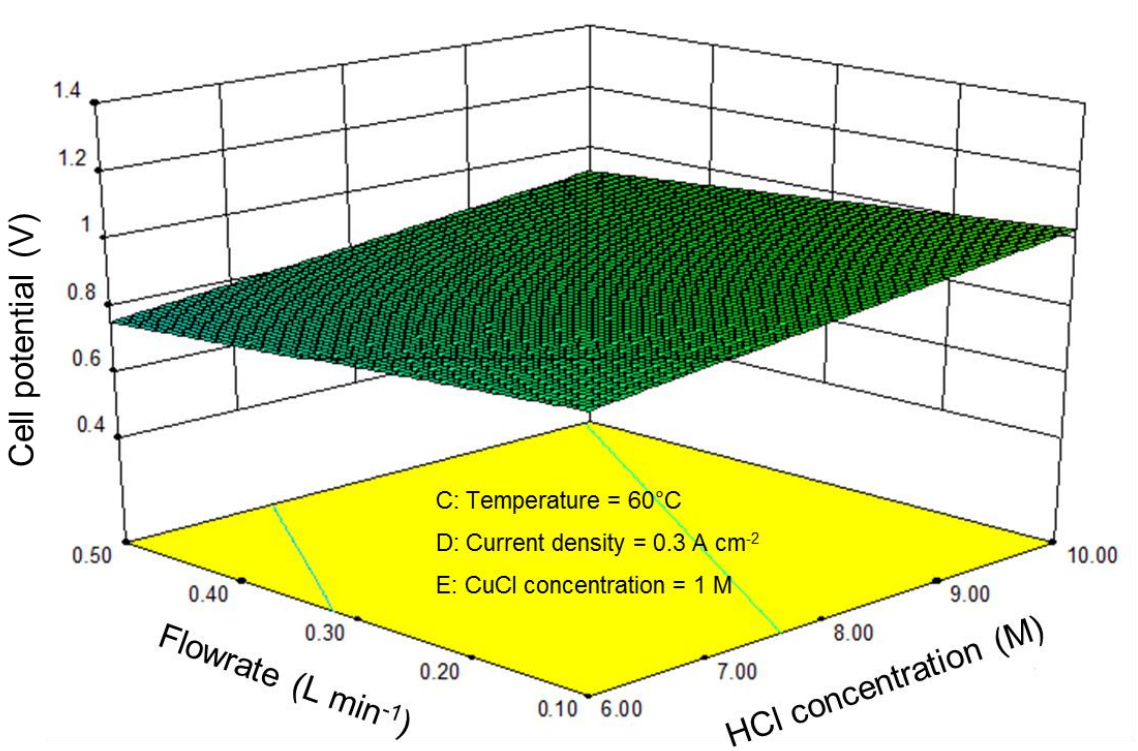

Figure 6.32 Influence of HCl concentration and flow rate on the cell voltage.

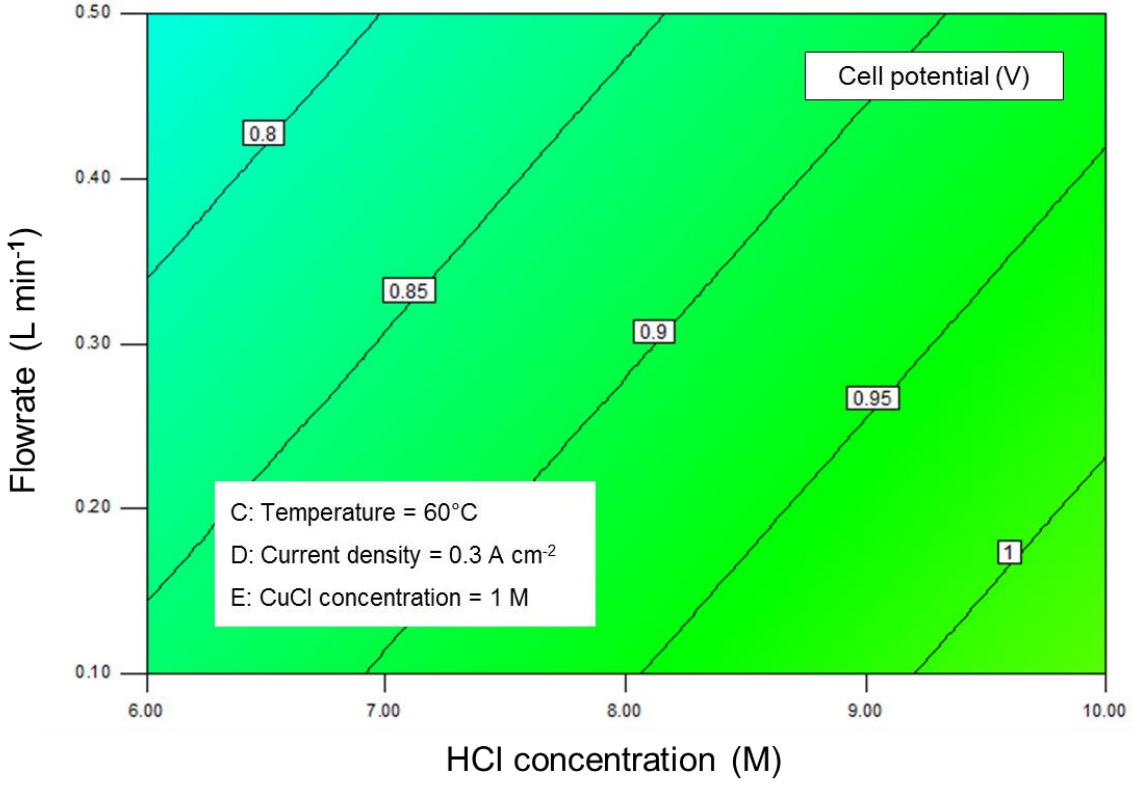

Figure 6.33 Influence of HCl concentration and flow rate on the cell voltage.

Figure 6.34 shows how three factors include HCl concentration, temperature, and flow rate combine to affect the cell potential when the applied current density and CuCl concentration are kept constant at 0.3A.cm^{-2} and 1M respectively. It is shown that the lower cell potential is predicted to be about 0.76V where the highest is estimated 1.12V. The combination of lowest HCl concentration, highest flow rate at the maximum operation temperature results in the lowest predicted value. Changing the current density to 0.5A.cm^{-2} would suggest the lowest cell potential of about 1.08V.

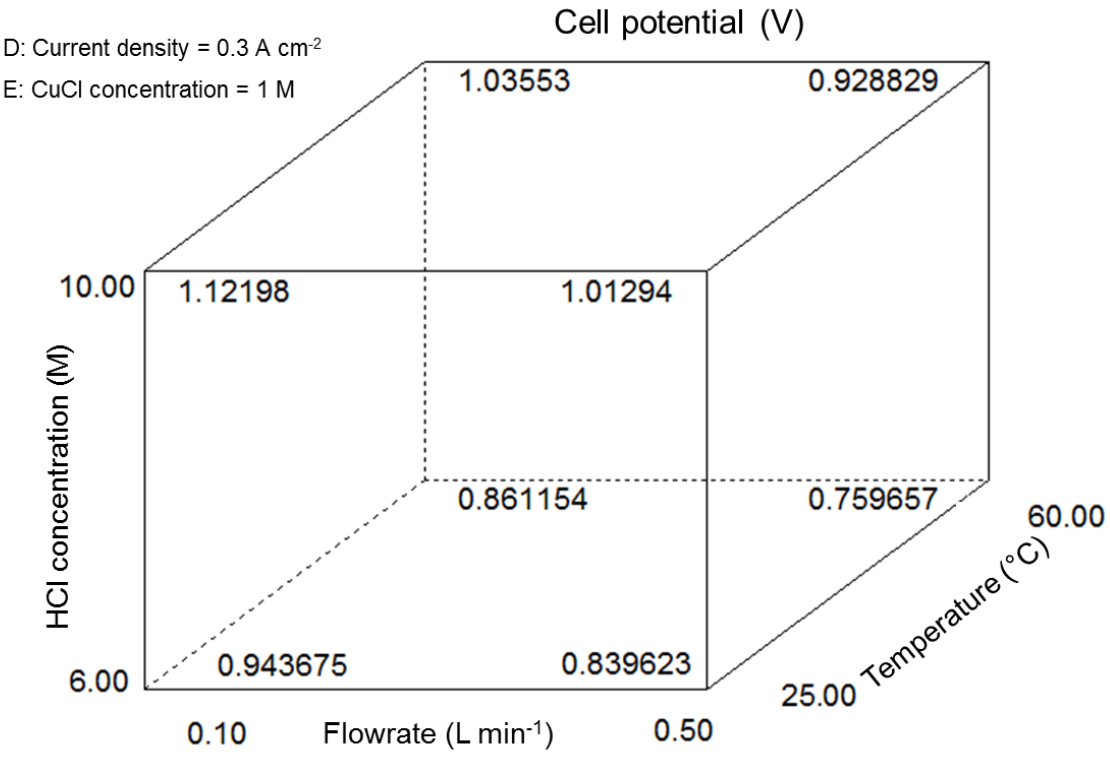

Figure 6.34 Three-factor effect on the cell potential.

.

For better understanding of the electrolysis performance, numerical optimization of the proposed model is carried out to search for a combination of factors that simultaneously satisfy the requirement of the cell potential to be minimized in the

specific range. The flow rate, temperature, and CuCl concentration are set to the fix value of 0.5L.min^{-1}, 60˚C, and 1M respectively. The cell potential is supposed to be minimized with the limit range of 0.7V to 0.9V. Numerical optimization finds a point in the fitted model that maximized the desirability function. Desirability is an objective function that reflects the desirable range for the response variable, which is the cell voltage. In this minimization problem, desirability is zero if the cell voltage is higher than 0.9V and it is one if the cell voltage is lower than 0.7V. Desirability varies from 0 to 1 if the cell potential is any value between 0.7V and 0.9V. The optimization algorithm begins at a random starting point and proceeds up the steepest slop to a maximum. Multiple starting points are chosen to improve chances of finding the best local maximum. Figures 6.35 and 6.36 show the results of optimization.

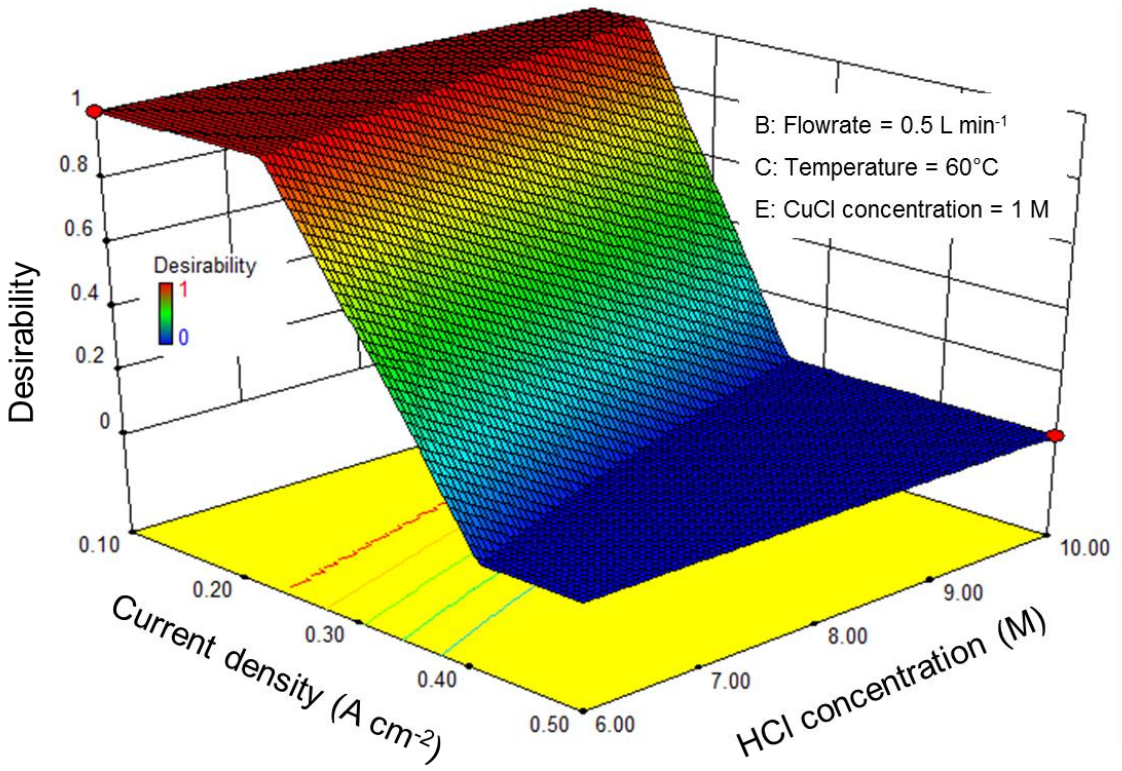

Figure 6.35 Variation of desirability with the current density and HCl concentration.

It is observed that to have a cell potential at the maximum point of 0.7V, the current density couldn't be higher than 0.25A.cm^{-2}, in the best possible operating condition. For the cell potential up to 0.9V, the applied current density could increase up to 0.4A.cm^{-2}.

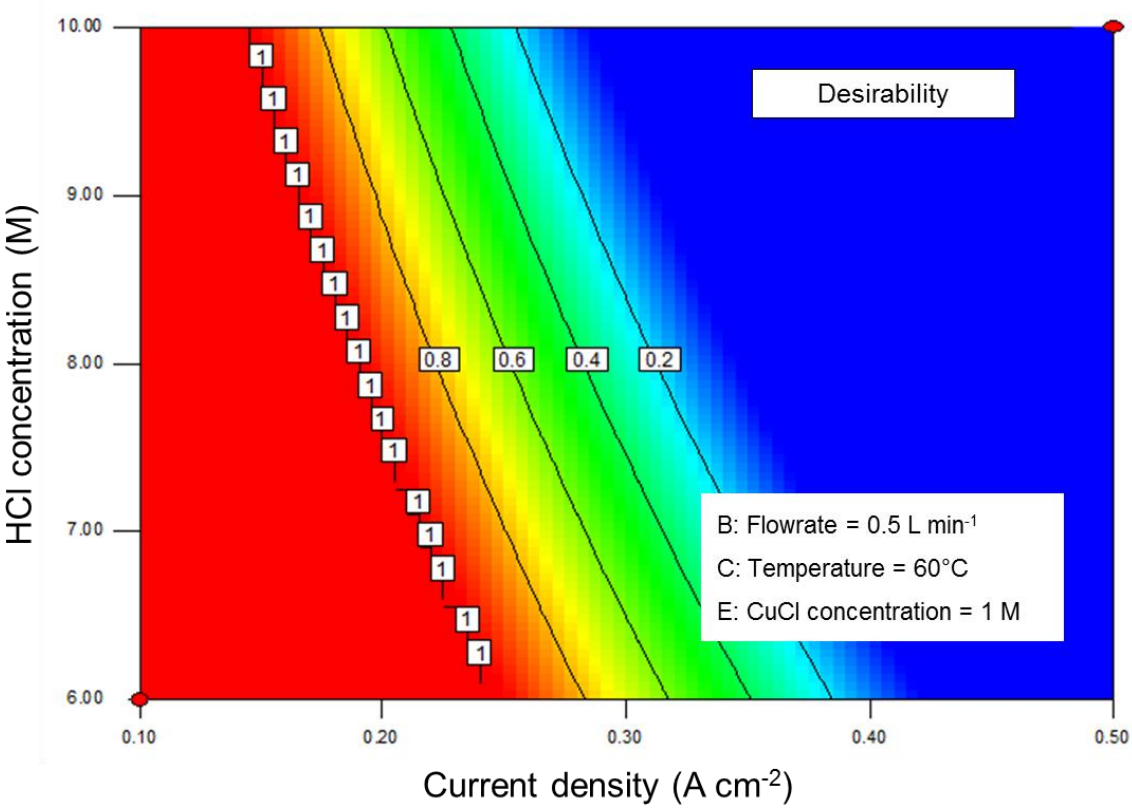

Figure 6.36 Variation of desirability with the current density and HCl concentration.

The hydrogen production rate in the electrolysis process is another important factor that needs careful attention. Figure 6.37 depicts variation of the hydrogen production rate with different applied current densities. The production rate is measured for all 51 experiments and it is on average 93% of its theoretical value. The higher applied current density indicates the faster hydrogen production rate and also the faster Cu^{++} to Cu^{+} conversion rate. Increasing the Cu^{++} concentration in the anolyte solution of

the CuCl electrolysis process manifests the higher cell voltage. However, the more concentrated Cu^{++} solution facilitates process integration of the electrolysis and hydrolysis reactions. It means there is a trade-off between the cell voltage and the energy required to separate Cu^{++} and Cu^{+} when the anolyte solution is recycled back to the hydrolysis reactor.

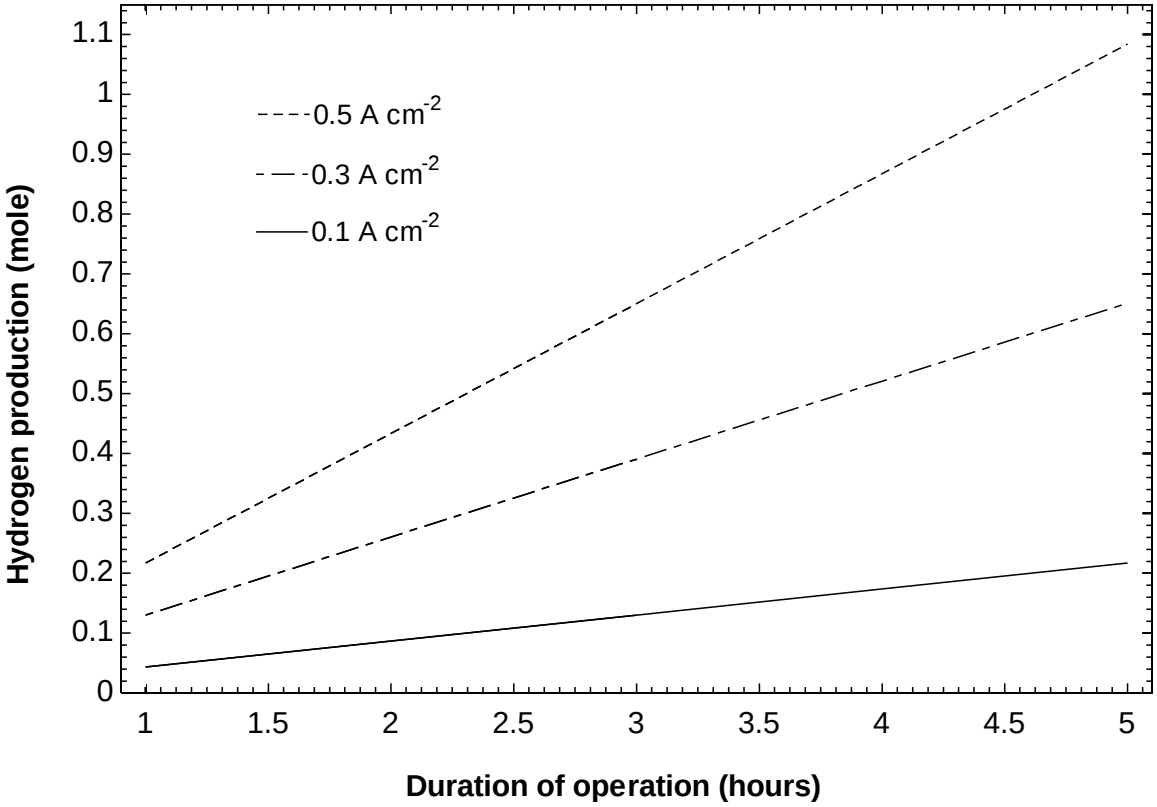

Figure 6.37 hydrogen production rates in the CuCl electrolysis process.

The correlation between the Cu^{++} to Cu^{+} molar ratio and the cell voltage is depicted in Figure 6.38. It is illustrated that the cell voltage increases almost 0.5V for the molar ratio of 75% which have been proposed to be assumed as the maximum acceptable ratio [91]. In order to have a clear insight into integration of the electrolysis process to

upstream and downstream processes in the Cu-Cl cycle, the conversion rate of the Cu^{++} to Cu^{+} in the electrolysis reaction should be quantified. For the electrolysis cell, every electron transferred is one conversion from Cu^{+} to Cu^{++}. It means that the number of electron transferred, which is directly correlated to the hydrogen production rate, is exactly equal to the number of Cu^{++} has been produced. This neglects any side reactions, but, because the potential the cell is working is pretty low, it is assumed that no side reaction is happened. Figures 6.39 and 6.40 depict the Cu^{++} to Cu^{+} molar ratio with the experiment running time for 3 liter solution with 1M and 0.5M CuCl concentrations, respectively. It is shown that the higher applied current density results in the faster conversion rate.

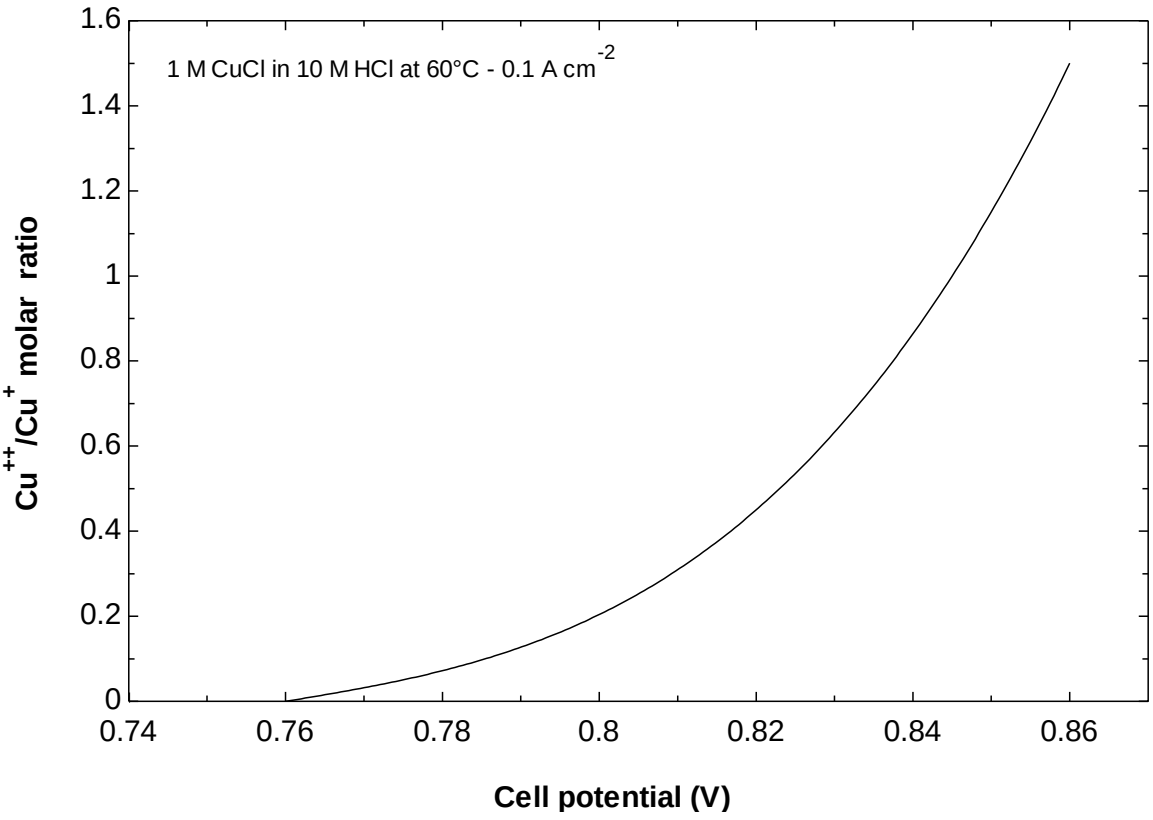

Figure 6.38 Cu^{++} to Cu^{+} ratio versus CuCl electrolysis cell potential.

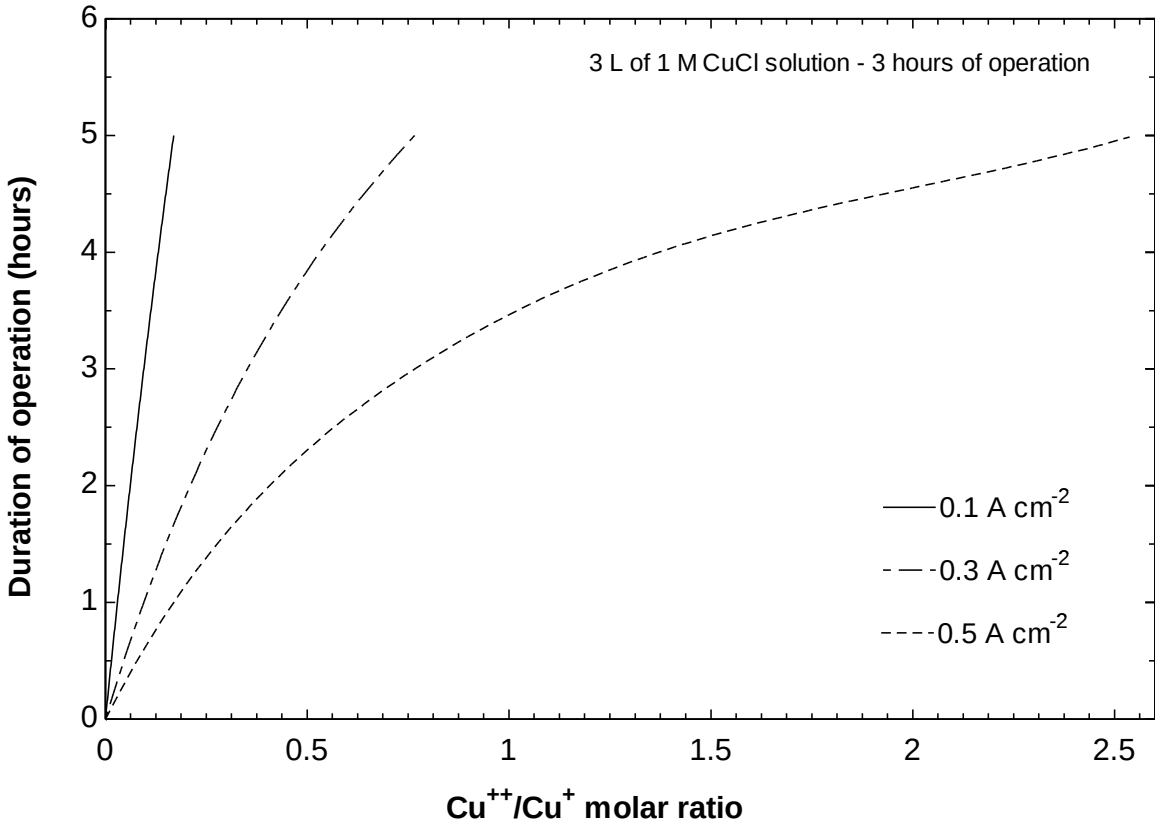

Figure 6.39 Duration of the operation versus Cu^{++} to Cu^{+} ratio, 1M CuCl solution.

The optimum duration of operation to reach the assumed maximum Cu^{++} to Cu^{+} ratio of 75% is dependent to the initial concentration of CuCl, the current density, and the capacity of the solution containers. It should be also mentioned that no copper deposition is observed on any component of the cell after all experiments. Measurements of copper species concentration in catholyte solution reveal an existence of a very small amount of copper which confirm a negligible effect of copper crossover on the cell performance. The amount of copper species in the catholyte with HCl concentration of 6M and 10M is measured $0.12 mg.L^{-1}$ and $0.075 mg.L^{-1}$ respectively. These values are the averages of 10 repeated measurements of 6 different samples for each concentration. It is revealed that the higher HCl concentration prevents copper crossing over the membrane.

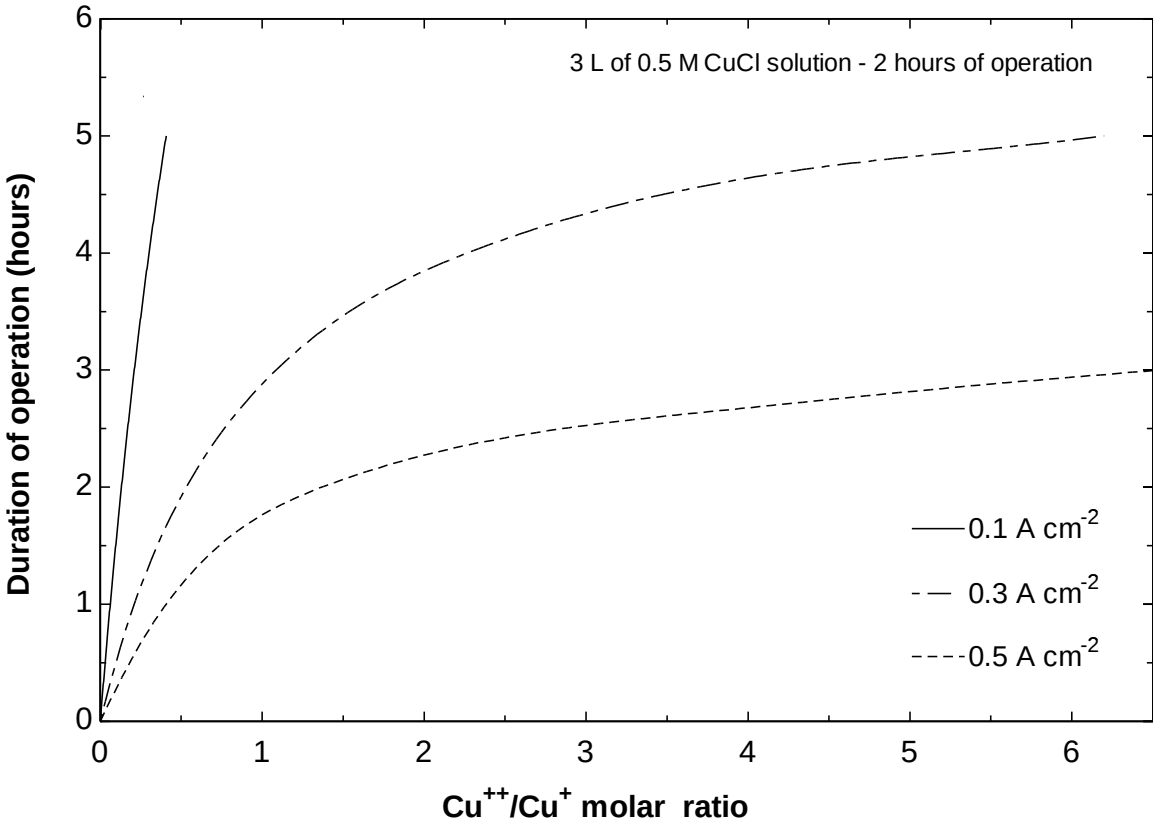

Figure 6.40 Duration of the operation versus Cu^{++} to Cu^{+} ratio, 0.5M CuCl solution.

The propagation of experimental uncertainties through calculation of the cell potential and the hydrogen production rate is shown in Table 6.2. Calculation of uncertainty for the cell potential is based on equation (6.1). Hydrogen production rate is calculated by the multiplication of H_2-N_2 mixture flow rate and the hydrogen concentration. It means that the propagation of uncertainty associated with the flow rate measurement and the concentration of produced hydrogen, measured by the hydrogen analyzer, are calculated to estimate uncertainty of the hydrogen production rate. It is demonstrated that uncertainties associated with the cell potential and hydrogen production rate are about 2.8% and 8.5%, respectively. The uncertainty values indicate high accuracy of the experimental results.

Table 6.2 Propagation of the experimental uncertainties.

Variable	Bias error	Precision eror	Uncertainty
Cell potential	0.019	0.021	0.028
Hydrogen production rate	0.067	0.053	0.085

6.3 Integration of a gasification process and the Cu-Cl cycle

Gasification is a promising technology that can convert waste materials into high-value fuels and chemicals. Since gasification processes can be combined with high-efficiency gas turbines, it also provides potential as a source of power generation. During the design and operation of gasification systems, comprehensive parametric studies are essential to ensure that feedstocks with different chemical compositions produce syngas with the right mixture of chemical species. The desired composition of syngas is related to the desired end products, such as heat, power, H_2, or chemicals such as methanol and ammonia. The gasification temperature, the oxygen fraction of input air and the amount of input steam are the main parameters that can be adjusted to change the operating conditions and performance of a gasifier. Figure 6.41 depicts the effects of equivalence ratio (ER) on the gasification temperature. In the gasification with air, an ER of 0.5 is corresponding to the point that the solid carbon is totally gasified. This occurred when the temperature researches to 1320˚C in which the exergy efficiency is maximized. It should be mentioned that since the ER is defined as the amount of oxygen is added to the gasification reactor proportional to the amount needed for complete combustion, an ER equal to 1 represents stoichiometric combustion of the fuel.

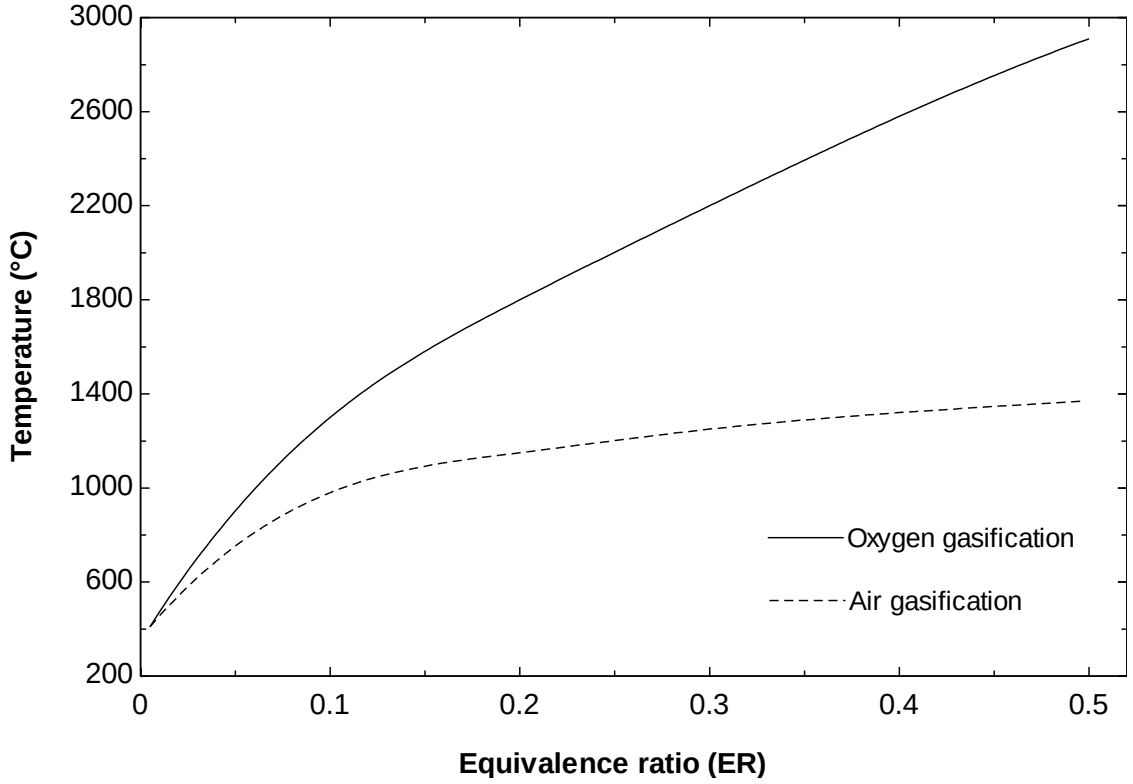

Figure 6.41 Variation of the gasification temperature with ER.

An sensitivity analysis of the gasification process confirms that using oxygen instead of air can effectively improve the combustion efficiency and significantly reduces the NOx emissions. As shown in Figure 6.41, using oxygen instead of air increases the gasification temperature to about 3000˚C. This occurs due to the decreased amount of nitrogen that generally performs as a heat carrier. In the higher temperature, the physical exergy of the produced syngas increases and the gasification exergy efficiency improves. Moreover, addition of oxygen instead of air has the benefit that a smaller amount of gas required to be heated up to the reactor temperature that results in reduction of the exergy loss in the gasifier. As illustrated in Figure 6.42, the exergy efficiency of the gasification process increases by 10% when air is substituted with oxygen.

It is shown in Figure 6.42 that the choice of oxygen or air as a gasification medium has a substantial effect on the gasification performance. Operation at lower ER, smaller gasifier, reduction in NOx emissions, and potential saving in the compression for the produced syngas is the other advantages of using oxygen instead of air. However, production of oxygen in an air separation unit (ASU), which is usually based on cryogenic systems, is costly and requires electricity. It means that the overall exergetic efficiency of the integrated ASU and a gasification process would be lower than a standalone gasification process. This indicates that an integration of a gasification process and the Cu-Cl cycle is a very attractive solution since the production of oxygen in the Cu-Cl cycle does not require additional input energy.

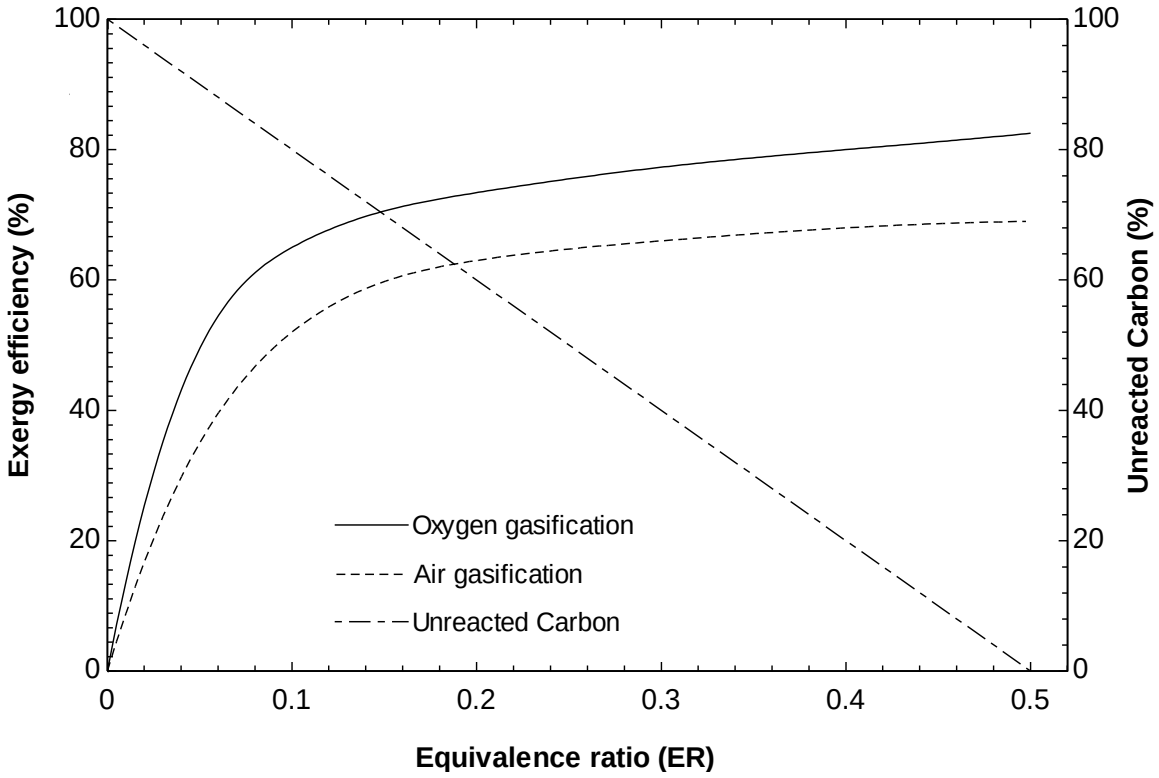

Figure 6.42 Variation of the gasification exergy efficiency with ER.

The energy efficiency of the Cu-Cl cycle is highly dependent to the amount of steam recovered for the hydrolysis reaction. It means that the cycle performance is very sensitive to amount of steam could be generated in HRSG unit when integrated with an IGCC system. In reference to the result presented in Figure 6.12, If the HRSG unit could satisfy excess steam requirement of the hydrolysis reaction up to 17 times of its stoichiometric value, the energy efficiency of the Cu-Cl cycle would increase up to 88% comparing to the cycle efficiency of 22.8% when no excess steam recovered. Heat recovery from the syngas cooling unit of an IGCC, which is mainly used for steam generation in the combined cycle of the original Texaco gasification design, can potentially satisfy steam requirement of the hydrolysis process in the Cu-Cl cycle. Assuming a fixed gas turbine inlet temperature, the IGCC overall efficiency will change if the steam bottoming cycle capacity is modified by integration of the gas cooling unit with the Cu-Cl cycle [7]. Figure 6.43 shows the results of the sensitivity analysis, and how the steam cycle efficiency affects the IGCC overall efficiency at different gas turbine inlet temperatures. It is shown that decreases in the capacity of the steam power generation in the combined cycle of IGCC reduces maximum 2.9% of the overall IGCC plant efficiency. Consequently, the energy efficiency of the coupled IGCC and the Cu-Cl cycle is estimated to be about 38%.

The higher gasification temperature increases the physical exergy of the produced syngas and improves the gasification exergy efficiency. Figures 6.44 and 6.45 depict variation of the gasification exergy efficiency with the temperature for both oxygen and air gasification processes, respectively. It is shown that the oxygen gasification has higher exergetic efficiency because of its higher operating temperature.

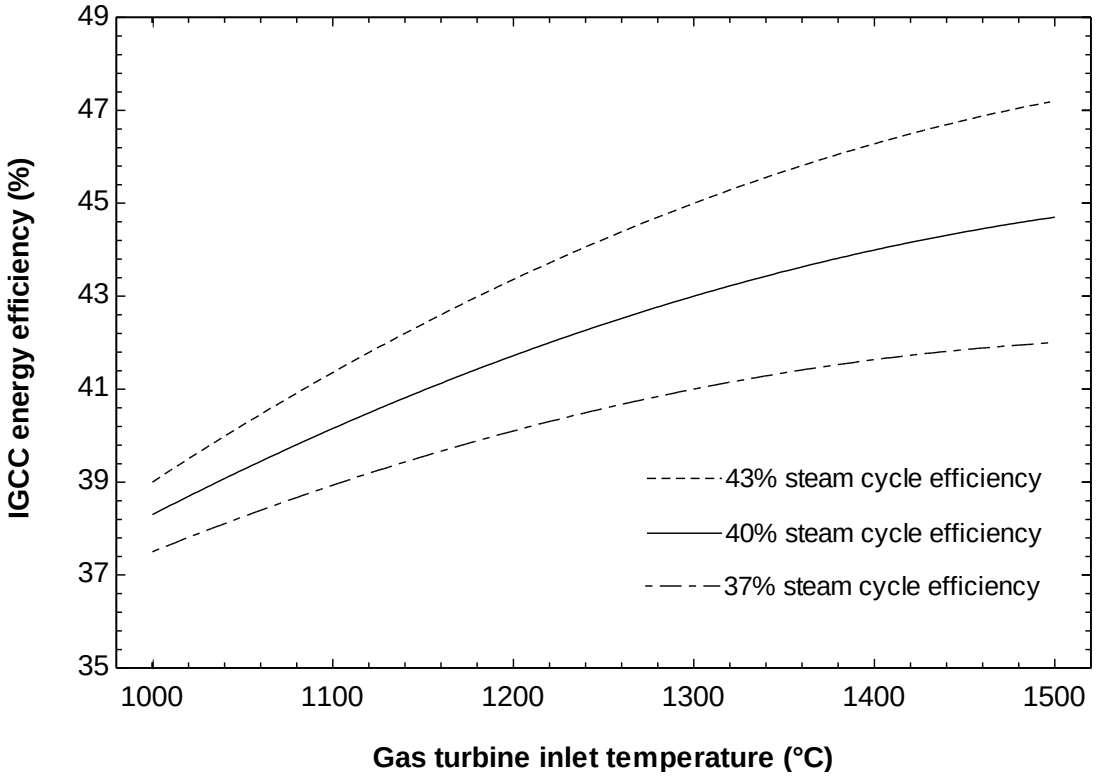

Figure 6.43 Variation of IGCC energy efficiency with the gas turbine inlet temperature and the steam cycle efficiency.

A gasification reaction with oxygen corresponds to a very high operating temperature which has its own problems. The higher temperature of the gasifier makes its operation complicated and increase the exergy loss potential. Consequently, steam could be added to the gasifier to moderate the operating temperature and replace part of oxygen supply. As long as the temperature is kept above 1320˚C, the reaction equilibrium is not changed. Figure 6.45 depicts the amount of steam required to replace oxygen in the gasification reaction. The inlet temperature of steam is assumed to be 250˚C. It is shown that at any point below the ER of 0.4, which corresponds to the temperature of 1320˚C, the slop of the steam to carbon ratio increases. It means that relatively more steam should be supplied to reach complete gasification. The temperature profile of the gasification process shows how steam could effectively moderate the operating temperature.

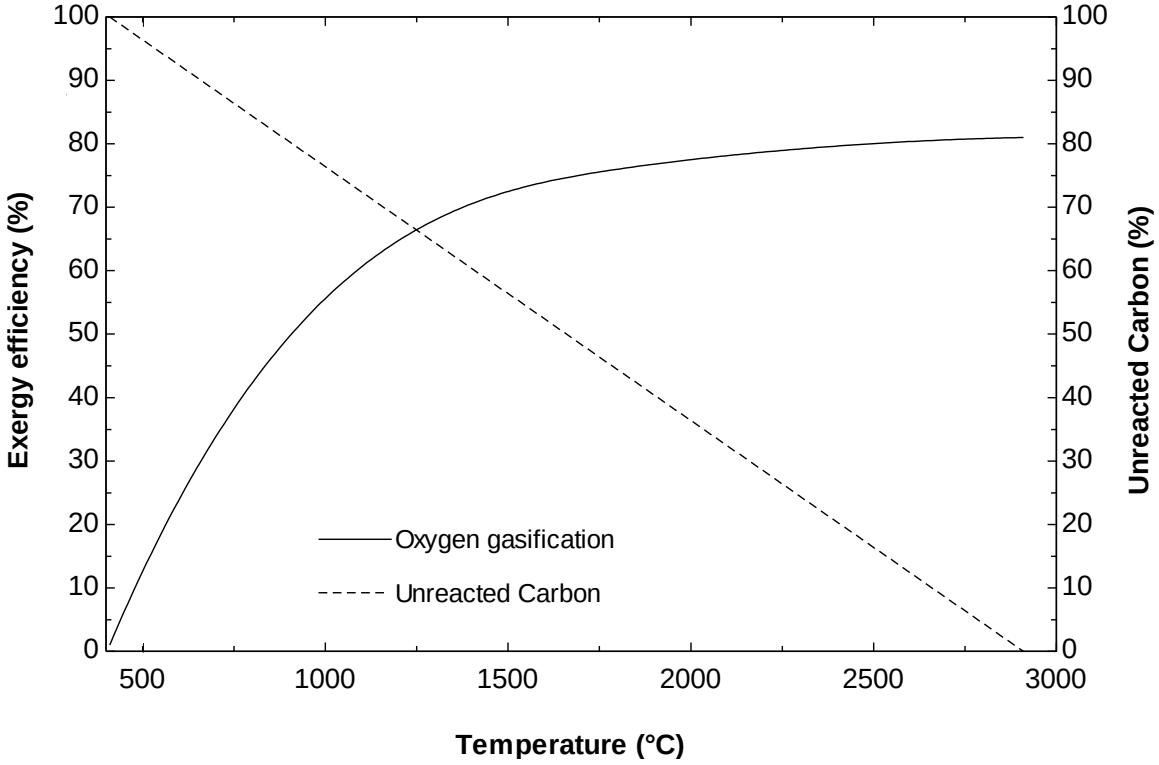

Figure 6.44 Variation of the exergy efficiency with temperature in oxygen gasification.

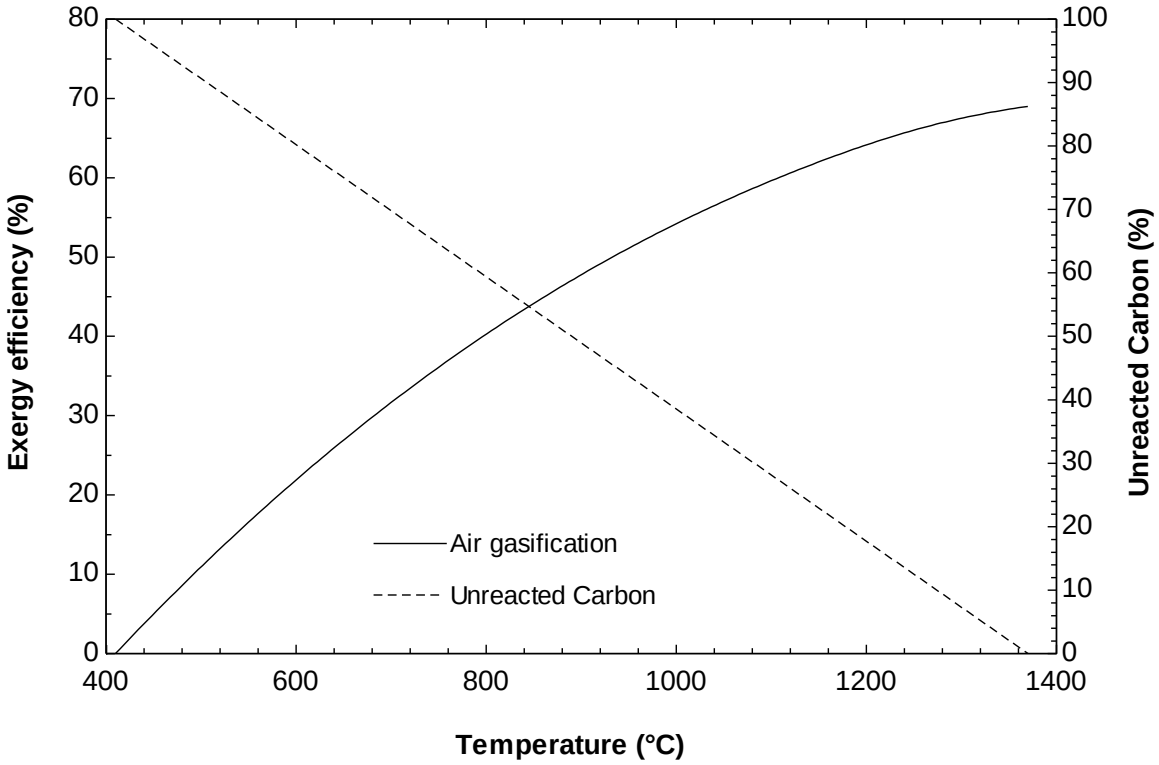

Figure 6.45 Variation of the exergy efficiency with temperature in air gasification.

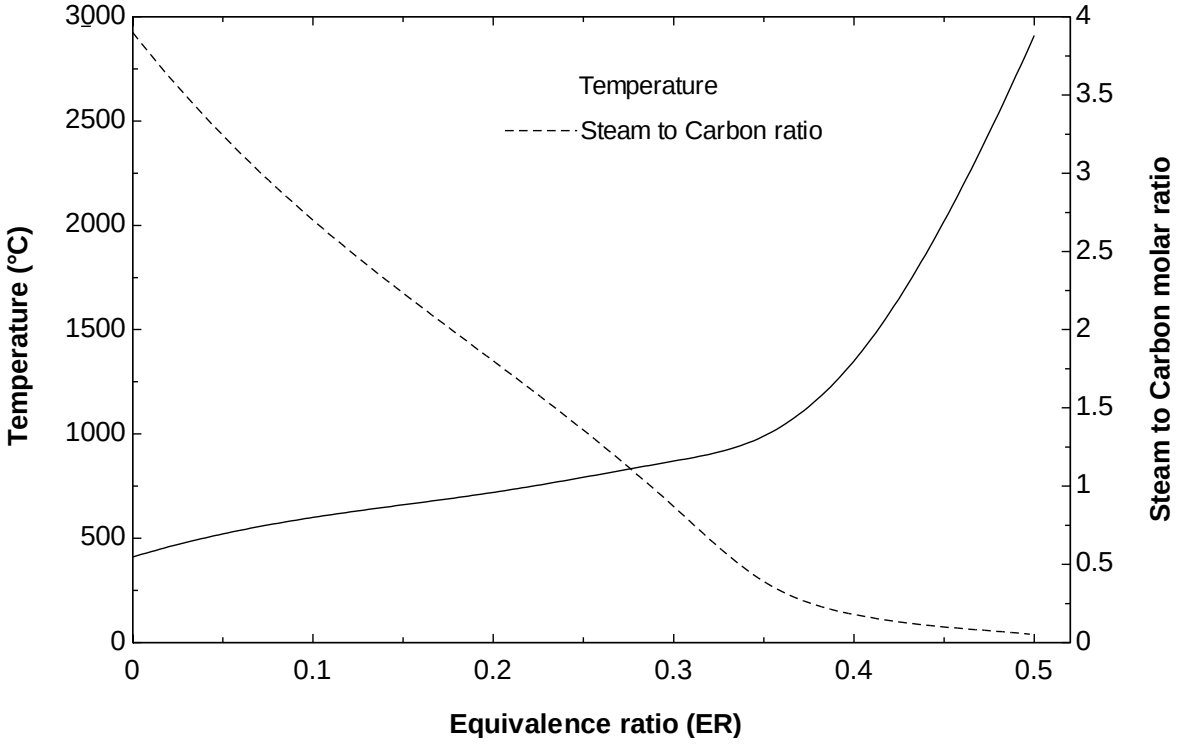

Figure 6.46 Variation of the steam to carbon ratio and gasification temperature with ER.

The effects of steam to carbon ratio on the gasification temperature and its exergetic efficiency are shown in Figure 6.47. It is illustrated that increasing the steam to carbon molar ratio beyond 0.5 significantly decrease both temperature and exergy efficiency. The optimum ratio should be chosen based on desired syngas composition. The effect of ER and its corresponding steam to carbon ratio on the syngas composition is illustrated in Figure 6.48. By increasing the ER, which leads to increase in the gasification temperature, the hydrogen content of the produced gas increases because of endothermic behavior of the water-gas reaction, equation (5.26). Moreover, the amount of CO in the product gas increases with a higher gasification temperature, due to exothermic and reversible behavior of the water-gas shift reaction, equation (5.27). The amount of

CO_2 in the syngas is higher in the beginning and then starts decreasing with a rising temperature.

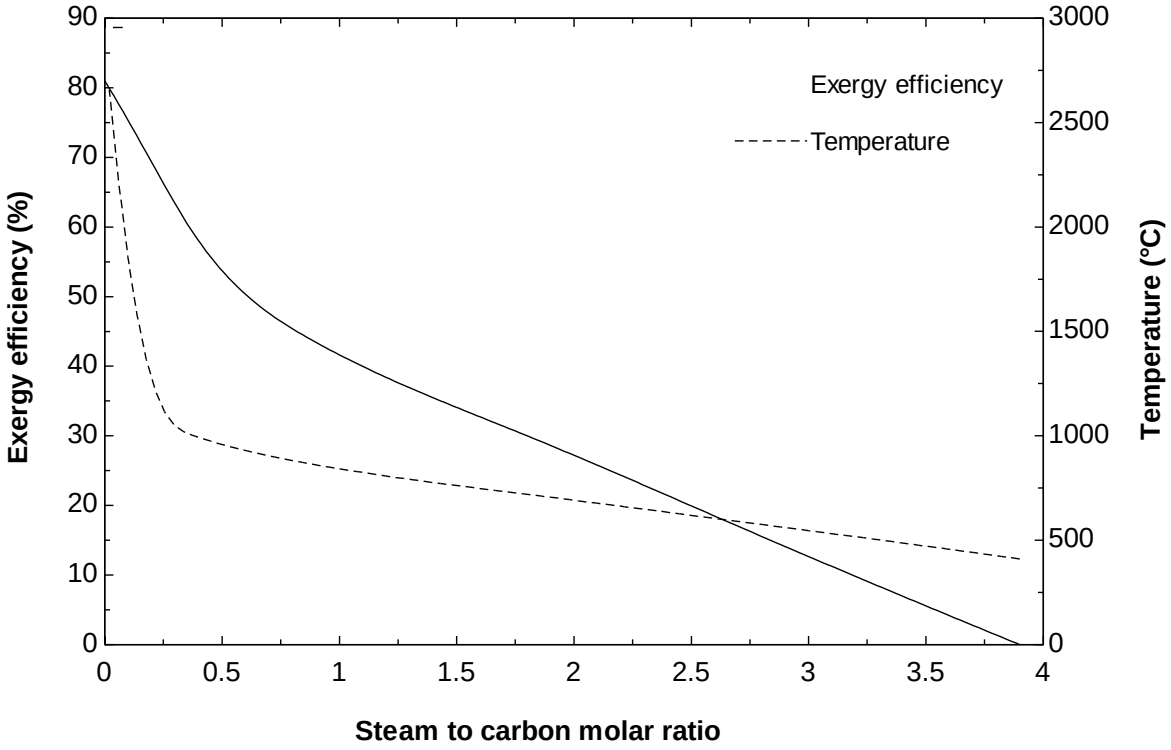

Figure 6.47 Variation of the gasification temperature and exergy efficiency with steam to carbon ratio.

Increasing the ER from 0.3 to 0.5 decreases the hydrogen content of a syngas and promotes formation of CO. The reason is that by decreasing the amount of steam in the gasifier, the partial oxidation reaction replaces the water-gas reaction and further rise of temperature helps CO formation in the exothermic water-gas shift reaction, equation (5.27). So, if the hydrogen content of a produce syngas required to be maximized, the optimum operating condition is ER equal to 0.3 corresponding to the steam to carbon molar ratio of 0.85. In this case, the optimum gasification temperature for a syngas with maximum hydrogen content is about 890˚C. Figure 4.49 depicts variation of the syngas H_2 and CO molar concentrations with the gasification temperature.

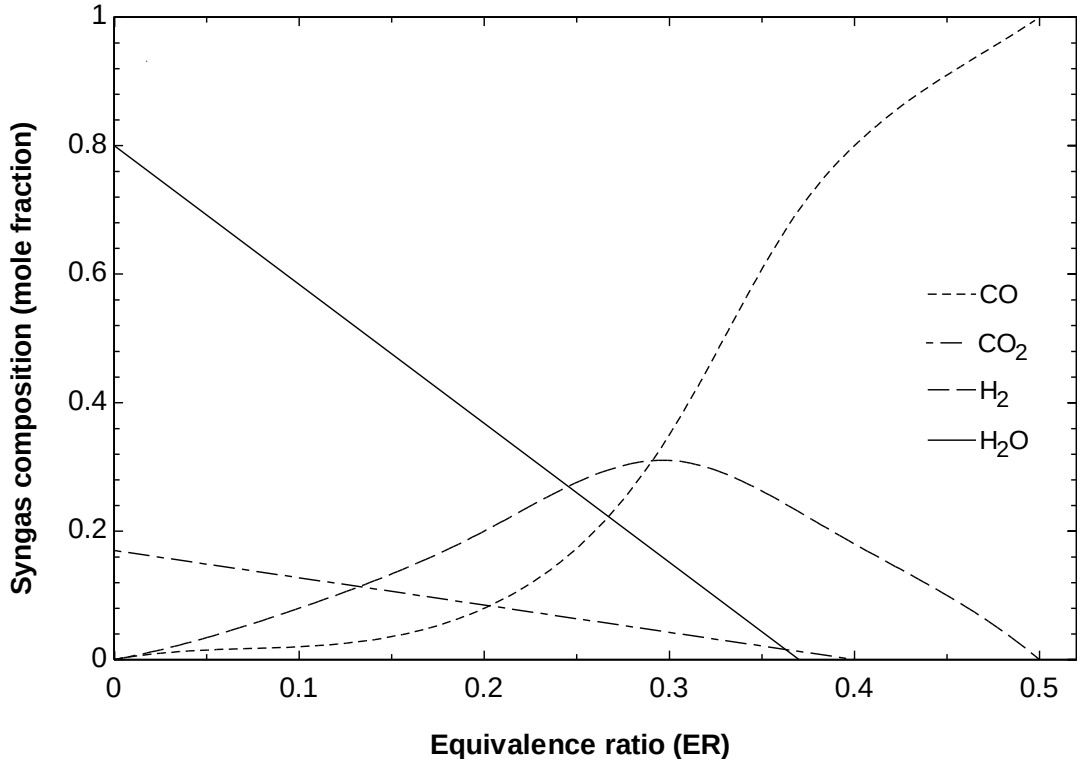

Figure 6.48 Variation of syngas composition with ER.

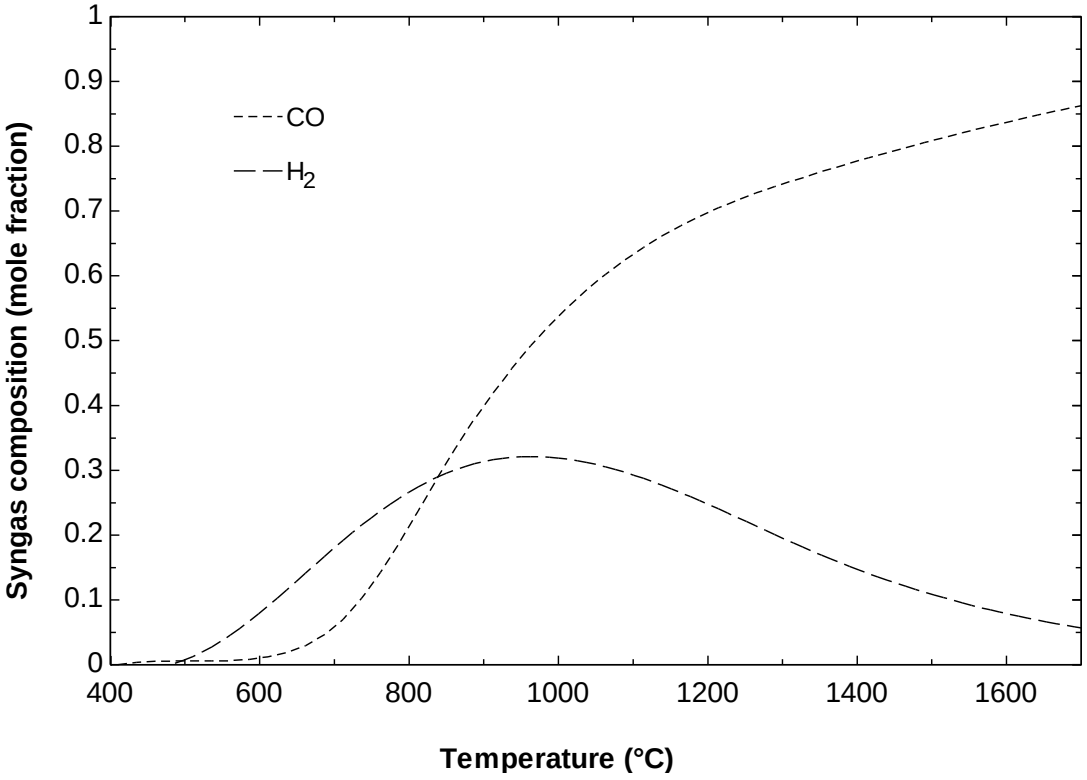

Figure 6.49 Variation of syngas composition with the gasification temperature.

The moisture content of a feedstock could significantly change the gasification temperature and LHV value of a produced syngas. Figure 6.50 shows the variation of the gasification temperature and LHV value of syngas with the moisture content of input fuel. As depicted, in equivalence ratio of 0.38 where water completely consumed in the gasification process, increasing the moisture content of a feedstock from 11.12wt% to 30wt% could decrease the reaction temperature from 1250˚C to 1010˚C. Furthermore, increasing the moisture content of fuel considerably decreases LHV of the produced syngas.

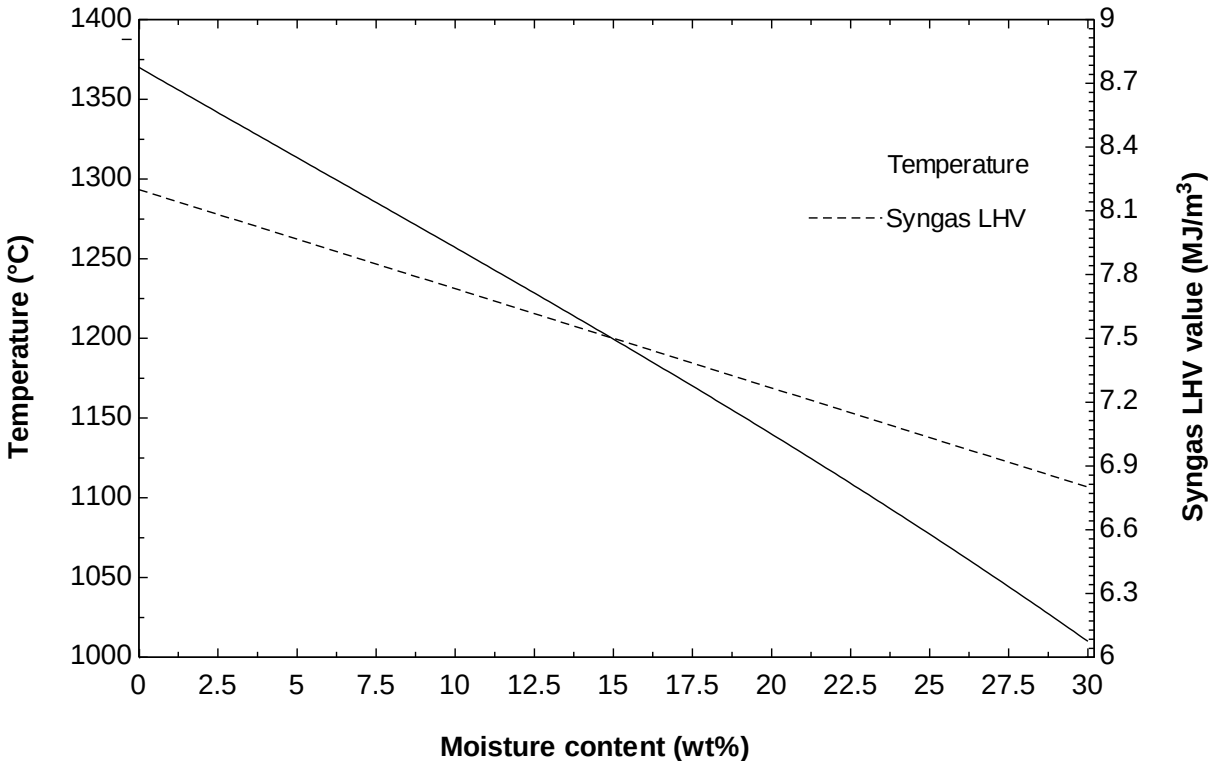

Figure 6.50 Variation of syngas LHV and gasification temperature with the fuel moisture content.

The influence of moisture content of the fuel on the exergy efficiency of the gasification process is very important and needs to be considered. Figure 4.51 illustrates

the effect of the fuel moisture content on the exergy efficiency of the oxygen and air gasification processes. It is shown that the higher moisture contents results in the lower exergy efficiency. This effect is slightly more significant in the air gasification process.

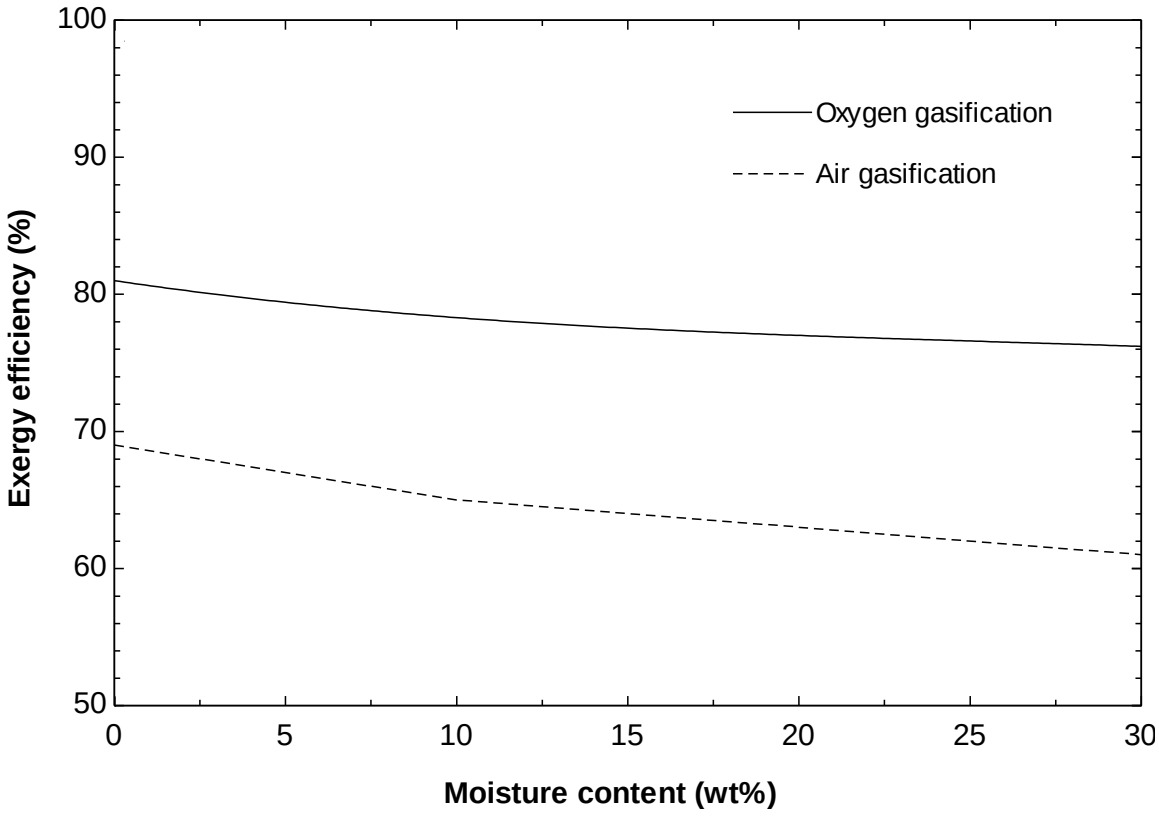

Figure 6.51 Variation of exergy efficiency with the fuel moisture content.

Chapter 7: Conclusions and Recommendations

7.1 Conclusions

In the process integration analysis of the hydrolysis and electrolysis processes, integrated process model of the hydrolysis and electrolysis processes of the Cu-Cl cycle was proposed using intermediate heat recovery steam generator (HRSG) and HCl-H_2O separation process. The separation process contains rectification and absorption processes which are internally coupled. Integrated process model of the proposed system was completely simulated. In this study:

- It was demonstrated that the steam generated in the HRSG unit satisfies the extra steam requirement of the hydrolysis reaction and the separation process effectively produces HCl acid up to the concentration of 22mol% for the electrolysis reaction.
- The influence of operation factors such as reflux ratio, feed composition, solvent flow rate, and temperature were analysed on the performance of the separation system.
- It was found that the reflux ratio has a dominant effect on operation of the rectification column. For a constant product flow rate, 50% increment in the reflux ratio could results in 10% improvement in the HCl concentration, but could adversely increase required heating duty up to 30%. Solvent flow rate had a great effect on operation of the absorption column.
- It was shown that 50% increment in the solvent flow rate reduces the concentration of the produce acid by 15%. The effects of number of stages in the columns on the

separation performance were also investigated and heat duty requirements and composition of products were calculated.

In the experimental development and factorial design of the electrolysis process, a lab-scale CuCl electrolysis process was designed, fabricated and tested. The effects of operating parameters including HCl and CuCl concentrations, applied current density, temperature, and solution flow rate on the cell potential and hydrogen production rate were experimentally investigated. Test bench and measurement techniques were introduced for better characterization of the experiment. In this study:

- Two-level fractional factorial design was performed, considering three replications and one centre point.
- The ANOVA analysis confirms the accuracy of the proposed model. The calculations are based on design of experiment methods to find a correlation between cell voltage and operational factors. The model permits prediction and comparison of all main effects and all interaction effects on the cell voltage to provide valuable insight into the integration of the electrolysis process.
- It was shown that the more concentrated HCl solution and higher applied current density led to a higher cell voltage.
- It was demonstrated that increasing the flow rate and temperature of the solution helps to reduce the cell potential. The effect of temperature is not significant.
- Combinatory effects of current density with flow rate and HCl concentration were also analysed and discussed. The new predictive model provides the opportunity to find the optimum operating conditions corresponding to the minimum cell potential.

- The hydrogen production rate in CuCl electrolysis process was estimated for different applied current densities. Good agreement between the theoretical and measured hydrogen production rates shows the H_2 production ratio of about 93%.
- The Cu^{++} to Cu^{+} conversion rate was calculated for solutions with different initial CuCl concentration and the effects of Cu^{++} to Cu^{+} ratio on the cell voltage was analysed and discussed.

In the system integration analysis of a gasification process and the Cu-Cl cycle, the effects of using oxygen instead of air on the gasification process are investigated where oxygen is provided by the Cu-Cl cycle. In this study:

- The influence of equivalence ratio (ER) on the gasification temperature and its exergetic efficiency was analyzed and compared for both air and oxygen gasification process.
- It was shown that oxygen gasification has higher temperature of operation and the advantage of 10% higher exergy efficiency in a complete gasification. Moreover, Operation at lower ER, smaller gasifier, reduction in NOx emissions, and potential saving in the compression for the produced syngas is the other advantages of using oxygen instead of air.
- An integration of the gasification process and the Cu-Cl cycle was found as an attractive option since production of oxygen with air separation units in typical IGCC power plants are costly and requires extra energy input.
- The effects of ER and steam to carbon ratio on the gasification temperature and composition of the produced syngas were analyzed and discussed. It was shown that if the hydrogen content of a produce syngas required to be maximized, the optimum

operating condition is ER equal to 0.3 corresponding to the steam to carbon molar ratio of 0.85. In this case, the optimum gasification temperature is about 1000˚C.

- Investigation on the influence of fuel moisture content on the gasification temperature and LHV of syngas was shown that the increasing the moisture content of a feedstock from 11.12wt% to 30wt% could decrease the reaction temperature from 1250˚C to 1010˚C and considerably decreases the LHV of syngas.
- It was shown that in an integrated system of IGGC and the Cu-Cl cycle, supplied heat by the syngas cooling section of an IGCC plant, previously used for steam generation, may be utilized as the major input of external heat required for the hydrolysis reaction of the Cu-Cl cycle, with minor modification on the IGCC steam cycle.

7.2 Recommendations

System integration analysis of the Cu-Cl cycle offers several main areas of future research as summarized below:

- In the proposed integrated process model of the hydrolysis and electrolysis processes, the required capital investment and operating cost for the hydrogen production capacity of 5kg per day should be further estimated. It is suggested that part of the recovered heat in HRSG unit is utilized to generate electricity for the electrolysis reaction. An organic rankine cycle (ORC) is a good option to generate electricity from low grade temperature heat sources.
- In the experimental study and statistical modeling of the CuCl electrolysis process:

- The similar modeling procedure is suggested to be carried out for different kind of membranes and electrode materials.
- Increasing the operating temperature beyond 60˚C causes considerable amount of HCl vapor escapes the system. This could result in a lower concentration of HCl acid in a long period of operation. It is suggested that the amount of loss is quantified. Increasing the system pressure allows working at higher temperature without having the HCl loss problem and also helps producing hydrogen at higher pressure. This is suggested to be further studied.
- The experiment test bench is designed to work in a semi-continuous mode. The hydrolysis and electrolysis processes are needed to be completely integrated and interactions of the operation factors should be experimentally investigated.
- Preparing the anolyte solution requires very careful attention to prevent pre-oxidation of CuCl to $CuCl_2$ which could adversely affect the electrolysis cell voltage. Purging nitrogen significantly solves the problem but searching for a more effective way should be further investigated. The amount of dissolved oxygen in the anolyte solution is also recommended to be quantified.
- Using more accurate flow measurement devices in the experiment would help to calculate the amount of hydrogen production more accurately.

- In the system integration of a gasification process and the Cu-Cl cycle, the capital investment requires to be estimated. Although, the influence of using oxygen instead of air on the gasification performance is thermodynamically studied, but the effects on the operating cost should be further studied. In the gasification model, heat losses from the gasifier to the environment and char formation are suggested to be included.

The effects of heat recovery in the hydrolysis reaction on the total operating cost of the Cu-Cl cycle are suggested to be evaluated.

References

[1] Olejarnik P. World Energy Outlook. International Energy Agency, France; 2010.

[2] Pachauri RK. Climate Change 2007: Synthesis Report. Contribution of Working Groups I, II and III to the Fourth Assessment Report of the Intergovernmental Panel on Climate Change. IPCC, 2007.

[3] Hirsch R, Bezdec R, Wending W, Peaking of world oil production: impacts, mitigation and risk management. US Department of Energy. National Energy Technology Laboratory. 2005.

[4] Schiermeier Q, Tollefson J, Scully T, Witze A, Morton O. Electricity without carbon. *Nature*. 2008; 454: 816-823.

[5] Environment Canada. Overview of the Reported Greenhouse Gas Emissions 2009. Cat. No. En81-6/1-2009E-PDF, Canada, 2010.

[6] Dincer I, Balta MT. Potential thermochemical and hybrid cycles for nuclear-based hydrogen production. *Int J Energy Res* 2011; 35:123-37.

[7] Aghahosseini S, Dincer I, Naterer GF. Integrated gasification and Cu–Cl cycle for trigeneration of hydrogen, steam and electricity. *Int J Hydrogen Energy* 2011; 36:2845-54.

[8] Ponomarev-Stepnoi N. Nuclear-hydrogen power. *Atomic Energy* 2004; 96:375–85.

[9] International Energy Agency. Energy technology perspectives. Organization of Economic Cooperation and Development; 2006.

[10] Dincer I. Environmental and sustainability aspects of hydrogen and fuel cell systems. *Int J Energy Research* 2007; 31:29–55.

[11] Marbán G, Valdés-Solís T. Towards the hydrogen economy? *Int J Hydrogen Energy* 2007; 32 1625-37.

[12] Duffey R, Miller A. From option to solution: nuclear contribution to global sustainability using the newest innovations. World Nuclear Association Symposium, London, U.K., September 2002.

[13] Turner J, Sverdrup G, Mann MK, Maness PC, Kroposki B, Ghirardi M, et al. Renewable hydrogen production. *Intl J Energy Research* 2008; 32:379-407.

[14] Dincer I. Technical, environmental and exergetic aspects of hydrogen energy systems. *Int J Hydrogen Energy* 2002; 27(3):265–85.

[15] Duffey R. Green atoms. *Power and Energy* 2005; 2(2):8–12.

[16] Lewis MA, Masin JG, Patrick AO. Evaluation of alternative thermochemical cycles, Part I: the methodology. *Int J Hydrogen Energy* May 2009; 34(9):4115-24.

[17] McQuillan BW, Brown LC, Besenbruch GE, Tolman R, Cramer T, and Russ BE. High efficiency generation of hydrogen fuels using solar thermo-chemical splitting of water. Annual Report GA-A24972, San Diego, CA. 2005.

[18] Petri MC, Yildiz B, and Klickman AE. US work on technical and economic aspects of electrolytic, thermochemical, and hybrid processes for hydrogen production at temperatures below 550°C. *Int J Nucl Hydrogen Prod Appl*. 2006; 1(1):79.

[19] Elder R. and Allen R. Nuclear heat for hydrogen production: Coupling a very high temperature reactor to a hydrogen production plant. *Prog Nucl Energy* 2009; 51:500.

[20] Muradov NZ, and VeziroÄlu TN. Carbon-neutral fuels and energy carriers. CRC Pressl Llc, Vol. 8, 2011.

[21] Naterer GF, Fowler M, Cotton J, Gabriel K. Synergistic roles of off-peak electrolysis and thermochemical production of hydrogen from nuclear energy in Canada. *Int J Hydrogen Energy* 2008; 33:6849–57.

[22] Lewis MA, Masin JG, O'Hare PA, Evaluation of alternative thermochemical cycles, Part I: The methodology. *Int J Hydrogen Energy* 2009; 34: 4115-24.

[23] Granowskii M, Dincer I, Rosen MA, Pioro I. Thermodynamic analysis of the use a chemical heat pump to link a supercritical water-cooled nuclear reactor and a thermochemical water-splitting cycle for hydrogen production. *J Power Energy Systems* 2008; 2:756–67.

[24] Funk JE. Thermochemical hydrogen production: past and present. *Int J Hydrogen Energy* 2001; 26(3):185–190.

[25] Steinfeld A. Solar thermochemical production of hydrogen - a review. *Solar Energy* 2005; 78:603–15.

[26] Suppiah S, Stolberg L, Boniface H, Tan G, McMahon S, York S, et al. Canadian nuclear hydrogen R&D programme: development of the medium-temperature Cu-Cl cycle and contributions to the high-temperature sulphureiodine cycle. Nuclear Production of Hydrogen, Fourth Information Exchange Meeting, Oakbrook, Illinois, USA; April 14-16, 2010.

[27] Naterer GF, Suppiah S, Lewis M, Gabriel K, Dincer I, Rosen MA, et al. Recent Canadian advances in nuclear-based hydrogen production and the thermochemical Cu–Cl cycle. *Int J Hydrogen Energy* 2009; 34: 2901–17.

[28] Lewis MA, Ferrandon MS, Tatterson DF, Mathias P. Evaluation of alternative thermochemical cycles - Part III further development of the Cu-Cl cycle. *Int J Hydrogen Energy* May 2009; 34(9):4136-45.

[29] Marin GD, Wang Z, Naterer GF, Gabriel K. Byproducts and reaction pathways for integration of the Cu-Cl cycle of hydrogen production. *Int. J. Hydrogen Energy* 2011; 36:13414-24.

[30] Naterer GF, Suppiah S, Stolberg L, Lewis M, Ferrandon M, Wang Z, Dincer I, et al. Clean hydrogen production with the Cu-Cl cycle - Progress of international consortium, I: Experimental unit operations. *Int J Hydrogen Energy* 2011; 36:15472-485.

[31] Naterer GF, Suppiah S, Stolberg L, Lewis M, Ferrandon M, Wang Z, Dincer I, et al. Clean hydrogen production with the Cu-Cl cycle - Progress of international consortium, II: Simulations, thermochemical data and materials. *Int J Hydrogen Energy* 2011; 36:15486-501.

[32] Ferrandon MS, Lewis MA, Tatterson DF, Gross A, et al. Hydrogen production by the Cu–Cl thermochemical cycle: Investigation of the key step of hydrolysing $CuCl_2$to Cu_2OCl_2 and HCl using a spray reactor. *Int J Hydrogen Energy* 2010; 35: 992-1000.

[33] Wang Z, Daggupati V, Marin G, Pope K, Xiong Y, Secnik E, Naterer GF, Gabriel K. Towards integration of hydrolysis, decomposition and electrolysis processes of the Cu-Cl thermochemical water splitting cycle. *Int J Hydrogen Energy* 2012; 37:16557-569.

[34] McKendry P. Energy production from biomass (part3): gasification technologies. *Bioresou Technol* 2002; 83 55-63.

[35] Aghahosseini S, Dincer I, Naterer GF, Environmental impact assessment of sustainable hydrogen, steam and electricity trigeneration through integrated gasification and Cu-Cl cycle. Proceedings of the Global Conference on Global Warming, Lisbon, Portugal; 2011.

[36] Sadhankar RR, Li J, Li H, Ryland DK, Suppiah S. Future hydrogen production using nuclear reactors. Engineering Institute of Canada - Climate Change Technology Conference, Ottawa, Canada; May, 2006.

[37] Sadhankar RR. Leveraging nuclear research to support hydrogen economy. In: 2nd green energy conference, Oshawa, Canada; June, 2006.

[38] Rosen MA, Naterer GF, Sadhankar R, Suppiah S. Nuclear-based hydrogen production with a thermochemical copper-chlorine cycle and supercritical water reactor. Canadian Hydrogen Association Workshop. Quebec, Canada; Oct. 19-20 2006.

[39] Dokiya M., Kotera Y. Hybrid cycle with electrolysis using Cu-Cl system. *Int J Hydrogen Energy* 1976; 1:117-121.

[40] Chukwu C, Naterer GF, Rosen MA. Process simulation of nuclear-produced hydrogen with a Cu-Cl cycle. 29th Conference of the Canadian Nuclear Society, Toronto, Ontario, Canada, June 1-4, 2008.

[41] Naterer GF, Suppiah S, Stolberg L, Lewis M, Wang Z, Daggupati V, et al. Canada's program on nuclear hydrogen production and thermochemical Cu-Cl cycle. *Int. J. Hydrogen Energy* 2010; 35(2):10905-26.

[42] Xiao ZF, Gammons CH, Williams-Jones AE. Experimental study of copper(I) chloride complexing in hydrothermal solutions at 40 to 300˚C and saturated water vapor pressure. *Geochimica et Cosmochimica Acta* 1998; 62: 2949-64.

[43] Ranganathan S, Easton EB. High performance ceramic carbon electrode-based anodes for use in the Cu–Cl thermochemical cycle for hydrogen production. *Int J Hydrogen Energy* 2010; 35:1001-7.

[44] El-Halwagi MM. Pollution prevention through process integration: systematic design tools. Academic Press, San Diego, USA; 1997.

[45] Linnhoff B, Hindmarsh E. The pinch design method for heat exchanger networks. *Chem Engng Sci* 1983; 38:745–63.

[46] Papoulias SA, Grossmann IE. A structural optimization approach in process synthesis-II. Heat recovery networks. *Comp Chem Eng* 1983; 7:707–21.

[47] Cerda J, Westerberg D, Mason D, Linhoff B. Minimum utility usage in heat-exchanger network synthesis: A transportation problem. *Chem Eng Sci* 1983; 38:373-383.

[48] Gundersen T, Naess L. The synthesis of cost optimal heat exchanger networks: an industrial review of the state of the art. *Comp Chem Eng* 1988; 12(6):503–30.

[49] Shenoy UV. Heat exchange network synthesis: process optimization by energy and resource analysis. Gulf Publishing Company, Houston, USA; 1995.

[50] El-Halwagi MM and Spriggs HD, Solve design puzzles with mass integration. *Chem Eng Prog* 1988; 94:25–44.

[51] Dunn RF, El-Halwagi MM. Selection of optimal VOC-condensation systems. *Waste Mgt* 1994; 14:103–13.

[52] Dunn RF, El-Halwagi MM. Optimal design of multi-component VOC-condensation systems. *J Haz Matls* 1994; 38:187–206.

[53] El-Halwagi MM, Srinivas BK, Dunn RF. Synthesis of heat induced separation networks. *Chem Eng Sci* 1995; 50:81–97.

[54] Dunn RF, Zhu M, Srinivas BK, El-Halwagi MM. Optimal design of energy-induced separation systems for VOC recovery. *AIChE Symp Ser* 1995; 90:74–85.

[55] Darton, R. C., Distillation and absorption technology: Current market and new developments, Part A. U.S. Department of energy, Washington DC, *Trans IchemE* 1992; 70:435 – 38.

[56] Smith R, Chemical process design and integration, Wiley, New York; 2005.

[57] Widagdo, S. and Seider, WD. Azeotropic Distillation. *AIChE Journal* 1996; 42(1):96–130.

[58] Rousseau ERW. Handbook of separation process technology, John Wiley & Sons, New York; 2009.

[59] Sattler K, Feindt HJ. Thermal separation processes: principles and design, Wiley-VCH, New York; 2008.

[60] Lei Z, Chen B, Ding Z. Special distillation processes, Elsevier Science, 2005.

[61] Stichlmair J, Fair JR. Distillation: principles and practices, Wiley-VCH, New York; 1998.

[62] Hilmen E. Separation of azeotropic mixtures: tools for analysis and studies on batch distillation operation. PhD diss., Norwegian University of Science and Technology, 2000.

[63] Pettersen T, Lien KM. Design of hybrid distillation and vapor permeation processes. *J Membr Sci* 1995; 102:21-30.

[64] Knapp JP, Doherty MF. A new pressure-swing-distillation process for separating homogeneous azeotropic mixtures. *Ind Eng Chem Res*. 1992; 31:346-57.

[65] Abu-Eishah SI, Luyben WL. Design and control of two-Column azeotropic distillation System. *Ind Eng Chem Process Des Dev* 1985; 24:132-140.

[66] Phimister JR, Seider WD. Semi-continuous, Pressure Swing Distillation. *Ind Eng Chem Res* 2000; 39: 122-130.

[67] Luyben, WL and Cheng HC. Heat-integrated distillation columns for ternary separations. *Ind Eng Chem Process Des Dev* 1995; 24:707-13.

[68] Carmo M and Gubulin J. Ethanol-water separation in the PSA process. *Adsorption*. 2002; 8:235-48.

[69] Wendt M, Königseder R, Li P, Wozny G. Theoretical and experimental studies on startup strategies for a heat-integrated distillation column system. *Chem Eng Res Design* 2003; 81:153-161.

[70] Löwe K and Wozny GA. New strategy for product switchover and startup for a heat- and Mass- integrated distillation system. *Chem Eng and Proc* 2001; 40:295-302.

[71] Huang K, Shan L, Zhu Q, Qian J. Adding rectifying/stripping section type heat integration to a pressure-swing distillation (PSD) process. *Appl Therm Eng* 2008; 28: 923-32.

[72] Green DW and Perry RH. Perry's Chemical Engineers' Handbook. 8th ed. McGraw-Hill, New York; 2008.

[73] Doherty MF, Knapp JP. Distillation, Azeotropic, and Extractive. *Kirk-Othmer Encyc Chem Technol*. 1993.

[74] Laroche L, Andersen H, Morari M, Bekiaris N. Homogeneous azeotropic distillation: comparing entrainers. *The Canadian Journal of Chemical Engineering* 1991; 69:1302-19.

[75] Zwart RWR, Boerrigter H. High efficiency co-production of synthetic natural gas (SNG) and Fischer-Tropsch (FT) transportation fuels from biomass. *Energy Fuels* 2005; 19:591-97.

[76] Dickenson R, Biasca F, Schulman B, Johnson H. Refiner options for converting and utilizing heavy fuel oil. *Hydrocarbon Process*. 1997; 76(2).

[77] Akunuri N. Modeling the performance, emissions, and cost of an entrained-flow gasification combined cycle system using ASPEN. Department of Civil Engineering, North Carolina State University; 26 August 1999.

[78] Faaij APC. Modern biomass conversion technologies. Mitigation Adaptation Strategies for Global Change 2006; 11(2):343-75.

[79] Bauen A. Future energy sources and systems e acting on climate change and energy security. *J Power Sources* 2006; 157(2):893-901.

[80] Heaven DL. Gasification converts a variety of problem feedstocks and wastes. *Oil Gas J* 1996; 94(22):49-54.

[81] Cormos CC. Evaluation of energy integration aspects for IGCC based hydrogen and electricity coproduction with carbon capture and storage. *Int J Hydrogen Energy* 2010; 35(14):7485-97.

[82] Wang ZL, Naterer GF, Gabriel KS, Gravelsins R, Daggupati VN. Comparison of different copper–chlorine thermochemical cycles for hydrogen production. *Int J Hydrogen Energy* 2009; 34:3267–76.

[83] Lewis MA. Cu-Cl cycle R&D – recent research for the hydrolysis reaction sensitivity studies. Cu-Cl cycle research and development at the Argonne National Laboratory. Canadian workshop on hydrogen production from non-fossil Sources. University of Ontario Institute of Technology; Oshawa, Ontario, Canada; December 20, 2007.

[84] Ferrandon MS, Lewis MA, Alvarez F, Shafirovich E. Hydrolysis of $CuCl_2$ in the Cu-Cl thermochemical cycle for hydrogen production: Experimental studies using a spray reactor with an ultrasonic atomizer. *Int J Hydrogen Energy* 2010; 35:1895-1904.

[85] Daggupati V, Naterer G, Gabriel K, Gravelsins R, Wang Z. Equilibrium conversion in CuCl cycle multiphase processes of hydrogen production. *Thermochimica Acta* 2009; 496:117 23.

[86] Lewis MA, Masin JG. The evaluation of alternative thermochemical cycles–Part II: The down-selection process. Int J Hydrogen Energy. 2009; 34 4125-4135.

[87] Pope K, Wang ZL, Naterer GF. Measured Steam Conversion and Chemical Kinetics in a Hydrolysis Packed Bed Reactor for Hydrogen Production. *Energy Procedia* 2012; 29:496-502.

[88] Balashov VN, Schatz R, Chalkova E, Akinfiev NN, Fedkin MV, Lvov SN. CuCl electrolysis for hydrogen production in the Cu–Cl thermochemical cycle. *J Electrochem Soc* 2011; 158(3):266-75.

[89] Wang Z, Naterer GF, Gabriel K, Gravelsins R, Daggupati V. New Cu-Cl thermochemical cycle for hydrogen production with reduced excess steam requirements, *Int J Green Energy* 2009; 6:616-26.

[90] Stolberg L. Electrolysis cell for the conversion of cuprous chloride in hydrochloric acid to cupric chloride and hydrogen gas. U.S. Patent No. 0051469; 2010.

[91] Suppiah S, Naterer GF, Lewis M, Trevani L, Easton B, Dincer I, et al. Thermo-mechanical design of nuclear-based hydrogen production. In: ORF workshop on nuclear-based thermochemical hydrogen production, Oshawa, February, 2011.

[92] Stolberg, L, Boniface H, McMahon S, Suppiah S, and York S. Development of the electrolysis reactions involved in the Cu-Cl thermochemical cycles. Proceedings of the International Conference on Hydrogen Production, Oshawa, CA, 2009.

[93] Gong, Y, Chalkova E, Akinfiev N, Balashov V, Fedkin M, and Lvov SN. CuCl-HCl electrolyser for hydrogen production via Cu-Cl thermochemical cycle. *ECS Trans* 2009; 19(10):21–32.

[94] Naterer GF, Suppiah S, Stolberg L, Lewis M, Wang Z, Dincer I, Rosen MA, et al. Progress of international hydrogen production network for the thermochemical Cu-Cl cycle. *Int J Hydrogen Energy* 2013; 38:740-59.

[95] Edge PS, Easton EB. Evaluation of anode electrode materials for Cu-Cl/HCl electrolysers for hydrogen production. *ECS Transactions* 2012; 41(31):111-20.

[96] Lewis MA, Ahmed S, Lvov S, Fan C. II.E.2 Membrane/Electrolyser development in the Cu-Cl thermochemical cycle. FY 2012 annual progress report, DOE hydrogen and fuel cells program, 2012.

[97] Kiva V, Hilmen E, Skogestad S. Azeotropic phase equilibrium diagrams: a survey. Chem Eng Sci 2003; 58:1903-53.

[98] Ray MS. Equilibrium-staged separations: a bibliography (1991). *Sep Sci Technol* 1993; 28:1361-1378.

[99] Wasylkiewicz SK, Kobylka LC, Castillo FJL. Pressure Sensitivity Analysis of Azeotropes. *Ind Eng Chem Res* 2003; 42:207-13.

[100] Seiler M, Jork C, Kavarnou A, Arlt W, Hirsch R. Separation of azeotropic mixtures using hyperbranched polymers or ionic liquids. *AIChE J* 2004; *50*(10): 2439-54.

[101] Guan J, Hu X, Simulation and analysis of pressure swing adsorption: ethanol drying process by the electrical analogue. Separation and purification technology. 2003; 31:31-35.

[102] Frank TC, Break azeotropes with pressure-sensitive distillation. *Chem Eng Prog* 1997; 93: 52-63.

[103] Wasylkiewicz SK, Doherty MF, Malone MF. Computing all homogeneous and heterogeneous azeotropes in multicomponent mixtures. *Ind Eng Chem Res* 1999; 38:4901-912.

[104] Gmehling J, Menke J, Krafczyk J, Fischer K. A data bank for azeotropic data-status and applications. *Fluid Phase Equilib* 1995; 103:51-76.

[105] Gmehling J, Menke J, Krafczyk J, Fischer K, Pereira Nunes S, Peinemann K. Azeotropic Data. Wiley-VCH, New York; 1996.

[106] Gmehling J, Bölts R. Azeotropic data for binary and ternary systems at moderate pressures. *Journal of Chemical & Engineering Data.* 1996; 41:202-09.

[107] Low K, Sørensen E. Optimal operation of extractive distillation in different batch configurations. *AICHE J* 2002; 48:1034-50.

[108] Lee FM, Pahl RH. Solvent Screening Study and conceptual extractive distillation process to produce anhydrous ethanol from fermentation broth. *Ind Eng Chem Proc DD* 1985; 24:168-172.

[109] García-Herreros P, Gómez JM, Gil ID, Rodríguez G. Optimization of the design and operation of an extractive distillation system for the production of fuel grade ethanol using glycerol as entrainer. *Ind Eng Chem Res.* 2011; 50:3977-3985.

[110] Meirelles A, Weiss S, Herfurth H, Ethanol dehydration by extractive distillation. *Journal of Chemical Technology and Biotechnology.* 1992; 53:181-188.

[111] Ligero E, Ravagnani T. Dehydration of ethanol with salt extractive distillation-a comparative analysis between processes with salt recovery. *Chemical Engineering and Processing: Process Intensification* 2003; 42:543-552.

[112] Furter W. Extractive distillation by salt effect. *Chem Eng Commun* 1992;116:35-40.

[113] Lei Z, Wang H, Zhou R, Duan Z. Influence of salt added to solvent on extractive distillation. *Chem Eng J* 2002; 87:149-156.

[114] Zhou R, Duan Z. Extractive distillation with salt in solvent. *Tsinghua Sci Technol* 1999; 4:1477-79.

[115] Lee FM, Ronald BE. Extractive distillation of hydrocarbons employing solvent mixture. U.S. Patent 4,921,581, issued May 1, 1990.

[116] Seiler M, Köhler D, Arlt W. Hyperbranched polymers: new selective solvents for extractive distillation and solvent extraction. *Sep Purif Technol.* 2003; 30:179-197.

[117] Lei Z, Zhou R, Duan Z. Separating 1-Butene and 1, 3-Butadiene with DMF and DMF with Salt by Extractive Distillation. *J Chem Eng Japan* 2002; 35:211-216.

[118] Jiménez L, Garvín A, Costa-López J. The production of butyl acetate and methanol via reactive and extractive distillation. I. Chemical equilibrium, kinetics, and mass-transfer issues. *Ind Eng Chem Res* 2002; 41:6663-69.

[119] Luyben WL. Comparison of extractive distillation and pressure-swing distillation for acetone-methanol separation. *Ind Eng Chem Res* 2008; 47:2696-2707.

[120] Demiral H, Yildirim ME. Recovery of acetic acid from waste streams by extractive distillation. *Water science and technology* 2003; 183-188.

[121] Slapak M, Van Kasteren J, Drinkenburg A. Design of a process for steam gasification of PVC waste. *Resour Conserv Recycling.* 2000; 30:81-93.

[122] Stichlmair JG, Herguijuela J. Separation regions and processes of zeotropic and azeotropic ternary distillation. *AICHE J* 1992; 38:1523-1535.

[123] Aker Chemetics, A division of Aker Solutions Canada Inc. Hydrochloric Acid Concentration. Last accessed on May 2013; http://www.akersolutions.com/.

[124] De Dietrich Process Systems GmbH. Concentration of Hydrochloric Acid above the azeotrope point. 2013; http://www.qvf.com/.

[125] Gmehling J, Möllmann C. Synthesis of distillation processes using thermodynamic models and the Dortmund data bank. *Ind Eng Chem Res* 1998; 37:3112-23.

[126] Jana AK. Heat integrated distillation operation. *Appl Energy* 2010; 87:1477-94.

[127] Fahmi, AA, Fawzi, AB, Rami J. Vapor–liquid equilibrium of ethanol–water system in the presence of molecular sieves. *Sep Sci Technol* 1999; 34(12):2355–68.

[128] Fawzi, AB, Fahmi AA, Jana S. Analysis of vapor–liquid equilibrium of ethanol–water system via headspace gas chromatography: effect of molecular sieves. *Purif Technol* 2000; 18:111–18.

[129] Cheng H, Zhou M, Xu CJ, Yu GC. Enhancement of fine adsorption particles on gas–liquid mass transfer. *I J Chem Ind Eng* (China) 1999a; 50:766–71.

[130] Cheng H, Zhou M, Zhang Y, Xu CJ, Yu GC. Enhancement of fine adsorption particles on gas–liquid mass transfer. *I J Chem Ind Eng (China)* 1999b; 50:772-77.

[131] Toonssen R, Woudstra N, Verkooijen AH. Exergy analysis of hydrogen production plants based on biomass gasification. *Int J Hydrogen Energy* 2008; 33: 4074-82.

[132] Li X, Grace J, Watkinson A, Lim C, Ergüdenler A. Equilibrium modeling of gasification: a free energy minimization approach and its application to a circulating fluidized bed coal gasifier. *Fuel* 2001; 80:195-207.

[133] Altafini CR, Wander PR, Barreto RM. Prediction of the working parameters of a wood waste gasifier through an equilibrium model. *Energy Conversion and Management* 2003; 44:2763-77.

[134] Zainal Z, Ali R, Lean C, Seetharamu K. Prediction of performance of a downdraft gasifier using equilibrium modeling for different biomass materials. *Energy conversion and management* 2001; 42:1499-1515.

[135] Abuadala A, Dincer I, Naterer GF. Exergy analysis of hydrogen production from biomass gasification. *Int J Hydrogen Energy* 2010; 35:4981-90.

[136] Sreejith C, Muraleedharan C, Arun P. Energy and exergy analysis of steam gasification of biomass materials: a comparative study. *Int J Ambient Energy* 2012; 34(1):35-52.

[137] Rao MS, Singh SP, Sodha MS, Dubey AK, Shyam M. Stoichiometric, mass, energy and exergy balance analysis of counter-current fixed-bed gasification of post-consumer residues. *Biomass and Bioenergy* 2004; 27:155-71.

[138] Hosseini M, Dincer I, Rosen MA. Steam and air fed biomass gasification: Comparisons based on energy and exergy. *Int J Hydrogen Energy* 2012; 37:16446-52.

[139] Jarungthammachote S, Dutta A. Thermodynamic equilibrium model and second law analysis of a downdraft waste gasifier. *Energy* 2007; 32 1660-69.

[140] Gil J, Corella J, Aznar MP, Caballero MA. Biomass gasification in atmospheric and bubbling fluidized bed: effect of the type of gasifying agent on the product distribution. *Biomass Bioenergy* 1999; 17:389-403.

[141] Kumar A, Eskridge K, Jones DD, Hanna MA. Steam–air fluidized bed gasification of distillers grains: Effects of steam to biomass ratio, equivalence ratio and gasification temperature. *Bioresour Technol* 2009; 100:2062-68.

[142] Lv P, Yuan Z, Ma L, Wu C, Chen Y, Zhu J. Hydrogen-rich gas production from biomass air and oxygen/steam gasification in a downdraft gasifier. *Renewable Energy* 2007; 32:2173-85.

[143] Prins MJ, Ptasinski KJ, Janssen FJ. From coal to biomass gasification: Comparison of thermodynamic efficiency. *Energy* 2007; 32:1248-59.

[144] Zhang Y, Li B, Li H, Liu H, Thermodynamic evaluation of biomass gasification with air in autothermal gasifiers. *Thermochimica Acta* 2011; 519:65-71.

[145] Cole-Parmer Canada Inc. Masterflex Peristaltic Pumps. Last accessed on June 2013; http://www.coleparmer.ca.

[146] ABB Measurement Products Canada, Continuous Gas Analysis, Advance Optima Series AO2020. Last accessed on June 2013; http://www.abb.com.

[147] Ion Power Inc., New Castle, DE, USA. Customized Nafion products. Last accessed on June 2013; http://www.ion-power.com.

[148] Gamry Instruments, Warminster, PA, USA. Electrochemical instrumentation and accessories. Last accessed on June 2013; http://www.gamry.com.

[149] Bard AJ, Faulkner LR. Electrochemical Methods: Fundamentals and Applications. 2nd ed., John Wiley & Sons, New York; 2000.

[150] Coleman HW, Steele WG. Experimentation, Validation, and Uncertainty Analysis for Engineers. John Wiley & Sons, New York; 2009.

[151] Kim JH, Simon TW, Viskanta R. Journal of heat transfer policy on reporting uncertainties in experimental measurements and results. *J Heat Transfer*. 1993; 115.

[152] Kirk RE and Othmer DF. Kirk-Othmer Encyclopedia of Chemical Technology. Hydrogen Chloride. Vol. 13. 5th ed., John Wiley & Sons, New York; 2005.

[153] Aspen Properties, Binary mixtures modeling software (calculations by Akzo Nobel Engineering edition) Aspen Technology; 2002-2003.

[154] Hilmen, EK. Separation of Azeotropic Mixtures: Tools for Analysis and Studies on Batch Distillation Operation. Norwegian University of Science and Technology, Dept. of Chemical Engineering. November 2000, Retrieved 24 March 2007.

[155] Towler G, Sinnott RK, Chemical Engineering Design: Principles, Practice and Economics of Plant and Process Design, Butterworth-Heinemann, 2012.

[156] Aspen physical property systems, Physical property methods. Aspen Technology Inc., Burlington, MA. July 2010.

[157] Montgomery DC. Design and analysis of experiments. 7th ed., John Wiley & Sons, New York; 2008.

[158] Anderson MJ, Whitcomb PJ. DOE Simplified: Practical Tools for Effective Experimentation. OR: Productivity; 2000.

[159] Mohr PJ, Taylor BN, Newell DB. CODATA recommended values of the fundamental physical constants: 2006. *Reviews of Modern Physics* 2008; 80:633.

[160] Shaw RG, Mitchell-Olds T. ANOVA for unbalanced data: an overview. *Ecology* 1993; 1638-45.

[161] McCloskey DN, Ziliak ST. The standard error of regressions. *J Econ Lit* 1996; 34:97-114.

[162] Shelton W, Lyons J. Texaco gasifier IGCC base cases. PEDIGCC-98-001 Report. NETL, DOE; 2000.

[163] Balmer RT. Modern Engineering Thermodynamics-Textbook with Tables Booklet, Academic Press, 2010.

[164] Karamarkovic R, Karamarkovic V. Energy and exergy analysis of biomass gasification at different temperatures. *Energy* 2010; 35:537-49.

[165] Bejan A, Moran MJ. Thermal Design and Optimization, John Wiley & Sons, New York; 1996.

[166] Anderson DR, Burnham KP, Thompson WL. Null hypothesis testing: problems, prevalence, and an alternative. *J Wildl Manage* 2000; 912-923.

[167] Hedges SB. The number of replications needed for accurate estimation of the bootstrap P value in phylogenetic studies. *Mol Biol Evol* 1992; 9:366-369.

[168] Allen JB, Larry RF. Electrochemical methods: fundamentals and applications. Department of Chemistry and Biochemistry University of Texas at Austin, John Wiley & Sons Inc., New York; 2001.